DISSERTATION

Modeling Static Recrystallization in Metallic Materials

Submitted for the degree "Doktor der technischen Wissenschaften", under direction of

Univ.Prof. Dipl.-Ing. Dr.techn. E. Kozeschnik
E308
Institute for Materials Science and Technology

Submitted at TU Wien
Faculty for Mechanical and Industrial Engineering

by
Heinrich Buken, MSc
Matr.Nr. 01429020
Halbgasse 24/1
1070 Wien
Austria

Vienna,8th of May 2018

_____
Personal Signature

This dissertation has been assessed by

_____   _____
Prof. Dr. Christof Sommitsch   Prof. Dr. Ronald Schnitzer
Technische Universität Graz   Montanuniversität Leoben

Declaration

I declare in lieu of oath, that I wrote this thesis and performed the associated research myself, using only literature cited in this volume.

(Heinrich Buken)

Vienna, 8th of May 2018

Acknowledgement

Abstract

This work presents a model to describe the recrystallization behavior of metallic materials. A physical model describing the process of recrystallization in terms of nucleation and growth is developed. The nucleation of recrystallization is calculated using models for subgrain evolution, dislocation kinetics and geometrical topological aspects. The growth is modeled with the help of driving pressures and grain boundary mobilities. The important influence factors on recrystallization such as temperature, strain rate, strain, composition of the material and initial grain size are described consistently by the model presented. The interactions of the generated recrystallization model with the precipitation kinetics, which are broadly represented by the thermokinetic software tool MatCalc, are particularly noteworthy. With the help of this interaction, recrystallization stop temperatures can be precisely described by interactions between grain boundaries and precipitates. With the help of a sophisticated physical approach to grain boundary mobility, which describes both the influences of precipitates and dissolved atoms, technical alloys in their microstructure evolution can also be represented within the developed model with a single set of input parameters. The results of the model are compared with numerous experiments from literature, whereby an excellent agreement between simulation and experiment can be observed.

Kurzfassung

In der vorliegenden Arbeit wird ein Modell zur Beschreibung des Rekristallisations-verhaltens von metallischen Werkstoffen vorgestellt. Dabei wird ein physikalisches Modell, welches den Vorgang der Rekristallisation in Begrifflichkeiten der Nukleation und des Wachstums beschreibt, entwickelt. Die Nukleation der Rekristallisation wird mit Hilfe der Subkornevolution, Versetzungskinetik und unter geometrisch-topologischen Aspekten berechnet. Das Wachstum wird mit Hilfe von Treibkräften und Korngrenzenmobilitäten modelliert. Die wichtigen Einflüsse auf die Rekristallisation wie die Temperatur, die Dehnrate, die Dehnung, die Zusammensetzung des Materials sowie die Anfangskorngröße werden von dem vorgestellten Modell in logischer Art und Weise beschrieben. Besonders hervorzuheben sind die Wechselwirkungen des erstellten Rekristallisationsmodells mit der Ausscheidungskinetik, welche durch das thermokinetische Softwaretool MatCalc bereitgestellt wird. Durch diese Interaktion lassen sich Rekristallisationsstoptemperaturen durch Wechselwirkungen zwischen Korngrenzen und Ausscheidungen genau beschreiben. Mit Hilfe eines ausgeklügelten physikalischen Ansatzes für die Korngrenzenmobilitäten, welcher sowohl die Einflüsse der Ausscheidungen als auch die Einflüsse der gelösten Atome beschreibt, können auch technische Legierungen in ihrer Mikrostrukturevolution mit einem unveränderten Set an Inputparametern des vorgestellten Modell abgebildet werden. Die Ergebnisse des Modells werden mit zahlreichen Experimenten aus der Literatur verglichen, wobei eine exzellente Übereinstimmung zwischen den Simulationen und Experimenten festgestellt werden kann.

Preface

This thesis is submitted in compliance with the requirements for the degree of doctor of technical sciences at the Vienna University of Technology. The doctoral work has been carried out at the Faculty of Mechanical and Industrial Engineering, Institute of Materials Science and Technology, Vienna, Austria.

The thesis is divided into two sections. In section A, an introduction to the field of recrystallization and precipitation modeling is given. Furthermore, the concept and functionality of the overall model is explained. In Section B, the concepts discussed in Section A are reported in detail in the form of five publications, which are:

1) H. Buken, E. Kozeschnik, Modelling static recrystallization in Al-Mg alloys, Metall. Mater. Trans. A Phys. Metall. Mater., (submitted), (2018).

2) H. Buken, E. Kozeschnik, A Model for Static Recrystallization with Simultaneous Precipitation and Solute Drag, Metall. Mater. Trans. A Phys. Metall. Mater. Sci. 48 (2017) 2812–2818.

3) H. Buken, P. Sherstnev, E. Kozeschnik, A state parameter-based model for static recrystallization interacting with precipitation, Model. Simul. Mater. Sci. Eng. 24 (2016) 35006.

4) H. Buken, E. Kozeschnik, State parameter-based modelling of microstructure evolution in micro-alloyed steel during hot forming, in: Mater. Sci. Eng. 119, 2016: p. 12023.

5) H. Buken, S. Zamberger, and E. Kozeschnik, A Model for the Influence of Micro-Alloying Elements on Static Recrystallization of Austenite, in: Proc. 6th Int. Conf. Recryst. Grain Growth (ReX&GG 2016), John Wiley & Sons, Inc., Hoboken, NJ, USA, 2016: pp. 113–118.

Moreover, the work that was performed throughout the years has been presented at numerous international and national conferences:

1) H. Buken, P. Sherstnev and E. Kozeschnik, „Modeling the interaction between precipitation and static recrystallization in micro-alloyed steel", oral presentation (invited), PTM 2015, Whistler, Canada, 28.06. - 03.07.2015

2) H. Buken and E. Kozeschnik, „Modelling the interaction of deformation and precipitation in V and Nb micro-alloyed steel", oral presentation, ICSMA 2015, Brno, Czech Republic, 09. - 14.08.2015

3) H. Buken and E. Kozeschnik, "State parameter-based modelling of microstructure evolution in micro-alloyed steel during hot forming"; oral presentation (invited), COMET-K2 Kompetenzzentrums MPPE, Leoben; Austria, 03. - 05.11.2015.

4) M. Rath, H. Buken, E. Kozeschnik, „Multi-class modeling of microstructure evolution during high-temperature deformation of Ni-base alloys - Theory and Application", oral presentation (invited), 62. Metallkunde Kolloquium, Lech am Arlberg, Switzerland, 11.04. - 13.04.2016

5) E. Kozeschnik, J. Kreyca, H. Buken, J. Svoboda, H. Riedel and F.D. Fischer, "Temperature and strain rate effects on strengthening of metallic materials", oral presentation (invited), Thermec 2016, Graz, Austria, 29.05. -03.06.2016

6) H. Buken, P. Sherstnev and E. Kozeschnik, „Simultaneous precipitation and recrystallization during hot deformation of Ti, Nb and V micro-alloyed steel", oral presentation, Thermec 2016, Graz, Austria, 29.05. -03.06.2016

7) H. Buken, J. Svoboda and E. Kozeschnik, "A Multi-class Approach for the Description of Static and Dynamic Recrystallization in Steel", oral presentation, 6th International Conference on Recrystallization and Grain Growth, Pittsburgh, USA, 17.07. - 21.07.2016.

8) H. Buken, S. Zamberger and E. Kozeschnik, „A model for the influence of micro-alloying elements on static recrystallization of austenite", 6th International Conference on Recrystallization and Grain Growth, Pittsburgh, USA, 17.07. - 21.07.2016.

9) H. Buken and E. Kozeschnik, "Recrystallization in Al- Mg alloys - A new modelling approach", oral presentation (invited): Metaldeform 2017, Samara, Russia; 04. - 07.07.2017.

10)   H. Buken and E. Kozeschnik: "Modelling the thermo-mechanical processing of micro-alloyed steel", oral presentation, Euromat 2017, Thessaloniki; 17.09. - 22.09.2017.

"Gute Sitten haben für die Gesellschaft mehr Wert als alle Berechnungen Newtons."

"Good manners are more valuable to society than Newton's calculations."

Friedrich II., der Große (1712-1786)

Table of Contents

Section A

1. Introduction

Although metalworking at elevated temperatures has been practiced for thousands of years, only in the last century, scientific progress has been made in detailed understanding of the metal-physical processes involved. Carpenter and Elam [1] were the first to distinguish the process of recrystallization from grain growth. Thereby, they developed the theory that the driving pressure for recrystallization stems up from the excess dislocations introduced by deformation, whose theory is valid until today. The grain boundaries moving during recrystallization grow at a rate directly proportional to this driving force. Zener [2] described in his work that the rate of growth of processes involving grain boundary motion (grain growth and recrystallization) can be highly dependent on the number density and size of precipitates present in the system. The experiments on static recrystallization in austenite by Medina et al [3] show that recrystallization can be severely hindered when precipitates interact with grain boundary motion. In addition to the Zener effect, impurities as well as alloying elements also influence the growth rate of grains, which has for instance been measured for Al-Mg alloys during grain growth and recrystallization [4]. In addition to the Zener drag and the Solute drag [5], which determine the compositional influence on the recrystallization behavior, other factors such as the degree of deformation, the strain rate, the temperature and the initial grain size exert considerable influence on the recrystallization behavior [6]. Numerous models already exist in literature [7–9] describing the recrystallization behavior as a function of these influencing factors. Nonetheless, most models rely on phenomenological assumptions or require a variety of fitting parameters that limit the predictive capability of these model to individual alloys.

This thesis is divided into two sections. The first section (Section A) contains an overview of the models developed and used during the dissertation and the accompanying explanations. First, the models for precipitation kinetics and microstructure development are discussed. Upon this, the results of the overall model are explained. The second section contains five scientific papers that constitute the major part of this work. The simulations in comparison to experimental results as well as the input parameters for the models are explained in detail in these papers.

2. Modelling Precipitation Kinetics

Since the microstructure kinetics can be strongly influenced by precipitates [2] and this effect is taken into account in this work, the most important evolution equations for the modeling of precipitation kinetics are explained in this chapter.

The occurrence of precipitation can basically be divided into three parts: Nucleation, growth and coarsening. The nucleation of precipitates is modelled in accordance to the classical nucleation theory, which is extended for multi-component systems. The transient rate of nucleation, J, which describes the creation of stable nuclei per unit volume and time, t, can be expressed as follows:

$$J = NZ\beta^* \exp\left(\frac{-G^*}{k_B T}\right) \exp\left(\frac{-\tau}{t}\right). \qquad (1)$$

The transient nucleation rate is mainly determined by the critical Gibbs energy for nucleus formation, G^*, the number of potential nucleation sites, N, the atomic attachment rate, β^*, the Zeldovich factor, Z, the Boltzmann-constant, k_B, the temperature, T, and the incubation time. τ. The critical Gibbs energy for nucleus formation is mainly evaluated by the balance of the volume free energy, G_{vol}, and the interface energy of the nucleus, γ. Differentiating this relation with respect to the nucleus size for a spherical nucleus and equating to zero delivers:

$$G^* = \frac{16}{3} \frac{\gamma^3}{\left(\Delta G_{\text{vol}} - \Delta G_{\text{s}}\right)^2}. \qquad (2)$$

Thereby the strain energy, G_{s}, considers the volumetric misfit between the precipitate and the matrix and increases the critical energy for nucleus forming. The calculation of the number of potential nucleation sites depends on the place of nucleus formation. In this work, a differentiation of nucleation sites between grain boundaries, N_{GB}, and dislocations, N_{Dis}, are taken into account.

$$N_{\text{Dis}} = \frac{\rho}{a} \qquad (3)$$

$$N_{\text{GB}} = \frac{A_{\text{GB}}}{a^2} \qquad (4)$$

The nucleation site contribution of dislocations is dependent on the actual dislocation density, ρ, and the nucleation site density of grain boundaries on the total grain boundary surface, A_{GB}, respectively [10].

The atomic attachment rate describes long-range diffusion of the precipitate forming elements through the matrix. For a multicomponent system, it is given by Svoboda et al. [11] as

$$\beta^* = \frac{4\pi r^{*2}}{a^4 \Omega} \left[\sum_{i=1}^{n} \frac{(c_{ki} - c_{0i})^2}{(c_{0i} D_{0i})} \right]^{-1}.$$ (5)

The extent of the atomic attachment rate ascends with the critical radius, r^*, the concentration of the element n in the matrix, c_{0i}, and the diffusion coefficient of the element in the matrix, D_{0i}. It decreases with the molar volume, Ω, and quadratically with a lower gap between the concentration of the element in the precipitate, c_{ki}.

The Zeldovich factor accounts for the probability of a nucleus to decompose at the point of critical nucleus size. The probability of a thermally excited critical nucleus with the energy, $k_B T$, at this condition is fifty percent. With increasing size, this probability decreases. According to Zeldovich [12] and Russel [13], the nucleation rate should include the Zeldovich factor as:

$$Z = \left[-\frac{1}{2\pi k_B T} \left(\frac{\partial^2 \Delta G^*}{\partial n_{at}^2} \right)_{n_{at}^*} \right]^{\frac{1}{2}},$$ (6)

where n_{at} is the number of atoms in the nucleus.

The incubation time, τ, relates the transient nucleation rate with the steady state nucleation rate. Thereby, this value is also dependent on the Zeldovich factor and the atomic attachment rate [14,15].

$$\tau = \left(2\beta^* Z^2 \right)^{-1}$$ (7)

After nucleation, the further growth and coarsening is modelled in accordance to Svoboda et al. [11], which includes the radius, r, and the composition of the precipitate:

$$G = \sum_{i}^{n} N_{0i} \mu_{0i} + \sum_{k=1}^{m} \frac{4\pi r_k^3}{3} \left(\lambda_k + \sum_{i=1}^{n} c_{ki} \mu_{ki} \right) + \sum_{k=1}^{m} 4\pi r_k^2 \gamma_k.$$ (8)

This mean field approach expresses the driving pressure for the growth and coarsening in terms of the Gibbs energy, G, in dependence of different components, precipitates, m, concentrations, chemical potentials, μ, interfacial energies and specific mechanical energies, λ. The Gibbs energy in the precipitate system is here the sum of three contributions: The Gibbs energy contributions of the matrix, of the precipitates and of the total precipitate-matrix interface in the system. During precipitation, three possibilities of free energy

dissipation are taken into account: Dissipation by interface migration, by diffusion inside the precipitates and by diffusion in the matrix. The integration of the kinetic parameters are performed by means of the software tool MatCalc and are based on the Kampmann-Wagner approach, which has been described in detail elsewhere [16].

The diffusion of the precipitate-forming elements in the bulk and at defects, such as grain boundaries and dislocations, have a deep impact on the precipitate evolution. In a recent contribution, Stechauner and Kozeschnik [17] reviewed self-diffusion coefficients along defects in Fe, Al and Ni for both at grain boundaries and at dislocations, where precipitates are preferentially located. To approximate the defect-effected diffusion for other elements, a ratio to bulk diffusion can be calculated and then multiplied with the corresponding bulk diffusion cefficient of the precipitate forming element. Figure 1 exemplarily shows the self-diffusion values of Al elaborated by Stechauner and Kozeschnik.
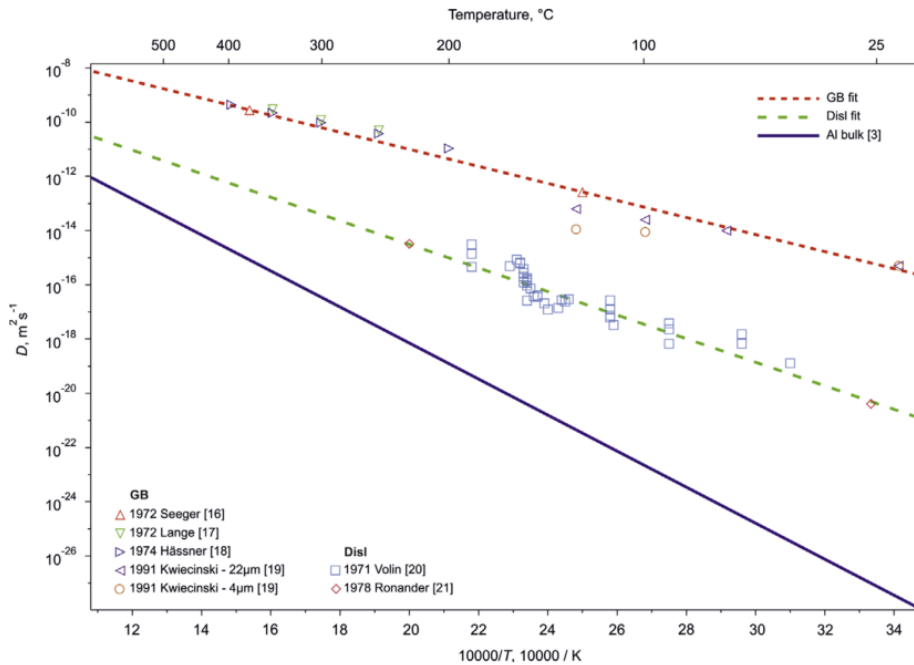
Figure 1:   Self diffusion coefficients at defects in Al [17]

Due to its cubic influence on the nucleation barrier, the interfacial energy has also a critical impact on the precipitation kinetics and can be calculated in an analytical approach independently from crystal structure and interface orientation by the approach of Sonderegger and Kozeschnik [18]:

$$\gamma = \alpha(r) \cdot \beta(T / T_\mathrm{C}) \cdot \left(\frac{n_\mathrm{S} z_\mathrm{S,eff}}{N_\mathrm{A} z_\mathrm{L,eff}} \Delta H_\mathrm{Sol} \right), \qquad\qquad (9)$$

with the number of atoms per surface area, n_S, the effective number of broken bonds at the interface, $z_\mathrm{S,eff}$, the Avogadro's number, N_A, the effective coordination number, $z_\mathrm{L,eff}$ and

the solution enthalpy, ΔH_{Sol}. The latter can directly be linked to the thermodynamic properties of the system and is thus a function of the chemical composition and the temperature. The curvature effect of the phase boundary is modelled in accordance to the approach of [19] and is captured with the function, $\alpha(r)$. In addition, the entropic contribution of the diffuse interface, $\beta(T/T_{\mathrm{C}})$, is adopted from ref. [20] and links the diffuse interface effect to a regular solution critical temperature, T_{C}. Principal results of the precipitation model are shown in chapter 4 and in section B of this thesis.

3. A New Model for Static Recrystallization

Recrystallization is a process that takes place via the elementary mechanisms of nucleation and growth [21]. Thereby, the excess dislocation energy is reduced by the formation of a new defect-poor microstructure. As part of my work on this subject, it has proved useful to describe the overall model in three steps:

(i)   The transformation of the microstructure comprises the nucleation and growth of the new grains. The **basic kinetic model** is developed here.

(ii)   The **physical description of important parameters** required by the kinetic model (i) for the correct calculation of recrystallization mainly includes a concise description of the grain boundary mobility and the driving forces for recrystallization. In this step, the important input parameters are formulated in such a general way that they can be used in several materials.

(iii) The **application of the model** to a particular material or a group of materials shows the predictive force and validity of the equations developed under (i) and (ii).

The basic kinetic model and the physical description of the most important input parameters (grain boundary mobilities and driving pressures) are explained in this chapter (subsequently). The application of the model with certain experiments is shown in the following chapter and in the papers attached (section B).

3.1   The Kinetic Model for Recrystallization

In their prominent work, Bailey and Hirsch [22] experimentally observed the nucleation mechanism for recrystallization, which is described as strain induced boundary migration (SIBM). A nucleation event becomes possible, when a subgrain being in contact with a high-angle grain boundary exceeds a critical size, r_{crit}, which is, according to Bailey and Hirsch, given by the quotient of the surface energy of the high-angle grain boundary (HAGB), γ_{HB}, and the driving pressure, P_D,

$$r_{crit}(t) = \frac{2\gamma_{HB}}{P_D(t)} = \frac{2\gamma_{HB}}{0.5Gb\rho(t)}, \qquad (10)$$

with the Burgers vector, b, the radius of the subgrain, r, the total dislocation density, ρ, and the shear modulus, G. Figure 2 shows the model of the nucleation of recrystallization within the Bailey Hirsch mechanism. In the Bailey-Hirsch approach, only the subgrains located at the grain boundary can develop into a high angle grain boundary.
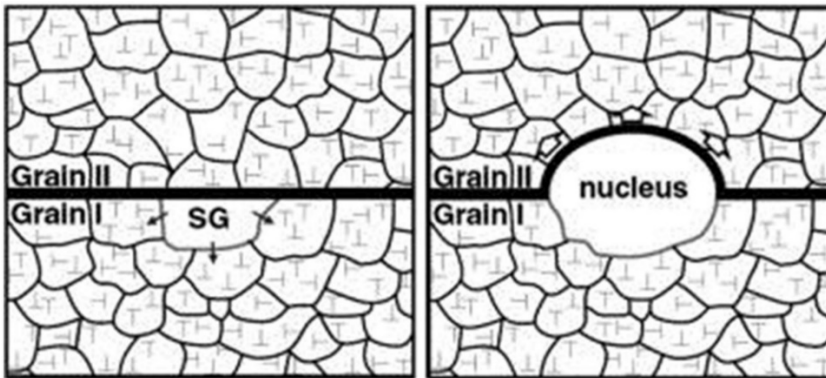
Figure 2:   Schematic illustration of a subgrain growing (left) and once it reaches the critical size (right) bulging into the deformed matrix as a new strain-free grain [23].

The nucleation rate, $\dot{N}_{rx}$, is formulated as function of the number density of potential nucleation sites, N_{pot}, a site saturation factor, B_{nuc}, and the flux of subgrains obtaining supercritical size, $\dot{F}_{sub}$, as

$$\dot{N}_{rx} = \dot{F}_{sub} N_{pot} B_{nuc}. \qquad (11)$$

The three components of the nucleation rate and their determination are explained below:

(i) $\dot{F}_{sub}$**:** Pantleon and Hansen [24] experimentally observed that the subgrains are distributed in a Rayleigh distribution . The fraction of subgrains, which are exceeding a critical size, can then be described as

$$F_{sub}(t) = \exp\left(-\frac{\pi}{4}X_{crit}^2(t)\right),\qquad(12)$$

where X_{crit} is the critical subgrain size divided by the mean subgrain size. A differentiation with respect to time delivers

$$\dot{F}_{sub} = -\frac{1}{2}\pi F(t)X_{crit}\dot{X}_{crit}.\qquad(13)$$

Thereby, the normalized critical subgrain size, X_{crit}, can be computed by means of the critical subgrain size and the mean subgrain size, r_{mean}, as

$$X_{crit}(t) = \frac{r_{crit}(t)}{r_{mean}(t)},\qquad(14)$$

and

$$\dot{X}_{Crit} = \frac{\dot{r}_{crit}}{r_{mean}} - \frac{r_{crit}\dot{r}_{mean}}{r_{mean}^2}.\qquad(15)$$

Figure 3 qualitatively illustrates the effect of the concept developed above on the modeled nucleation of recrystallization. The shaded area shows the proportion of the total population of subgrains, which become stable recrystallization nuclei in the course of the progressing subgrain growth process or the increasing value of the stored energy.
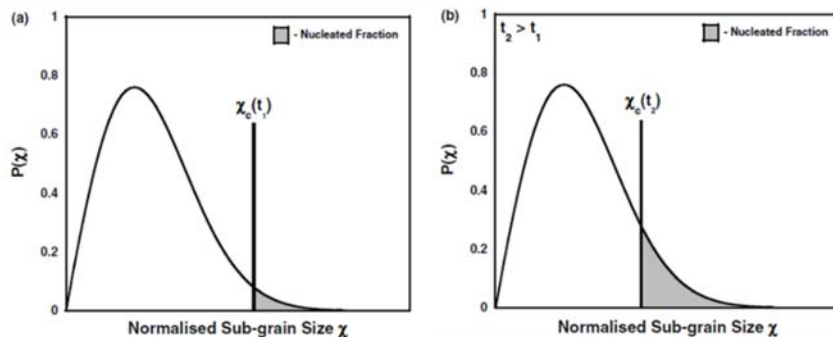

Figure 3: Portion of subgrains reaching supercritical size from the total population during nucleation of recrystallization [23].

(ii) N_{pot} **:** The potential nucleation sites can be calculated from the quotient of the specific grain boundary area, a_{av}, per unit volume of material and the area covered by a single critical subgrain being located at the high angle grain boundary. Zhu et al. [25] developed, on a mathematical basis, a term describing the effect of different deformation modes (plane strain compression, axisymmetric compression and axisymmetric tensile deformation) on the specific grain boundary area. We adopt the results of Zhu et al. in the present work and account for these with the function, f, depending on the deformation strain, ε. The function calculates the relative enlargement of the specific surface area caused by deformation. The total number of potential nucleation sites, N_{pot}, can then be formulated as,

$$N_{pot} = \frac{a_{av}}{\pi r_{crit}^2} f(\varepsilon). \tag{16}$$

Just as in the publication by Zhu et al., we describe the shape of one individual grain as a truncated octahedron (tetrakaidecahedron). The total available grain boundary area of all grains can then be described with the mean grain radius, R, the number density of the original grains, N_0, and the surface area of one grain, S_{HAG} :

$$a_{av} = 0.5 N_0 S_{HAG} = 0.5 \left(\frac{1}{8\sqrt{2}(1.5R)^3} \right) \left(\left(6 + 12\sqrt{3}\right)(1.5R)^2 \right). \tag{17}$$

(iii) B_{nuc} **:** With increasing density of newly recrystallized grains, the possible locations for new nuclei are occupied by the already recrystallized microstructure. The following term computes the fraction of grain boundary area left for further nucleation as:

$$B_{Nuc} = 1 - \frac{N_{rx} \pi (r_{crit})^2}{a_{av}}. \tag{18}$$

As shown in the equations developed above, the subgrain evolution is highly important for the nucleation of recrystallization. The subgrain growth can be divided into two parts: a part that describes the growth due to curvature, $\dot{r}_G^+$, and a part that describes shrinkage during deformation, $\dot{r}_S^-$.

$$\dot{r}_{mean} = \dot{r}_S^- + \dot{r}_G^+. \tag{19}$$

The shrinkage of the subgrain size due to deformation is known in literature as the "similitude" principle, which has been introduced by Nes [26] and Estrin [27]. Both authors

formulate an empirical equation describing the subgrain size via the inverse of dislocation density:

$$\dot{r}_s^- = \frac{\partial}{\partial t}\left(\frac{K_{\text{Sim}}}{\sqrt{\rho(t)}} \right),$$

(20)

with the material constant, K_{Sim}.

The growth of the subgrains can be described by the curvature approach, which is observed and simulated by many authors [28–30] in independent experiments. Within such an approach, the growth rate of the subgrain is described using the product of subgrain mobility, $M_{\text{eff,LB}}$, and the driving pressure for subgrain growth, $P_{\text{D,SGG}}$:

$$\dot{r}_G^+ = M_{\text{eff,LB}} P_{\text{D,SGG}}.$$

(21)

According to a recent contribution by Brechet et al. [31], the driving pressure can be calculated by taking into account the repelling pressure of dislocations due to the internal dislocation density, $\rho_{\text{int}} = \rho - \rho_{\text{RS}}$, where ρ_{RS} is the wall dislocation density:

$$P_{\text{D,SGG}} = \frac{2\gamma_{LB}}{r_{\text{mean}}} - \frac{Gb^2}{\sqrt{2\delta r_{\text{mean}}}}\sqrt{\rho_{\text{int}}},$$

(22)

with the interaction width of the low-angle grain boundary (LAGB), δ, and the subgrain boundary energy, γ_{LB}. The models for the calculation of the single dislocation density populations are presented in chapter 3.2. The evolution of the important input quantity of the subgrain mobility, which includes the influences of solute drag and Zener drag, is explained in the following subchapter. The approach described above can be used to describe the nucleation of recrystallization. The growth of these new grains is described in the following.

The newly formed high-angle grains grow into the deformed microstructure with a driving pressure (generated from the increased dislocation density), P_D, and an effective grain boundary mobility, $M_{\text{eff,HB}}$, [32].

The growth rate, $\dot{R}_{\text{rx}}$, decreases with increasing recrystallization, as less deformed microstructure remains in which the new grains could grow. Therefore, we scale the growth equation with the recrystallized volume fraction, X_{rx}:

$$\dot{R}_{\text{rx}} = M_{\text{eff,HB}} P_D (1 - X_{\text{rx}}).$$

(23)

The recrystallized volume fraction, $\dot{X}_{rx}(\dot{V}_{rx})$, can be calculated using the nucleation rate and the growth rate developed above. Assuming that the grains have the shape of a truncated octahedron (tetrakaidecahedron), the evolution equation is formulated as follows:

$$\dot{X}_{rx} = 27\sqrt{2}\left(R_{rx}^3 \dot{N}_{rx} + 3N_{rx}R_{rx}^2 \dot{R}_{rx}\right) = \frac{\dot{V}_{rx}}{V_{tot}}.$$

(24)

It should be noted that the driving pressure and mobility play a central role in both, nucleation and growth, of recrystallized grains. In nucleation, the development of the driving pressure determines the size of the critical nucleation radius. The growth equation above shows that both, mobility and driving force, equally control growth. Due to the importance of these two parameters, their development is described separately in chapter 4.2.

3.2 Mobilities and Driving Pressures

In the previous chapter, the kinetic model for recrystallization has been described. The result of the model reacts very sensitively to the important state parameters. The most important ones, which are used in most of the works from literature as fitting parameters, are, in this context, the grain boundary mobility and the driving pressure. In the following part, physical models for the calculation of these quantities are presented and developed.

Unlike other approaches, the solute drag and Zener drag effects are included in the **grain boundary mobility**. First, we examine the grain boundary mobility of a pure material without taking into account precipitation effects and foreign atom influences. Turnbull [33] was the first to model the temperature dependence of grain boundary mobility using self-diffusion at the grain boundary, D_{GB}:

$$M_{\text{free;HB}} = \eta_{\text{free,HB}} \cdot M_{TB} = \eta_{\text{free,HB}} \cdot \frac{\omega D_{GB} V_m}{b^2 RT}, \qquad (25)$$

with the grain boundary width, ω, the efficiency factor, $\eta_{\text{free,HB}}$, the Turnbull mobility, M_{TB}, the ideal gas constant, R, the molar volume, V_m, and the temperature, T. Similar approaches have been presented by other authors [34,35] but all have in common that the temperature dependence of the mobility is mainly given by temperature dependence of the grain boundary diffusion coefficient.

In order to calculate the **influence of precipitation** on the (sub)grain boundary movement, we use the expression developed by Zener [2] for the retarding pressure, P_Z, due to precipitation and extend it for different size classes, i, and precipitate types, k:

$$P_Z(k,i) = \frac{3}{2} \gamma_{HB} \sum_i \sum_k \frac{f_{k,i}}{r_{k,i}}, \qquad (26)$$

with $r_{k,i}$ being the mean precipitate radius and $f_{k,i}$ being the precipitated phase fraction. At this point, the model for microstructure development is linked to the precipitation model (see chapter 3) in MatCalc. Within the MatCalc model for precipitation evolution, the precipitate radii and phase fractions required for the Zener pressure are calculated.

In contrast to many other approaches [8,36,37], we include the Zener pressure into the grain boundary mobility and not into the driving pressure. We formulate a precipitate affected mobility, $M_{\text{prec,HB}}$, by means of the ratio of the driving force and the Zener force [32]:

$$M_{\text{prec,HB}} = \begin{cases} \left(\dfrac{P_{\text{D}} - P_{\text{Z}}}{P_{\text{D}}}\right) M_{\text{free,HB}} + \left(1 - \dfrac{P_{\text{D}} - P_{\text{Z}}}{P_{\text{D}}}\right) M_{\text{pinned,HB}} & , P_{\text{D}} > P_{\text{Z}} \\ M_{\text{pinned,HB}} & , P_{\text{D}} \leq P_{\text{Z}} \end{cases} \qquad (27)$$

The advantage of this procedure is that the velocity of grain boundary movement never becomes zero, even in cases where the Zener pressure is larger than the driving pressure for recrystallization, but is only severely slowed down to the value of the pinned mobility, $M_{\text{pinned,HB}}$, which has been observed experimentally in many contributions e.g. [38,39]. If the precipitates bring the grain boundary to a stop, the precipitates, which are present at the grain boundary, can coarsen faster due to the high-velocity diffusion conditions there, which leads to a local reduction of the Zener pressure since the phase fraction remains equal, the radii become larger and the number density of precipitates reduces. As a result, the grain boundary can continue to progress locally even if the mean Zener pressure of the deformed microstructure is larger than the driving pressure. Figure 4 illustrates this process.
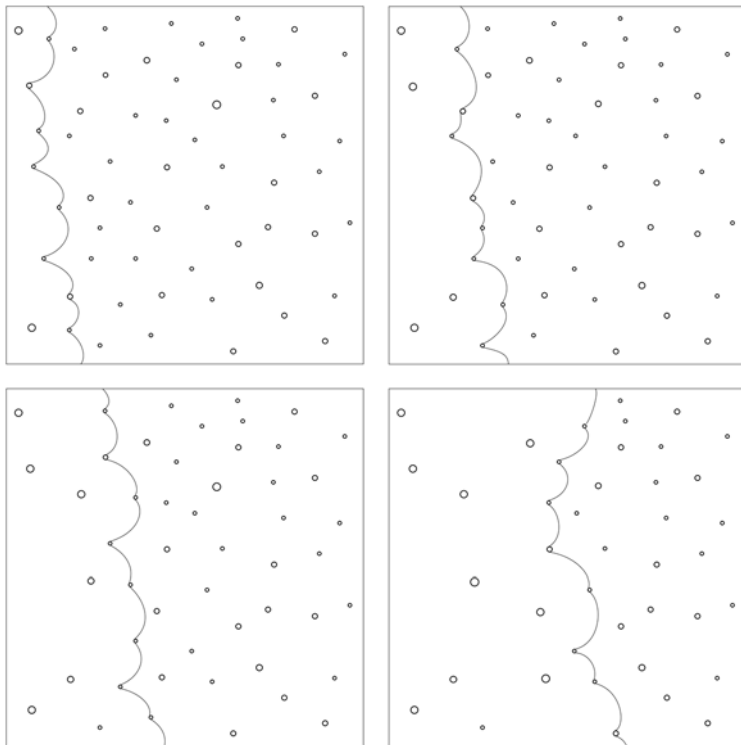
**Figure 4:**   High angle boundary passing through a precipitate enriched matrix [32]

In addition to precipitation, atoms also exert an influence on grain boundary motion, which is known in literature as the **solute drag effect** [5,40]. In this work it is modeled on the basis of the prominent work of Cahn [5]. According to Cahn, the dragging effect of solute atoms should be incorporated into the mobility term with

$$M_{\mathrm{SD}} = \frac{1}{\alpha C_{\mathrm{GB}}}, \qquad\qquad (28)$$

where, M_{SD} is the solute drag-affected grain boundary mobility , α is an inverse mobility including the trapping effect of the solute drag exerting element and C_{GB} is the concentration of the considered element at the grain boundary. The inverse mobility determines the temperature dependence with the cross boundary diffusion, D_{CB}, and the interaction energy, E_{B}, and is given as:

$$\alpha = \frac{\omega (RT)^2}{E_{\mathrm{B}} D_{\mathrm{CB}} V_{\mathrm{M}}} \left(\sinh \left(\frac{E_{\mathrm{B}}}{RT} \right) - \left(\frac{E_{\mathrm{B}}}{RT} \right) \right). \qquad\qquad (29)$$

It should be mentioned that the analyses on the solute drag of Cahn [5] go further than the technically relevant equations described here. Cahn distinguishes in his work a so-called "fast branch" from a "slow branch" depending on the concentration of the element exerting the solute drag and the driving force for moving the grain boundary. Analyses by Rehman and Zurob [7] and by Cram et al. [41] in various materials have shown that, during recrystallization, modelling can only be carried out with the aid of the slow branch. Within the framework of this work, only the "slow branch" is considered.

The total mobility approach, which includes both the influences of the precipitates and those of the solutes, can be summarized as follows:

$$M_{\mathrm{eff,HB}} = \left(\frac{1}{M_{\mathrm{prec,HB}}} + \frac{1}{M_{\mathrm{SD}}} \right)^{-1}. \qquad\qquad (30)$$

The above approach automatically determines the resulting grain boundary mobility depending on the precipitation and solute state. Figure 5 shows a sketch of the presented mobility approach.
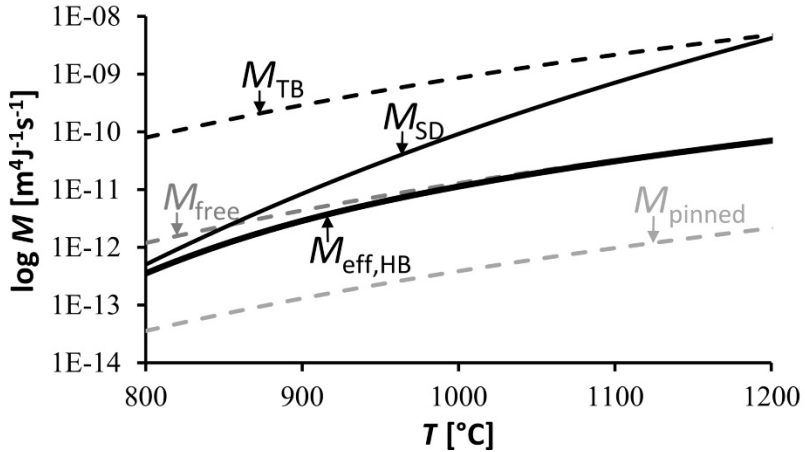
Figure 5:   Mobility-chart for a V- alloyed austenite before precipitation [42]

The free mobility is a fraction of the Turnbull mobility. Since the coarsening of grain boundary precipitates has the same temperature dependence as the free mobility [43] the pinned mobility is also considered as a fraction of the Turnbull mobility. The effective grain boundary mobility is calculated from free mobility and solute drag mobility if no precipitates are yet present. When precipitates are formed, the effective mobility moves in the direction of the pinned mobility depending on the amount of driving pressure and Zener pressure.

The subgrain growth is based on dislocation climb, according to Winning [44] and Sandstrom [45]. Therefore, Sandstrom [45] formulates a **mobility approach for subgrains**, which calculates the temperature dependence of the subgrain mobility of a pure material using bulk diffusion, D_B:

$$M_{\text{free;LB}} = \eta_{\text{free,LB}} \cdot M_{\text{SS}} = \eta_{\text{free,LB}} \cdot \frac{D_B b^2}{k_B T}, \qquad\qquad (31)$$

with the Sandstrom mobility, M_{SS}, and the Boltzmann constant, k_B. Just as in the above-described Turnbull approach for the high angle boundaries, a linear adjustment parameter is required, which does not change the temperature-dependence of the mobility. In their simulative studies, Zurob and co-workers [23,46] observe that subgrain growth can strongly depend on the solute content. Jones and Hansen [47] experimentally confirmed that second phase particles also prevent subgrain boundaries from growing. This means that both effects, which are also observed in the case of high angle grain boundaries, are also present during subgrain growth. To include these effects in the subgrain growth, we transfer the retarding effect of both mechanisms from the mobility system of the high angle grain boundaries to that of the small angle grain boundaries as:

$$M_{\text{eff,LB}} = \left(\frac{M_{\text{eff,HB}}}{M_{\text{free,HB}}} \right) M_{\text{free,LB}}.$$

<div align="right">(32)</div>

The **dislocation density evolution** is developed within an extended Kocks-Mecking model [48], which accounts for dislocation generation, dynamic recovery and static recovery. Buken and Kozeschnik [42] presented an approach based on the original model by Sherstnev et al. [49], which includes the effect of geometrically necessary dislocations:

$$\dot{\rho} = \frac{M\sqrt{\rho}}{Ab}\dot{\varepsilon} - 2B\frac{d_{\text{ann}}}{b}\rho\, M\dot{\varepsilon} - 2CD_{\text{Dis}}\frac{Gb^3}{k_B T}(\rho^2 - \rho_{\text{RS}}^2),$$

<div align="right">(33)</div>

with the critical dislocation annihilation distance, d_{ann}, the Taylor factor, M, the strain rate, $\dot{\varepsilon}$, the substitutional self-diffusion coefficient at dislocations, D_{Dis}, and material-dependent coefficients A, B, C. The geometrically necessary dislocation density can be computed by means of the Read-Shockley model [50] as

$$\rho_{\text{RS}} = \frac{\tan(\theta_{\text{mean}})}{br_{\text{mean}}},$$

<div align="right">(34)</div>

with the mean subgrain misorientation angle, θ_{mean}.

The models described above for the most important state parameters of the recrystallization model (boundary mobilities and dislocation densities) can be used to predict the recrystallization behavior of a wide variety of materials. In the last two subchapters, the functionality of the model was outlined. Finally, Figure 6 describes, how the important influencing parameters of recrystallization (composition, grain size, deformation rate, strain and temperature) affect the entire model.
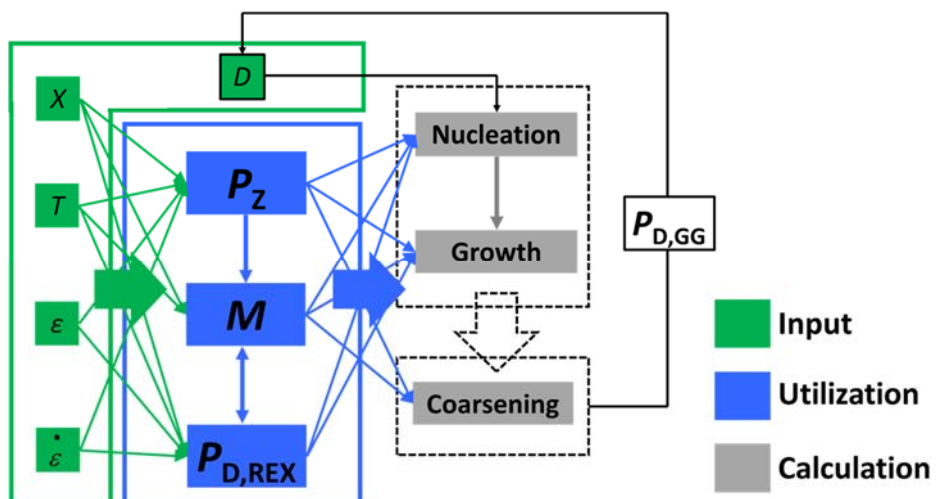

Figure 6:   Simplified mapping of the effect of material and heat treatment parameters on the recrystallization model

4. Static Recrystallization in Microalloyed Steels and Al-Mg Alloys

In this chapter, the most important final parameters for the recrystallization model for both, microalloyed steel in the austenite condition and Al alloys, are explained. In particular, the input parameters of the models for driving pressures and mobilities presented in chapter 4.2. Short application examples of the model are also given but the main demonstration of the functionality is given in the attached papers.

The diffusion values (also at defects like grain boundaries and dislocations) play a major role both in recrystallization (mobility and recovery) and in the precipitation kinetics. Therefore, a reliable source for these values is extremely important to generate a simulation success. In a new review publication, Stechauner and Kozeschnik [17] have reviewed these values which are used in this work.

The grain boundary mobilities in a pure material are determined with the aid of grain growth tests. A temperature-dependent mobility is determined with a known driving force, which results from the potential of the reduction of the total surface energy and the measured grain sizes [51]. Huang and Humphreys performed grain growth experiments in pure Aluminum and different Al-Mg alloys. Applying the Turnbull approach for the free mobility delivers a linear prefactor for the free mobility for pure Al of $\eta_{\text{free,HB}}(\text{Al}) = 0.4$. Zhou and Zurob [52] measured the grain size evolution during grain growth in C-Mn steels in the austenitic range. The Turnbull approach covers the measured grain boundary mobility with a linear prefactor of $\eta_{\text{free,HB}}(\text{Fe}_\gamma) = 0.0075$.

The solute drag effect is included in the mobilities on basis of the Cahn model. This model requires the definition of a binding energy for each solute drag-exerting element, which segregates into the grain boundary, and a cross boundary diffusion coefficient, i.e. the diffusion coefficient for the crossing of the grain boundary. In their simulations with that model, Rehman and Zurob [7] and Buken and Kozeschnik [42] determined the cross boundary diffusion coefficient as approximately two times that of the bulk diffusion coefficient, $D_{\text{CB}} = 2D_{\text{B}}$. In case of Al-Mg alloys, numerous grain growth experiments exist, which allows for a straightforward adjustment of the binding energy such that the calculated energies fit the measured solute drag containing grain boundary mobilities. Applying the Cahn model to the measured mobilities of Huang and Humphreys [4] delivers a trapping

energy between Al-grain boundaries and Mg-atoms of $E_{B, Mg} = 5kJ/mol$. Figure 7 shows the calculated mobilities in comparison to the experimentally observed ones.
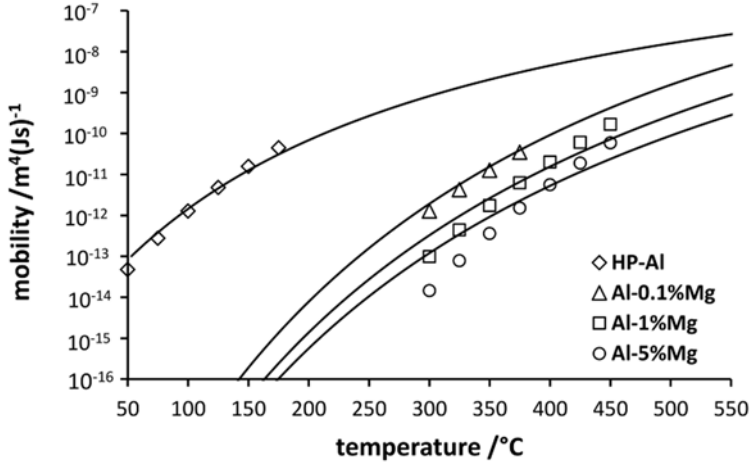
Figure 7: Calculated (lines) and measured (markers) mobilities for Al-Mg alloys [53]

Within the scope of the present work, the solute drag impact of the common micro-alloying elements (Nb, Ti, and V) in austenite have been analyzed. The binding energy for the Cahn model of Nb could be taken directly from the literature [7], which is given with $E_{B, Nb} = 2kJ/mol$. The trapping energy of V has been analyzed in the work of Buken and Kozeschnik [42], which delivered a value of $E_{B,V} = 2kJ/mol$. In their contribution, Andrade et al. [54] stated that the strength of the solute drag effect of Ti lies in between V and Nb. Buken et al. [55] confirmed that by simulation analysis where a trapping energy for Ti $E_{B,Ti} = 10kJ/mol$ delivers plausible recrystallization kinetics in comparison to independent experiments.

The parameters for the development of the dislocation density (*A, B, C*) can be determined using experimentally observed flow curves. The Taylor approach can be used to model the proportion of strength through dislocation hardening together with the dislocation evolution equation presented in chapter 4.2. Figure 8 shows simulated flow curves (only the dislocation density fraction) and the corresponding dislocation densities for different Al-Mg alloys at room temperature.
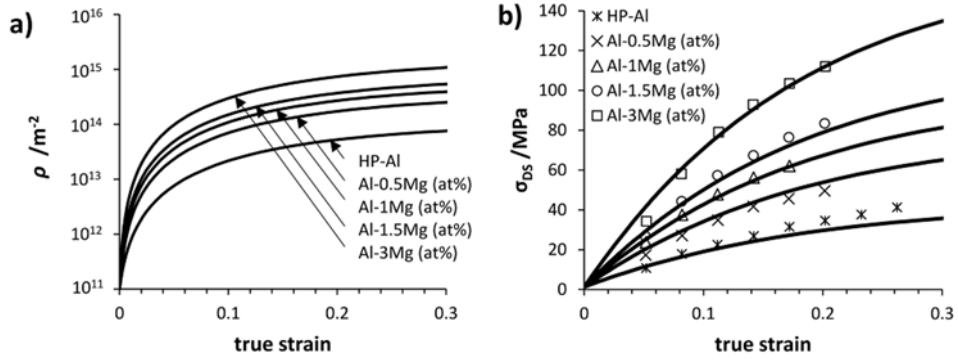
Figure 8: a) simulated dislocation densities b) corresponding flow curves for different Al-Mg alloys [53]

The presented (most important) input parameter for microalloyed austenite and Al-Mg alloys are summarized in Table 1 and Table 2.

Table 1: Parameters for recrystallization of Al- alloys

Symbol	Value	Unit	Ref.
D_B	$1.4 \times 10^{-5} \exp(-127200/RT)$	m²/s	[17]
D_{Dis}	$1.5 \times 10^{-6} \exp(-83200/RT)$	m²/s	[17]
D_{GB}	$2.0 \times 10^{-5} \exp(-60200/RT)$	m²/s	[17]
D_{CB}	$2D_B$	m²/s	[7,42]
$A; B; C$	-16,6 $\ln(C_{Mg})$+44.6; 2; 4×10^{-5}	-	[56]
K_{Sim}	A	-	[32]
$E_{B,Mg}$	5000	J/mol	[4]
$C_{GB,Mg}$	C_{Mg}	mol/ mol	[7,42]
γ_{HB}	$0.65-0.0005 \times T[K]$	J/m³	[53]
γ_{LB}	$0.5\gamma_{HB}$	J/m³	[32]
ω	10^{-9}	m	[32,52]
δ	$50b$	m	[53]
θ_{mean}	3°	-	[42]
$\eta_{free,HB}$	0.4	-	[4]

Table 2:   Parameters for recrystallization of microalloyed steel

Symbol	Value	Unit	Ref.
D_B	7.0×10^{-5} exp(-286000/RT)	m²/s	[17]
D_{Dis}	4.5×10^{-5} exp(-185000/RT)	m²/s	[17]
D_{GB}	5.5×10^{-5} exp(-145000/RT)	m²/s	[17]
D_{CB}	$2D_B$	m²/s	[7,42]
$A;B;C$	50; 5; 5×10-5	-	[32]
K_{Sim}	A	-	[32]
$E_{B,Nb}$	20000	J/mol	[7]
$E_{B,Ti}$	10000	J/mol	
$E_{B,V}$	2500	J/mol	
$C_{GB,(Nb,Ti,V)}$	$C_{0,(Nb,Ti,V)}$	mol/mol	[7,42]
γ_{HB}	$1.3111 - 0.0005 \times T[K]$	J/m³	[57]
γ_{LB}	$0.5\gamma_{HB}$	J/m³	[32]
ω	10^{-9}	m	[32,52]
δ	$50b$	m	[53]
θ_{mean}	3°	-	[42]
$\eta_{free,HB}$	0.0075	-	[52]

The application of the model and the parameters presented above allows a prediction of the recrystallization behavior of **(i) microalloyed steel** and **(ii) Al-Mg alloys**.

(i)   Figure 9 shows the recrystallized fraction of three V micro-alloyed steels experimentally determined by Medina. The V content increases from alloy V1 to alloy V3, resulting in an increase in the driving force for precipitation formation and, thus also in the Zener pressure in comparison, which leads to a reduction in the recrystallization plateau and slows down recrystallization. Figure 10 shows the associated TTP diagrams, showing that the changed precipitation kinetics from alloy V1 to alloy V3 are largely responsible for the difference in recrystallization behavior.
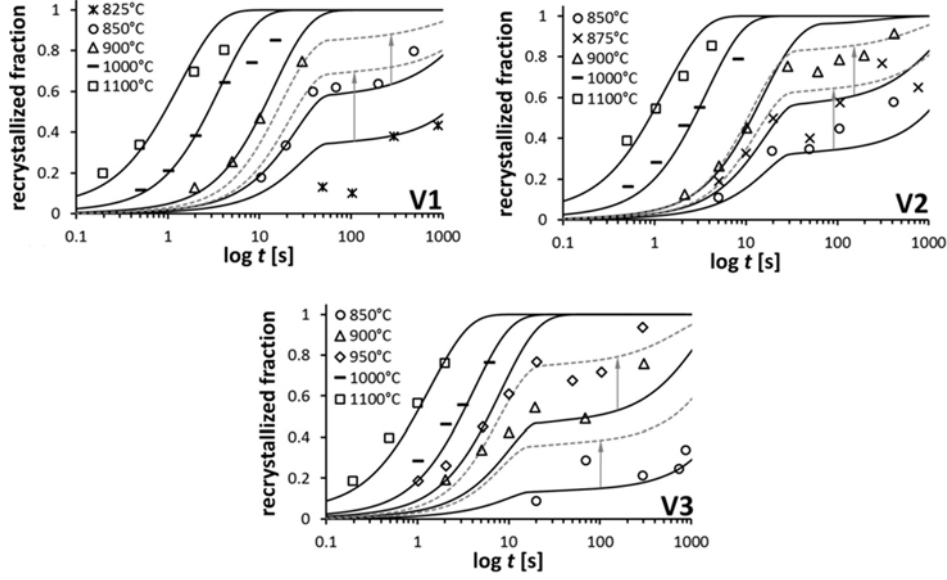
Figure 9: Simulated vs. experimentally observed recrystallization kinetics for three different V micro-alloyed steel [42]
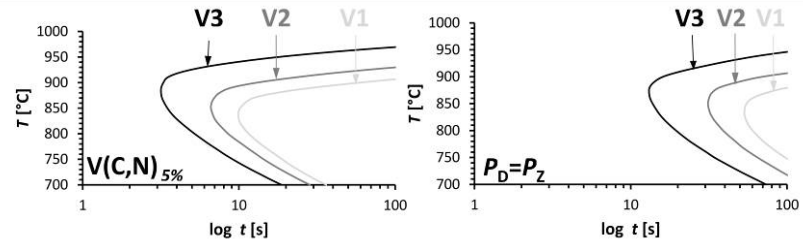
Figure 10: Simulated TTP diagrams for V(C,N) precipitation

(ii) Figure 11 shows the simulated recrystallization kinetics and experimentally determined data points of Koizumi et al. [58] on six different Al-Mg alloys with a tenfold increase in the Mg content. It is noticeable that the recrystallization rate decreases first and later increases with the increase in Mg content. This is due to two common effects: On the one hand, Mg increases the dislocation density, which occurs during the work hardening (see Figure 8) and, on the other hand, the grain boundary mobility is reduced by increasing solute drag effects (see Figure 7). Figure 12 underlines the recrystallization response of both effects in comparison to experimentally measured values.
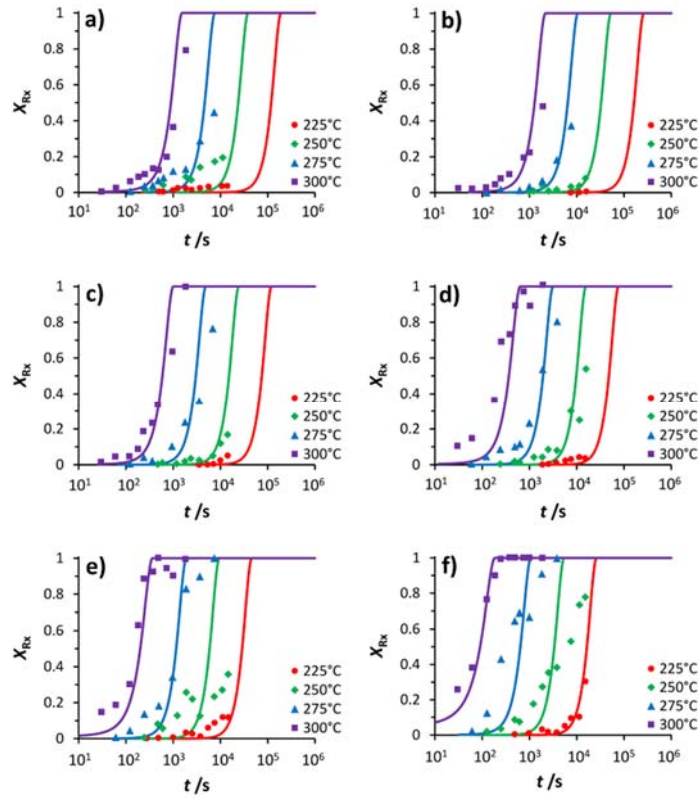
Figure 11: Calculated and experimental recrystallization kinetics at different temperatures for a) Al-0.5%Mg, b) Al-1%Mg, c) Al-2%Mg, d) Al-3%Mg, e) Al-4%Mg and f) Al-5%Mg [53]
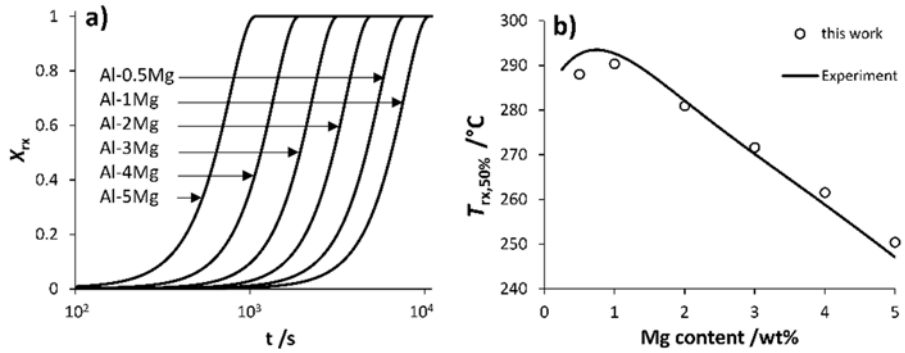
Figure 12: a) Simulated recrystallization kinetics at 275°C for all considered alloys. b) Simulated 50% recrystallization temperature (markers) and experimental data from ref. [58] (line).

5. Summary and Conclusion

As a result of this work, a new recrystallization model is presented, which describes recrystallization in terms of nucleation and growth on a physical basis. The nucleation is described by a distribution of subgrains, of which only those with a supercritical size nucleate. The growth of the nuclei is largely dependent on the dislocation density and grain boundary mobility. Models for both important influencing parameters are presented. The grain boundary mobilities are physically developed and include both the influences of solute drag and Zener drag. The latter can be calculated with the help of the precipitation development from the thermo-kinetic software tool MatCalc. To evaluate the quality of the overall model, input parameters for Al alloys and steel are calculated in a comprehensible way. The application of the model shows excellent agreement with experimental measurements within the material groups considered.

The present model is capable of reproducing many experiments of different materials with a consistent set of parameters. This is only possible until the limits of the model are reached. Thus, this dissertation does not describe how dynamic recrystallization is modeled. The forming of new nuclei in newly formed nuclei cannot be mapped within a "single-class" approach, as described in the present thesis. Nevertheless, with the help of this work, the important physical processes during recrystallization including traceable input variables (mobilities) and driving pressures can be revealed. A potential multi-class model, which has a larger range of application, should also have the mechanisms and input variables described in this thesis.

6. References

[1]   Carpenter H and Elam C 1920 Crystal growth and recrystallization in metals *J. Inst. Met.* **24** 83–154

[2]   Smith C S 1948 Introduction to Grains, Phases, and Interfaces—an Interpretation of Microstructure *Trans. AIME* **175** 15–51

[3]   Gómez M, Medina S F, Quispe a. and Valles P 2002 Static Recrystallization and Induced Precipitation in a Low Nb Microalloyed Steel. *ISIJ Int.* **42** 423–31

[4]   Huang Y and Humphreys F J 2012 The effect of solutes on grain boundary mobility during recrystallization and grain growth in some single-phase aluminium alloys *Mater. Chem. Phys.* **132** 166–74

[5]   Cahn J W 1962 The impurity drag effect in grain boundary motion *Acta Metall.* **10** 789–98

[6]   Medina S F and Mancilla J E 1996 Static recrystallization modelling of hot deformed microalloyed steels at temperatures below the critical temperature *ISIJ Int.* **36** 1077–83

[7]   Rehman M K and Zurob H S 2013 A novel approach to model static recrystallization of austenite during hot rolling of Nb microalloyed steel. Part I: Precipitate-free case *Metall. Mater. Trans. A Phys. Metall. Mater. Sci.* **44** 1862–71

[8]   Furu T, Marthinsen K and Nes E 1990 Modelling recrystallisation *Mater. Sci. Technol.* **6** 1093–102

[9]   Zurob H S, Hutchinson C R, Brechet Y and Purdy G 2002 Modelling recrystallization of microalloyed austenite: effect of coupling recovery, precipitation and recrystallization *Acta Mater.* **50** 3075–92

[10]   Kozeschnik E 2012 *Modeling Solid-State Precipitation* (New York: Momentum Press)

[11]   Svoboda J, Fischer F D, Fratzl P and Kozeschnik E 2004 Modelling of kinetics in multi-component multi- phase systems with spherical precipitates I: Theory *Mater. Sci. Eng. A* **385** 166–74

[12]   Zeldovich J B 1943 On the theory of new phase formation Cavitation *Acta Physicochim. E.R.SS* **18** 1–22

[13]   Russel K C 1980 Nucleation in solids: The induction ans steady state effects *Adv. Colloid Interface Sci.* **13** 205–318

[14]   Feder J, Russel C, Lothe J and Pound G M 1966 Homogeneous Nucleation and Growth of Droplets in Vapor *Adv. Phys.* **15** 111–78

[15]   Wakeshiima H 1954 Time Lag in Self- Nucleation *J. Chem. Phys.* **22** 1614–5

[16]   Kampmann R and Wagner R 1984 Decomposition of alloys: the early stages *Acta Scr. Met. Ser.* 91–103

[17]   Stechauner G and Kozeschnik E 2014 Assessment of substitutional self-diffusion along short-circuit paths in Al, Fe and Ni *Calphad* **47** 92–9

[18]   Sonderegger B and Kozeschnik E 2009 Generalized Nearest-Neighbor Broken-Bond Analysis of Randomly Oriented Coherent Interfaces in Multicomponent Fcc and Bcc Structures *Metall. Mater. Trans. A* **40** 499–510

[19]   Sonderegger B and Kozeschnik E 2009 Size dependence of the interfacial energy in the generalized nearest-neighbor broken-bond approach *Scr. Mater.* **60** 635–8

[20]   Sonderegger B and Kozeschnik E 2010 Interfacial Energy of Diffuse Phase Boundaries in the Generalized Broken-Bond Approach *Metall. Mater. Trans. A* **41** 3262–9

[21]   Anderson W A and Mehl R F 1945 Recrystallization of Aluminium in terms of the rate of nucleation and the rate of growth 140–72

[22]   Bailey J E and Hirsch P B 1962 The Recrystallization Process in Some Polycrystalline Metals *Proc. R. Soc. A Math. Phys. Eng. Sci.* **267** 11–30

[23]   Zurob H S, Bréchet Y and Dunlop J 2006 Quantitative criterion for recrystallization nucleation in single-phase alloys: Prediction of critical strains and incubation times *Acta Mater.* **54** 3983–90

[24]   Pantleon W and Hansen N 2001 Dislocation boundaries—the distribution function of disorientation angles *Acta Mater.* **49** 1479–93

[25]   Zhu Q, Sellars C M and Bhadeshia H K D H 2007 Quantitative metallography of deformed grains *Mater. Sci. Technol.* **23** 757–66

[26]   Nes E 1997 Modelling of work hardening and stress saturation in FCC metals *Prog. Mater. Sci.* **41** 129–93

[27]   Estrin Y ., Tóth L S ., Molinari A . and Bréchet Y . 1998 A dislocation-based model for all hardening stages in large strain deformation *Acta Mater.* **46** 5509–22

[28]   Ørsund R and Nes E 1989 Subgrain growth during annealing of heavily deformed metals *Scr. Metall.* **23** 1187–92

[29]   Sandström R 1977 Subgrain Growth Occuring by Boundary Migration *Acta Mater.* **25** 905–11

[30]   Huang Y and Humphreys F J 2000 Subgrain Growth and Low Angle Boundary **48** 2017–30

[31]   Bréchet Y J M, Zurob H S and Hutchinson C R 2009 On the effect of pre-recovery on subsequent recrystallization *Int. J. Mater. Res.* **100** 1446–8

[32]   Buken H, Sherstnev P and Kozeschnik E 2016 A state parameter-based model for static recrystallization interacting with precipitation *Model. Simul. Mater. Sci. Eng.* **24** 35006

[33]   Turnbull D 1951 Theory of Grain Boundary Migration Rates *JOM* **3** 661–5

[34]   Vandermeer R A and Hu H 1994 On the grain growth exponent of pure iron **42** 3071–5

[35]   Rollet A D, Gottstein G, Shvindlerman L S and Molodov D A 2004 Grain boundary mobility- a brief review *Zeitschrift für Met.* **95** 226–9

[36]   Humphreys F J 1997 A unified theory of recovery, recrystallization and grain growth, based on the stability and growth of cellular microstructures—I. The basic model *Acta Mater.* **45** 4231–40

[37]   Crooks M J, Garrat-Reed A J, Vander Sande J B and Owen W S 1981 Precipitation and recrystallization in some Vanadium and Vandium- Niobium microalloyed steels *Metall. Mater. Trans. A* **12A** 1999–2012

[38]   Medina S F and Mancilla J E 1996 Static recrystallization modelling of hot deformed steels containing several alloying elements *ISIJ Int.* **36** 1070–6

[39]   Abad R, Fernández a. I, López B and Rodriguez-Ibabe J M 2001 Interaction between Recrystallization and Precipitation during Multipass Rolling in a Low Carbon Niobium Microalloyed Steel. *ISIJ Int.* **41** 1373–82

[40]   Svoboda J, Fischer F D and Leindl M 2011 Transient solute drag in migrating grain boundaries *Acta Mater.* **59** 6556–62

[41]   Cram D G, Fang X Y, Zurob H S, Bréchet Y J M and Hutchinson C R 2012 The effect of solute on discontinuous dynamic recrystallization *Acta Mater.* **60** 6390–404

[42]   Buken H and Kozeschnik E 2017 A Model for Static Recrystallization with Simultaneous Precipitation and Solute Drag *Metall. Mater. Trans. A Phys. Metall. Mater. Sci.* **48** 2812–8

[43]   Kirchner H O K 1971 Coarsening of grain-boundary precipitates *Metall. Trans.* **2** 2861–4

[44] Winning M, Rollett A D, Gottstein G, Srolovitz D J, Lim A and Shvindlerman L S 2010 Mobility of low-angle grain boundaries in pure metals *Philos. Mag.* **90** 3107–28

[45] Sandstrom R 1977 Subgrain Growth Occuring by Boundary Migration *Acta Metall.* **25** 905–11

[46] Rehman K and Zurob H S 2013 Novel Approach to Model Static Recrystallization of Austenite during Hot-Rolling of Nb-Microalloyed Steel: Effect of Precipitates *Mater. Sci. Forum* **753** 417–22

[47] Jones A R and Hansen N 1981 The interaction between particles and low angle boundaries during recovery of aluminium-alumina alloys *Acta Metall.* **29** 589–99

[48] Kocks U F and Mecking H 2003 Physics and phenomenology of strain hardening: The FCC case *Prog. Mater. Sci.* **48** 171–273

[49] Sherstnev P, Lang P and Kozeschnik E 2012 Treatment of Simultaneous Deformation and Solid- State Precipitation in Thermo-Kinetic Calculations *European Congress on Computational Methods in Applied Sciences and Engineering*

[50] Read W T and Shockley W 1950 Dislocation Models of Crystal Grain Boundaries *Phys. Rev.* **78** 275–89

[51] Hillert M 1965 On the theory of normal and abnormal grain growth *Acta Metall.* **13** 227–38

[52] Zhou T, O'Malley R J and Zurob H S 2010 Study of grain-growth kinetics in delta-ferrite and austenite with application to thin-slab cast direct-rolling microalloyed steels *Metall. Mater. Trans. A Phys. Metall. Mater. Sci.* **41** 2112–20

[53] Buken H and Kozeschnik E 2018 Modelling static recrystallization in Al-Mg alloys *Acta Mater.* **(in Print)**

[54] Andrade H L, Akben M G and Jonas J J 1983 Effect of molybdenum, niobium, and vanadium on static recovery and recrystallization and on solute strengthening in microalloyed steels *Metall. Trans. A* **14** 1967–77

[55] Buken H, Zamberger S, Kozeschnik E and Kozeschnik E 2016 A Model for the Influence Of Micro-Alloying Elements on Static Recrystallization of Austenite *Proceedings of the 6th International Conference on Recrystallization and Grain Growth (ReX&GG 2016)* (Hoboken, NJ, USA: John Wiley & Sons, Inc.) pp 113–8

[56]   Sherby O D, Anderson R A and Dorn J E 1951 Effect of Alloying Elements on the Elevated Temperature Plastic Properties of Alpha Solid Solutions of Aluminum *JOM* **3** 643–52

[57]   Zurob H S, Brechet Y and Purdy G 2001 A model for the competition of precipitation and recrystallization *Acta Mater.* **49** 4183–90

[58]   Koizumi M, Kohara S and Inagaki H 2000 Kinetics of recrystallization in Al- Mg alloys *Zeitschrift für Met.* **91** 460–7

Section B

Paper I

Modelling static recrystallization in Al-Mg alloys

Heinrich Buken and Ernst Kozeschnik

Modelling static recrystallization in Al-Mg alloys

Heinrich Buken[a,b] and Ernst Kozeschnik[a,b]

[a] Institute of Materials Science and Technology, TU Wien, Getreidemarkt 9, 1060 Vienna, Austria
[b] MatCalc Engineering GmbH, Getreidemarkt 9, 1060 Vienna, Austria

In the present work, the influence of Mg on recrystallization kinetics in Al is analyzed by computer simulation. A comprehensive state parameter-based microstructure model is developed, which describes recrystallization in terms of nucleation and growth. The mechanism of solute drag is fully incorporated, thus accounting for the decrease of grain boundary mobility in the presence of impurity atoms. On basis of the present approach, the solute binding energy between Mg atoms and grain boundaries is assessed and compared to experimentally measured values. Furthermore, the influence of Mg on dislocation production during strain hardening is modeled. The simulations of the composition and temperature-dependent recrystallization kinetics are verified on experimental studies where excellent agreement is achieved. Both, simulation and experiment show that increasing Mg content first decelerates and, later on, accelerates recrystallization kinetics.

Keywords: Recrystallization; Solute Drag; Microstructure Evolution; Strain hardening

Introduction

The proper control of microstructure evolution during processing of Mg-based aluminium alloys is a key factor for determining the final mechanical-technological properties of the material. Mg is a widely used element in Al-alloys, especially in the 5xxx and 6xxx series. On one hand, Mg segregates into grain boundaries and reduces the mobility of the moving boundary by several orders of magnitude in comparison to pure Al [1]. This so-called solute drag effect [2] is caused by solute atoms being dragged along with the moving grain boundary, thus excerting a restraining force against the movement of the grain boundary. As a result, microstructural processes involving the motion of high angle grain boundaries (HAGB) and low angle grain boundaries (LAGB) can be severely slowed down by the presence of impurity atoms [1,3]. On the other hand, an increased Mg content

promotes a higher strain-hardening rate, which, at identical strain, induces a higher dislocation density [4,5]. As a result, the driving pressure for recrystallization increases, thus accellerating the observed recrystallization kinetics. Koizumi et al. [6] have performed recrystallization experiments in Al-Mg alloys, observing that an increase of the Mg content first leads to a deceleration of the rate of recrystallization, followed by an acceleration at further increasing Mg content. These results will form the basis of experimental verification of the present model.

In literature, several approaches are available describing recrystallization phenomena in metallic materials. With particular focus on Al alloys, earlier models [7,8] mostly utilize JMAK-based equations [9] for describing the kinetics of static recrystallization. In these models, several semi-empirical parameters are commonly utilized to adjust the simulated recrystallizing kinetics to experimentally measured recrystallized fractions. Since JMAK-based models do not incorporate explicit mechanism-based descriptions for nucleation and growth of recrystallizing grains, they can only take limited account of basic physical phenomena, such as, the solute drag effect, precipitate-dislocation interactions in precipitation hardening alloys or the influence of impurities on dislocation generation during strain hardening.

Recently, Zurob et al. [10,11] presented a physically-based model describing recrystallization with explicit expressions for nucleation and growth. In their work, the nucleation rate for recrystallization is evaluated from microstructural state parameters, such as, the subgrain size and the dislocation density, which, in combination with growth equations, delivers information on the recrystallized fraction within the deformed microstructure. The solute drag impact is included in the grain boundary mobility within the Cahn approach [2]. When applying the model to Al, however, Zurob et al. [10] utilized experimentally determined mobilities taken from literature instead of calculating composition-dependent mobilities based on physical relationships. Furthermore, this work does not take into account that the alloy composition has an important impact on the dislocation evolution during and after deformation. Consequently, no variation in the alloy composition of various Al alloys is elaborated in this work and recrystallization kinetics is evaluated only for a single Mg content of 1 wt%.

In the present work, we develop a state parameter-based model in which all relevant microstructural parameters are numerically integrated forward in time. The evolution equations incorporate full composition and temperature dependence for grain boundary mobilities as well as dislocation generation during strain hardening. The

calculated grain boundary mobilities are compared to experimentally measured values to illustrate the predictive potential of our mobility approach. In addition, we develop relations by which we describe the driving pressure for recrystallization as a function of the Mg content through a composition-dependent dislocation generation term. The predictions of our recrystallization model are finally compared with experimentally measured values from literature. The entire model and input parameters are explained in detail subsequently.

The recrystallization model

2.1 Nucleation and growth

The nucleation rate of newly formed recrystallized grains, $\dot{N}_{rx}$, is formulated as the product of the number density of potential nucleation sites, N_{pot}, a site saturation factor, B_{nuc}, which accounts for the grain area that is already covered by recrystallized grains and which is, therefore, no longer available for further nucleation, as well as the flux of subgrains reaching supercritical size, $\dot{F}_{sub}$, as

$$\dot{N}_{rx} = N_{pot} B_{nuc} \dot{F}_{sub} \cdot \qquad (1)$$

Bailey and Hirsch [12] suggested that the main nucleation mechanism for recrystallization is given by the process of strain-induced boundary migration. This process is initiated when a subgrain being in contact with a high-angle grain boundary (HAGB) exceeds a critical size, r_{crit}, determined by the quotient of the surface energy of the HAGB , γ_{HB}, and the driving pressure, P_D, as determined by the total dislocation density, ρ, with

$$r_{crit}(t) = \frac{2\gamma_{HB}}{P_D(t)} = \frac{2\gamma_{HB}}{0.5Gb\rho(t)}, \qquad (2)$$

with the shear modulus, G, the Burgers vector, b, and r denoting the radius of the subgrain. The number density of potential nucleation sites can be calculated from the quotient of the specific grain boundary area, a_{av}, per unit volume of material and the area covered by a single supercritical subgrain being located at the high angle grain boundary. The former is influenced by the degree of deformation of the grain, where the surface area increases with increasing strain. We map this process into our simulations using the analysis of Zhou et al. [13] who described the evolution of surface area of the grains during deformation in the form of a function, f, depending on the deformation strain, ε

. This function represents the ratio of the specific surface area of the deformed grain compared to that of the undeformed grain. The total number of potential nucleation sites, N_{pot}, then reads

$$N_{pot} = \frac{a_{av}}{\pi r_{crit}^2} f(\varepsilon). \tag{3}$$

To calculate the specific grain boundary area of one individual undeformed grain, we assume the grain to have the shape of a truncated octahedron (tetrakaidecahedron). The total available grain boundary area of all deformed grains can be formulated in dependence of the mean grain radius, R, the number density of the original grains, N_0, and the surface area of one grain, S_{HAG}, as

$$a_{av} = 0.5 N_0 S_{HAG} = 0.5\left(\frac{1}{8\sqrt{2}(1.5R)^3}\right)\left((6 + 12\sqrt{3})(1.5R)^2\right). \tag{4}$$

With the continuous production of new recrystallization nuclei, the deformed grain boundary surface continues to become occupied leading to a continuous decrease of the nucleation rate. In a first approximation, the following term is utilized to take this effect into account:

$$B_{Nuc} = 1 - \frac{N_{rx}\pi(r_{crit})^2}{a_{av}} . \tag{5}$$

To describe the distribution of subgrain sizes, we utilize a Rayleigh distribution as experimentally observed by Pantleon and Hansen [14] and also used in the model of Rehman and Zurob [11]. The fraction of subgrains, which are larger than the critical size, can then be expressed as

$$F_{sub}(t) = \exp\left(-\frac{\pi}{4}X_{crit}^2(t)\right), \tag{6}$$

where X_{crit} is the critical subgrain size normalized with respect to the mean subgrain size. The fraction of subgrains, which become supercritical and serve as new stable recrystallization nuclei, is found after differentiation with respect to time as

$$\dot{F}_{sub} = -\frac{1}{2}\pi F(t) X_{crit} \dot{X}_{crit}. \tag{7}$$

The normalized critical subgrain size and its derivative, $\dot{X}_{crit}$, are calculated in dependence of the actual mean subgrain size, r_{mean}, and the critical subgrain size, as

$$X_{crit}(t) = \frac{r_{crit}(t)}{r_{mean}(t)} \tag{8}$$

and

$$\dot{X}_{\text{Crit}} = \frac{\dot{r}_{\text{crit}}}{r_{\text{mean}}} - \frac{r_{\text{crit}}\dot{r}_{\text{mean}}}{r_{\text{mean}}^2} \, . \qquad\qquad (9)$$

Successfully nucleated recrystallized grains grow into the deformed grains by dissipation of the stored deformation energy. We model this process by formulating a growth rate, $\dot{R}_{\text{rx}}$, as the product of a driving pressure, P_{D}, (identical to the one in eq. (2)) and an effective high-angle grain boundary mobility, $M_{\text{eff, HB}}$, [15] with

$$\dot{R}_{\text{rx}} = M_{\text{eff, HB}} P_{\text{D}} (1 - X_{\text{rx}}) \, . \qquad\qquad (10)$$

The growth rate is scaled with the recrystallized volume fraction, X_{rx}, in order to account for hard impingement of the recrystallized grains.

Since the driving pressure for nucelation and growth of recrystallized grains is provided by the stored deformation energy, i.e., the dislocation density, this quantity and its evolution as function of temperature, strain rate and chemical composition of the alloy play a central role in modeling recrystallization kinetics. This is equally true for the growth rate of recrystallized grains, eq. (10), as well as the nucleation rate as defined in eqs. (1) and (2). Consequently, particular emphasis of the present work has been directed into accurate modeling of this microstructural state parameter.

The evolution of the dislocation density is described by means of an extended Kocks-Mecking model [16] considering the processes of dislocation generation as well as dynamic and static recovery. In this context, we closely follow the approach introduced by Sherstnev et al. [17], describing the rate of the total dislocation density evolution as

$$\dot{\rho} = \frac{M\sqrt{\rho}}{Ab}\dot{\varepsilon} - 2B\frac{d_{\text{ann}}}{b}\rho \, M\dot{\varepsilon} - 2CD_{\text{Dis}}\frac{Gb^3}{k_B T}(\rho^2 - \rho_{\text{RS}}^2), \qquad\qquad (11)$$

with the Taylor factor, M, the critical dislocation annihilation distance, d_{ann}, the substitutional self-diffusion coefficient at dislocations, D_{Dis}, the strain rate, $\dot{\varepsilon}$, and material-dependent coefficients A, B, C. In contrast to the original Sherstnev et al. model, where the driving force for static recovery is given by the difference of actual and equilibrium dislocation density, we introduce a limiting degree of static recovery, here, given by the amount of geometrically necessary dislocations, ρ_{RS}, for maintaining the subgrain microstructure. In the Read-Shockley model [18], the mean subgrain misorientation angle, θ_{mean}, and the mean subgrain size in a periodic network of subgrains define the geometrically necessary dislocation density as

$$\rho_{RS} = \frac{\tan(\theta_{mean})}{br_{mean}}.$$
(12)

Finally, the individual pieces of information about nucleation density and growth rate can be combined to calculate the increase of the recrystallized volume fraction as

$$\dot{X}_{rx} = 27\sqrt{2}\left(R_{rx}^3 \dot{N}_{rx} + 3N_{rx}R_{rx}^2 \dot{R}_{rx}\right) = \frac{\dot{V}_{rx}}{V_{tot}}.$$
(13)

In evaluation of the grain volume of all recrystallized grains in the matrix, V_{rx}, we again assume that the grain geometry can be approximated by a truncated octahedron. Since the model refers to unit volume of material, the total volume, V_{tot}, is 1m³.

A major advantage of the present nucleation model is that it avoids the (extensive) use of fitting paramters in the form of activation energies. Instead, the essential temperature and composition-dependencies of the nucleation rate, eq. (1), are incorporated within the evolution equations for the mean subgrain size, r_{mean}, as well as the composition and temperature-dependent evolution of the critical nucleation radius, r_{crit}, eq. (2), which in turn is determined by the dislocation density evolution, eq. (11). The composition and temperature-dependency of the growth rate is also inherently incorporated in the high-angle grain boundary mobility, $M_{eff,HB}$, as well as the driving pressure, P_D. As a result, the present model utilizes only a minimum number of undetermined input parameters with most of the temperature dependence of physical quantities already being determined by the temperature dependence of independently measured quantities, such as the bulk and grain boundary self-diffusion coefficients as well as solute drag binding energies as obtained from application of the corresponding Cahn model [2].

2.2 Subgrain evolution

As emphasized in the previous section, the nucleation rate for recrystallization is substantially determined by the evolution of the mean subgrain size in relation to the critical subgrain size for recrystallization nuclei. In the present approach, the evolution of mean subgrain size is formulated in differential form as superposition of a shrinkage term, $\dot{r}_S^-$, and a growth term, $\dot{r}_G^+$, with

$$\dot{r}_{mean} = \dot{r}_S^- + \dot{r}_G^+$$
(14)

A convenient parameterization of this general equation can be achieved with application of (i) the "principle of similutude", as introduced by Estrin [19] and Nes [20] and (ii) the driving force – mobility concept, as already used to describe the growth rate of recrystallizing grains, eq. (10). The former relates the mean subgrain size with the average dislocation density in the deformed material and can be written in differential form as

$$\dot{r}_s^- = \frac{\partial}{\partial t}\left(\frac{K_{Sim}}{\sqrt{\rho(t)}}\right).$$ (15)

In this (empirical) expression, K_{sim} represents a material-dependent shrinkage coefficient for the effect of dislocation storage on subgrain size evolution. Application of this relation has been investigated by Gil Sevillano [21] in several different groups of materials, where the viability of the principle of similitude has been confirmed repeatedly.

In an investigation of the evolution of subgrains during annealing, Sandstrom [3] observed that the rate of subgrain growth is inversely proportional to the current subgrain size. Based on this work, Orsund and Nes [22] described the growth of subgrains in terms of mobility and driving pressure. Later, Huang and Humphreys [23] experimentally investigated subgrain growth in pure Al and also successfully applied a model that describes the growth rate via mobilities and driving pressures. We adopt this approach, here, for the subgrain growth rate as

$$\dot{r}_G^+ = M_{eff,LB}P_{D,SGG},$$ (16)

with the effective LAGB mobility, $M_{eff,LB}$, and the driving pressure for subgrain growth, $P_{D,SGG}$.

In conventional approaches to subgrain growth (e.g., refs. [3,22,23]), usually, only the interface curvature-dependent contribution to the driving pressure is considered. In a recent work, Brechet et al. [24] extend this approach and formulate an additional restraining pressure generated by the intrinsic dislocation density. The integral driving pressure for subgrain growth then reads

$$P_{D,SGG} = \frac{2\gamma_{LB}}{r_{mean}} - \frac{Gb^2}{\sqrt{2\delta r_{mean}}}\sqrt{\rho_{int}},$$ (17)

with the subgrain boundary energy, γ_{LB}, the interaction width of the LAGB, δ, and the internal dislocation density, $\rho_{int} = \rho - \rho_{RS}$, describing the statistically distributed dislocations.

The subgrain boundary mobility, eq. (22) later, incorporates the temperature-dependence of the subgrain growth rate as well as the impact of impurity atoms, i.e. the solute drag effect. The parameterization of this quantity is outlined in the following section.

2.2 Boundary mobility

The grain and subgrain boundary mobilities are most important input parameters determining the recrystallization kinetics. To model the HAGB mobility, we use the same approach that has recently been successfully applied to recrystallization kinetics simulations in micro-alloyed steel [25] with

$$M_{\text{eff,HB}} = \left(\frac{1}{M_{\text{free,HB}}} + \frac{1}{M_{\text{SD}}} \right)^{-1} , \qquad (18)$$

where $M_{\text{free,HB}}$ is the mobility of the free undisturbed boundary and M_{SD} is the solute drag-affected mobility capturing the influence of impurity atoms. The former can be calculated from the work of Turnbull [26] as

$$M_{\text{free;HB}} = \eta_{\text{free,HB}} \cdot M_{\text{TB}} = \eta_{\text{free,HB}} \cdot \frac{\omega D_{\text{GB}} V_{\text{m}}}{b^2 RT} , \qquad (19)$$

with the efficiency factor, $\eta_{\text{free, HB}}$, the grain boundary width, ω, the grain boundary self-diffusion coefficient, D_{GB}, the molar volume, V_{m}, the ideal gas constant, R, and the temperature, T. The diffusion coefficient along grain boundaries has been independently assessed recently by Stechauner and Kozeschnik [27] and their values are adopted, here. The efficiency factor for the free mobility is adjusted to the experimental data of [1] and delivers good results for $\eta_{\text{free}} = 0.4$.

The effect of solute drag is accounted for on basis of the classical Cahn approach [2], where the solute drag mobility, M_{SD}, is inversely proportional to the concentration of impurity atoms in the grain boundary, C_{GB}, and an inverse mobility, α, as

$$M_{\text{eff,LB}} = \left(\frac{M_{\text{eff,HB}}}{M_{\text{free,HB}}} \right) M_{\text{free;LB}} \qquad (20)$$

where E_{B}, is the interaction energy between the solute drag-exerting element and the grain boundary and D_{CB} is the diffusion coefficient across the grain boundary. The concentration of Mg in the HAGB is assumed to be identical to the matrix concentration [11,25]. If the Mg content in the alloy increases, the grain boundary mobility decreases due to the increasing amount of atoms that must be dragged along with the moving

boundary. In the limit of zero Mg, the calculated integral mobility approximates the free mobility since the solute drag mobility approaches infinity. Figure 1 compares the calculated grain boundary mobilities to experimental data, where fair agreement is achieved.
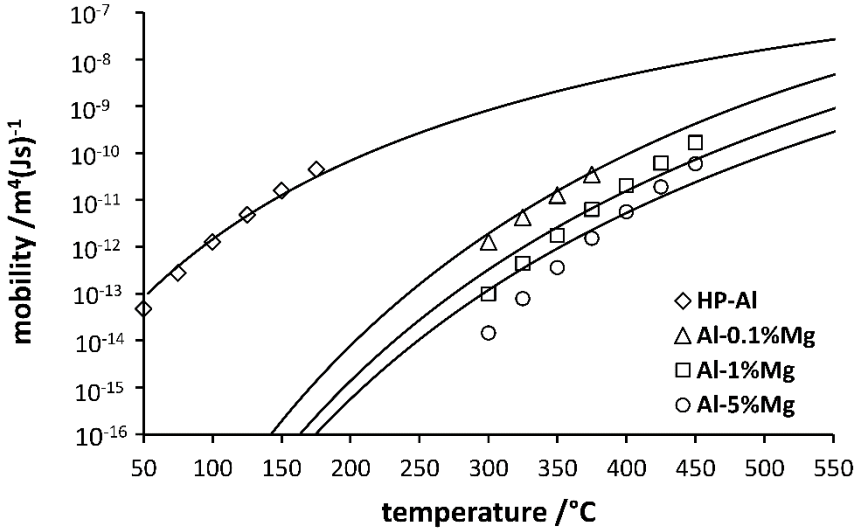

Figure 1: Calculated (solid lines) and experimental grain boundary mobility for Al-5%Mg, Al-1%Mg, Al-0,1Mg% and high purity-Al (from Ref [1]) at different temperatures.

Sandstrom [3] and Winning et al. [28] suggest that dislocation climb provides a viable mechanism for subgrain boundary movement. On this basis, Sandstrom [3], formulates a mobility approach where the subgrain boundary mobility, M_{SS}, is mainly a function of the bulk diffusion coefficient, D_B, which is applicable to pure alloys. We introduce a temperature-independent linear prefactor, $\eta_{free,LB}$, which determines the value of the effective free boundary mobility as

$$M_{free;LB} = \eta_{free,LB} \cdot M_{SS} = \eta_{free,LB} \cdot \frac{D_B b^2}{k_B T} \qquad (21)$$

with the Boltzmann constant, k_B. In their simulations, Rehman and Zurob [11,29] observe that the growth rate of subgrains is slowed down by dissolved atoms. Therefore, they introduce a model that correlates the rate of subgrain growth with the mean distance of solute atoms. Unfortunately, a separate parameter must be defined for each type of solute and obstacle, which is somehow decoupled from the parameters of the remaining simulation structure.

In contrast to the Rehman and Zurob approach, we interpret the influence of solute atoms on subgrain growth again as somehow proportional to the effect of solutes on grain boundary movement as delivered by the Cahn model [2]. Although not directly derived here on a physical basis, a subgrain boundary retardation factor is introduced, which is derived from the ratio of free and solute drag mobilities of the high-angle grain boundaries as

$$M_{eff,LB} = \left(\frac{M_{eff,HB}}{M_{free,HB}} \right) M_{free,LB} \qquad\qquad (\; 21 \;)$$

The major advantage of this approach is the fact that no additional independent calibration parameters must be introduced for the subgrain boundary mobility. The temperature-dependence of the mobility is determined by the model of Sandstrom [3], whereas the composition-dependence of the subgrain boundary mobility is related to that of the high-angle grain boundary.

2.3 Verification experiments

To verify the simulation, we analyze the work of Koizumi et al. [6] who experimentally investigate the recrystallization kinetics of five different Al-alloys with Mg matrix concentrations, C_{Mg}, of 0.5 wt%, 1 wt%, 2 wt%, 3 wt%, 4 wt% and 5 wt%. In their analysis, they first cast the alloys and measured a grain size of 300μm after pre-annealing at 450°C for 7 hours. Subsequently, cold reduction with a total strain of 0.95 is applied and the specimens are finally tempered at temperatures of 225, 250, 275 and 300°C. During tempering, the specimens are periodically extracted from a salt bath and analyzed metallographically in order to obtain the recrystallized fraction evolution. Since the aim of the present investigation is to model the influence of temperature and composition (solute drag and dislocation evolution accompanying strain hardening) on recrystallization kinetics, we only vary parameters (temperature and composition), which are important to these effects.

2.4 Model input parameters

The bulk and grain boundary diffusion coefficients entering the present model are taken from a recent analysis by Stechauner and Kozeschnik [27]. These values mainly determine the temperature-dependence of the free boundary mobilities and the static recovery kinetics of dislocations and subgrain boundaries. For the HAGB-energy, a value of 0.65-0.0005·T[K] is assumed, which incorporates the temperature-dependence of the

shear modulus as reported in ref. [30]. The resulting specific HAGB energy spans a range of 0.35 J/m²- 0.4 J/m² for the considered testing temperatures from 225°C- 300°C, which is well in line with the grain boundary energy value suggested by Murr [31].

A similar Ansatz for determining the HAGB-energy was used by Zurob et al. [32] for austenite. The dislocation evolution parameters *A*, *B*, *C* are adjusted to the experimental flow curve measurements of Sherby et al. [4] by means of applying the Taylor equation [5] with a dislocation strengthening parameter of 0.2 [33]. Thereby, only the *A*-parameter is a function of the Mg-content in the system, capturing the influence of Mg on the dislocation evolution kinetics. Table 1 summarizes the input parameters for the simulation.

Table 1: List of simulation parameters

Symbol	Designation	Value	Unit	Ref.
D_{B}	Al bulk diffusion coefficient	$1.4 \cdot 10^{-5}$ exp(-127200/RT)	m²/s	[27]
D_{Dis}	dislocation pipe diffusion	$1.5 \cdot 10^{-6}$ exp(-83200/RT)	m²/s	[27]
D_{GB}	grain boundary diffusion	$2.0 \cdot 10^{-5}$ exp(-60200/RT)	m²/s	[27]
D_{CB}	cross boundary diffusion	$2D_{\mathrm{B}}$	m²/s	[11,25]
A, B, C	strengthening parameters	$-16{,}6 \cdot \ln(C_{\mathrm{Mg}})+44.6; 2; 4 \cdot 10^{-5}$	-	This work, [4]
K_{Sim}	Similitude parameter	A	-	[15]
E_{B}	binding energy	5000	J/mol	This work, [1]
$C_{\mathrm{GB, Mg}}$	HAGB-concentration of Mg	C_{Mg}	mol/mol	[11,25]
γ_{HB}	HAGB-energy	0.65-0.0005·T[K]	J/m³	This work
γ_{LB}	LAGB-energy	$0.5\gamma_{\mathrm{HB}}$	J/m³	[34]
ω	grain boundary width	10^{-9}	m	[15,35]
b	Burgers vector	$2.86 \cdot 10^{-10}$	m	[36]
δ	dislocation interaction width	$50\,b$	m	This work
G	shear modulus	29438.4-15.052T[K]	MPa	[30]
θ_{mean}	mean misorientation angle	3°	-	[37]

$\eta_{\text{free,HB}}$	HAGB-prefactor	0.4	-	[1]
$\eta_{\text{free,LB}}$	LAGB-prefactor	1	-	[38]
α_{Taylor}	strengthening coefficient	0.2	-	[33]

3. Results and discussion

In this section, the results of our simulation are compared with the experimental data of Koizumi et al. [6], who carried out recrystallization kinetics measurements on a series of Al-Mg alloys (see section 2.3). In the considered experiments, the recrystallized volume fraction is measured metallographically so that there is more confidence in the measured values than in strength relaxation-based methods, such as double-hit compression tests or hardness measurements [39]. The simulations are carried out with the thermokinetic software tool MatCalc, in which we use the identical set of input parameters (section 2.4) for each simulation (material and temperature variation). The results of our simulation in comparison to the experiments performed by Koizumi et al. [6] are shown in figure 1.
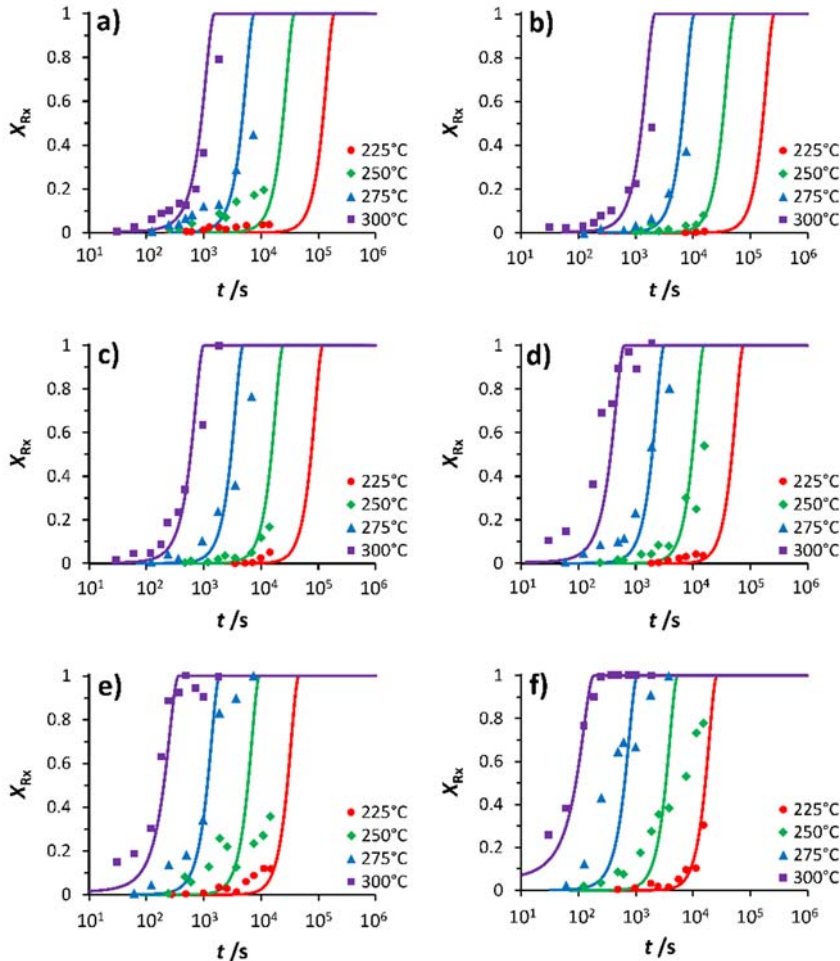

Figure 2: Calculated recrystallization kinetics at different temperatures for a) Al-0.5%Mg, b) Al-1%Mg, c) Al-2%Mg, d) Al-3%Mg, e) Al-4%Mg and f) Al-5%Mg

Koizumi et al. [6] observe approximately one order of magnitude difference in recrystallization time for each chemical composition of Al-Mg alloys, when the annealing

temperature increases by 25 K. The main reason for this behavior lies in the variation of grain boundary mobility, by which the temperature dependence of the growth rate is determined. The solute drag effect of Mg on grain boundary movement, as quantified in this work on the basis of the experiments of Huang and Humphreys [1] with a binding energy of 5 kJ / mol in the Cahn model [2], provides an additional important mechanism into the entire simulation model.

Fig. 2 demonstrates that our simulations fully reproduce the experimental observation that increasing Mg content first accelerates and then decelerates the rate of recrystallization, see Perryman [40]. A minimum of the recrystallization rate can be found in the Koizumi experiments [6] at a Mg content of approximately 1 wt%. This behavior can be described by the interplay of two mechanisms triggered by Mg atoms in the Al-matrix: On one hand, increasing Mg content decreases the grain boundary mobility due to the solute drag effect exerting a retarding pressure on the boundary during migration [2]. Consequently, this effect acts as a retarding process on recrystallization (Eq. 10). To quantify this mechanism, Fig. 1 displays the simulated boundary mobility for various concentrations of Mg in the matrix (section 2.2) compared to experimental data.

On the other hand, the dislocation evolution is heavily dependent on the Mg content. In a recent contribution, Muzyk et al. [41] pointed out that Mg has a strong influence on the stacking fault energy in Al-alloys. Kocks and Mecking [16] suggest that the strain hardening potential in materials should scale with the stacking fault energy. Thornten [42] describes that the change in stacking fault energy influences the cross-slip mechanism of dislocations at high temperatures and thus leads to a lower rate of dynamic recovery. In their recent analysis, Kreyca and Kozeschnik [43] show that both, the rate of dislocation generation and that of dislocation annihilation due to dynamic recovery, are influenced by the Mg content.

In our present simulation approach, we account for this aspect by adjusting the dislocation generation parameter, A, in dependence of the Mg-content as suggested by Kreyca and Kozeschnik [43] at room temperature. The calculated dislocation density evolution can then be compared to experimental stress-strain curves by applying the Taylor equation [5]. Thereby, the strain-induced dislocation strengthening contribution to the material, σ_{DS}, is expressed as

$$\sigma_{DS} = \sigma_0 + \alpha_{\text{Taylor}} MGb \sqrt{\rho} , \qquad (22)$$

where σ_0 is the basic yield strength containing solid solution and grain boundary hardening.

To apply the above formula, we use Eq. 11 together with the parameters *A, B, C* given in table 1. Unfortunately, Koizumi et al. [6] do not provide values for strengthening during cold deformation. Therefore, we compare with measurements of Sherby et al. [4], who analysed the flow behaviour of different Al-Mg alloys. Figure 3 shows our simulated flow curves and dislocation densities for high-purity Al, Al- 0.5%Mg, Al-1%Mg, Al-1.5%Mg and Al- 3%Mg, where excellent agreement is achieved.
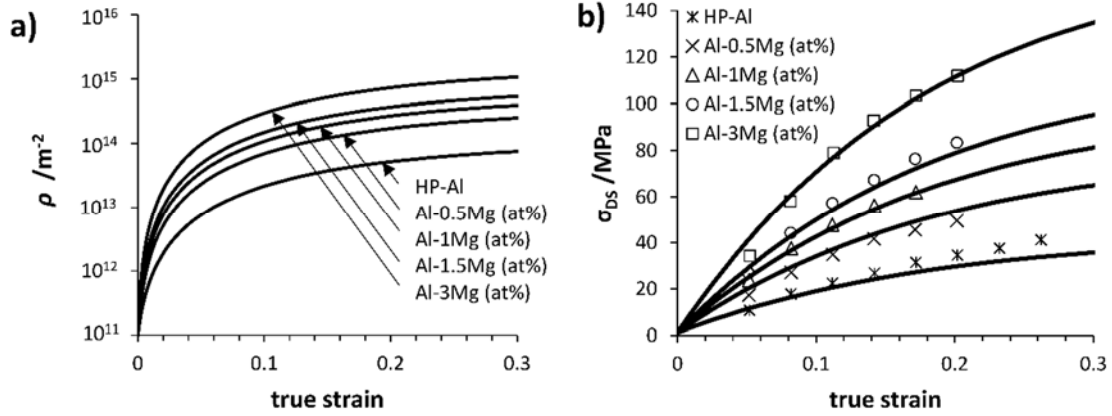

Figure 3:   a) dislocation generation in dependence of different Mg-contents (high purity-Al, Al- 0.5%Mg, Al-1%Mg, Al-1.5%Mg, Al- 3%Mg) at 25°C b) resulting dislocation strengthening contribution in comparison to experimental data of [4] at 25°C

The two mechanisms referenced above, solute drag and dislocation density evolution, severely interact in our simulation. As a consequence, the observed recrystallization kinetics can be likewise accelerated and decelerated, depending on the Mg content. Figure 4 summarizes the influence of the Mg content on recrystallization kinetics. In image 4a), the simulated recrystallized volume fractions at 275°C are compared, showing that the recrystallization kinetics are faster in Al-0.5%Mg compared to Al-1%Mg. A further increase in Mg always leads to an increase of the recrystallization kinetics. Diagram 4b) shows the simulated (markers) and measured (line) 50% recrystallization temperatures. Excellent agreement between the experimental observations and the simulations based on the present model is observed.
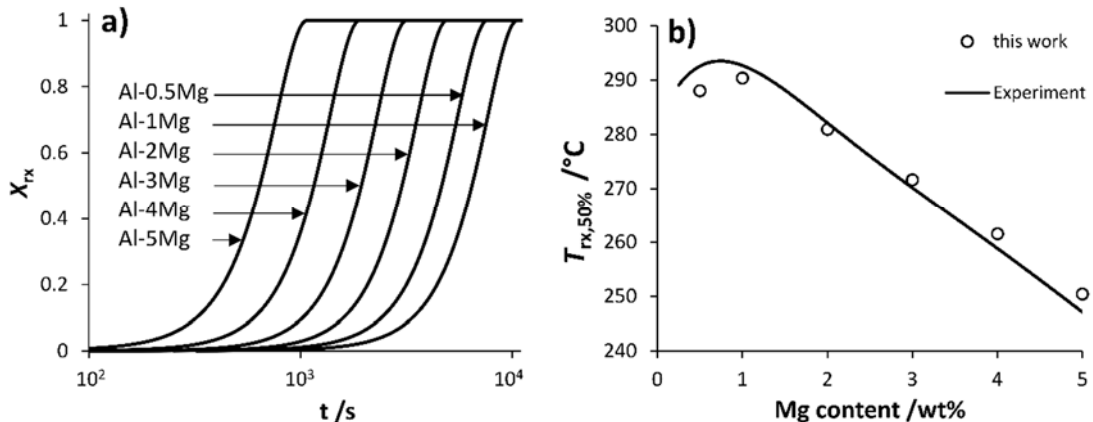
Figure 4:   a) simulated recrystallization kinetics at 275°C for all considered alloys. b) simulated 50% recrystallization temperature (markers) and experimental data from ref. [6] (line).

4. Summary

In the present work, we propose a comprehensive state parameter-based model for static recrystallization in terms of nucleation and growth of recrystallizing grains. Both, the HAGB mobilities and the dislocation densities are evolved on basis of physical evolution expressions and they are individually analyzed and compared to independent experiments. On one hand, the Mg content-dependent dislocation density evolution promotes recrystallization with increasing alloy content due to increased dislocation production. On the other hand, the solute drag effect retards recrystallization due to an increasingly retarding effect on boundary mobility. The mutual interplay of these effects can be observed in both the simulation and the experiment.

Bibliography

[1]   Y. Huang, F.J. Humphreys, The effect of solutes on grain boundary mobility during recrystallization and grain growth in some single-phase aluminium alloys, Mater. Chem. Phys. 132 (2012) 166–174. doi:10.1016/j.matchemphys.2011.11.018.

[2]   J.W. Cahn, The impurity drag effect in grain boundary motion, Acta Metall. 10 (1962) 789–798. doi:10.1016/0001-6160(62)90092-5.

[3]   R. Sandstrom, Subgrain Growth Occuring by Boundary Migration, Acta Metall. 25 (1977) 905–911. doi:10.1016/0001-6160(77)90177-8.

[4]   O.D. Sherby, R.A. Anderson, J.E. Dorn, Effect of Alloying Elements on the Elevated Temperature Plastic Properties of Alpha Solid Solutions of Aluminum,

JOM. 3 (1951) 643–652. doi:10.1007/BF03397360.

[5]   G.I. Taylor, The Mechanism of Plastic Deformation of Crystals. Part I. Theoretical, Proc. R. Soc. A Math. Phys. Eng. Sci. 145 (1934) 362–387. doi:10.1098/rspa.1934.0106.

[6]   M. Koizumi, S. Kohara, H. Inagaki, Kinetics of recrystallization in Al- Mg alloys, Zeitschrift Für Met. 91 (2000) 460–467.

[7]   F.J. Humphreys, A unified theory of recovery, recrystallization and grain growth, based on the stability and growth of cellular microstructures—I. The basic model, Acta Mater. 45 (1997) 4231–4240. doi:10.1016/S1359-6454(97)00070-0.

[8]   T. Furu, K. Marthinsen, E. Nes, Modelling recrystallisation, Mater. Sci. Technol. 6 (1990) 1093–1102. doi:10.1179/026708390790189957.

[9]   M. Avrami, Kinetics of Phase Change. II Transformation-Time Relations for Random Distribution of Nuclei, J. Chem. Phys. 8 (1940) 212–224. doi:10.1063/1.1750631.

[10]   H.S. Zurob, Y. Bréchet, J. Dunlop, Quantitative criterion for recrystallization nucleation in single-phase alloys: Prediction of critical strains and incubation times, Acta Mater. 54 (2006) 3983–3990. doi:10.1016/j.actamat.2006.04.028.

[11]   M.K. Rehman, H.S. Zurob, A novel approach to model static recrystallization of austenite during hot rolling of Nb microalloyed steel. Part I: Precipitate-free case, Metall. Mater. Trans. A Phys. Metall. Mater. Sci. 44 (2013) 1862–1871. doi:10.1007/s11661-012-1526-5.

[12]   J.E. Bailey, P.B. Hirsch, The Recrystallization Process in Some Polycrystalline Metals, Proc. R. Soc. A Math. Phys. Eng. Sci. 267 (1962) 11–30. doi:10.1098/rspa.1962.0080.

[13]   Q. Zhu, C.M. Sellars, H.K.D.H. Bhadeshia, Quantitative metallography of deformed grains, Mater. Sci. Technol. 23 (2007) 757–766. doi:10.1179/174328407X157308.

[14]   W. Pantleon, N. Hansen, Dislocation boundaries—the distribution function of disorientation angles, Acta Mater. 49 (2001) 1479–1493. doi:10.1016/S1359-6454(01)00027-1.

[15]   H. Buken, P. Sherstnev, E. Kozeschnik, A state parameter-based model for static recrystallization interacting with precipitation, Model. Simul. Mater. Sci. Eng. 24 (2016) 35006. doi:10.1088/0965-0393/24/3/035006.

[16]   U.F. Kocks, H. Mecking, Physics and phenomenology of strain hardening: The

FCC case, Prog. Mater. Sci. 48 (2003) 171–273. doi:10.1016/S0079-6425(02)00003-8.

[17] P. Sherstnev, P. Lang, E. Kozeschnik, Treatment of Simultaneous Deformation and Solid- State Precipitation in Thermo-Kinetic Calculations, in: Eur. Congr. Comput. Methods Appl. Sci. Eng., 2012.

[18] W.T. Read, W. Shockley, Dislocation Models of Crystal Grain Boundaries, Phys. Rev. 78 (1950) 275–289. doi:10.1103/PhysRev.78.275.

[19] Y.. Estrin, L.S.. Tóth, A.. Molinari, Y.. Bréchet, A dislocation-based model for all hardening stages in large strain deformation, Acta Mater. 46 (1998) 5509–5522. doi:10.1016/S1359-6454(98)00196-7.

[20] E. Nes, Modelling of work hardening and stress saturation in FCC metals, Prog. Mater. Sci. 41 (1997) 129–193. doi:10.1016/S0079-6425(97)00032-7.

[21] J. Gil Sevillano, P. Van Houtte, E. Aernoudt, Large strain work hardening and textures, Prog. Mater. Sci. 25 (1980) 69–412. doi:10.1016/0079-6425(80)90003-1.

[22] R. Ørsund, E. Nes, Subgrain growth during annealing of heavily deformed metals, Scr. Metall. 23 (1989) 1187–1192. doi:10.1016/0036-9748(89)90324-4.

[23] Y. Huang, F.J. Humphreys, Subgrain growth and low angle boundary mobility in aluminium crystals of orientation {110}|<001>, Acta Mater. 48 (2000) 2017–2030. doi:10.1016/S1359-6454(99)00418-8.

[24] Y.J.M. Bréchet, H.S. Zurob, C.R. Hutchinson, On the effect of pre-recovery on subsequent recrystallization, Int. J. Mater. Res. 100 (2009) 1446–1448. doi:10.3139/146.110194.

[25] H. Buken, E. Kozeschnik, A Model for Static Recrystallization with Simultaneous Precipitation and Solute Drag, Metall. Mater. Trans. A Phys. Metall. Mater. Sci. (2016) 1–7. doi:10.1007/s11661-016-3524-5.

[26] D. Turnbull, Theory of Grain Boundary Migration Rates, JOM. 3 (1951) 661–665. doi:10.1007/BF03397362.

[27] G. Stechauner, E. Kozeschnik, Assessment of substitutional self-diffusion along short-circuit paths in Al, Fe and Ni, Calphad. 47 (2014) 92–99. doi:10.1016/j.calphad.2014.06.008.

[28] M. Winning, A.D. Rollett, G. Gottstein, D.J. Srolovitz, A. Lim, L.S. Shvindlerman, Mobility of low-angle grain boundaries in pure metals, Philos. Mag. 90 (2010) 3107–3128. doi:10.1080/14786435.2010.481272.

[29]   K. Rehman, H.S. Zurob, Novel Approach to Model Static Recrystallization of Austenite during Hot-Rolling of Nb-Microalloyed Steel: Effect of Precipitates, Mater. Sci. Forum. 753 (2013) 417–422. doi:10.4028/www.scientific.net/MSF.753.417.

[30]   E.I. Galindo-Nava, J. Sietsma, P.E.J. Rivera-Díaz-Del-Castillo, Dislocation annihilation in plastic deformation: II. Kocks-Mecking Analysis, Acta Mater. 60 (2012) 2615–2624. doi:10.1016/j.actamat.2012.01.028.

[31]   L.E. Murr, Interfacial Phenomena in Metal and Alloys, Addison-Wesley Publishing Company, Reading, 1977. doi:10.1002/piuz.19770080108.

[32]   H.S. Zurob, C.R. Hutchinson, Y. Brechet, G. Purdy, Modelling recrystallization of microalloyed austenite: effect of coupling recovery, precipitation and recrystallization, Acta Mater. 50 (2002) 3075–3092. doi:10.1016/S1359-6454(02)00097-6.

[33]   M.. Kassner, Taylor hardening in five-power-law creep of metals and Class M alloys, Acta Mater. 52 (2004) 1–9. doi:10.1016/j.actamat.2003.08.019.

[34]   H. Buken, E. Kozeschnik, State parameter-based modelling of microstructure evolution in micro-alloyed steel during hot forming, in: Mater. Sci. Eng. 119, 2016: p. 12023. doi:10.1088/1757-899X/119/1/012023.

[35]   T. Zhou, R.J. O'Malley, H.S. Zurob, Study of grain-growth kinetics in delta-ferrite and austenite with application to thin-slab cast direct-rolling microalloyed steels, Metall. Mater. Trans. A Phys. Metall. Mater. Sci. 41 (2010) 2112–2120. doi:10.1007/s11661-010-0246-y.

[36]   H. Frost, M. Ashby, Deformation mechanism maps: the plasticity and creep of metals and ceramics, 1982.

[37]   H. Buken, E. Kozeschnik, A Model for Static Recrystallization with Simultaneous Precipitation and Solute Drag, Metall. Mater. Trans. A Phys. Metall. Mater. Sci. 48 (2017) 2812–2818. doi:10.1007/s11661-016-3524-5.

[38]   Y. Huang, F.J. Humphreys, Subgrain growth and low angle boundary mobility in aluminium crystals of orientation {110} 〈001〉, Acta Mater. 48 (2000) 2017–2030. doi:10.1016/S1359-6454(99)00418-8.

[39]   H.S. Zurob, C.R. Hutchinson, Y. Brechet, G.R. Purdy, Rationalization of the softening and recrystallization behaviour of microalloyed austenite using mechanism maps, Mater. Sci. Eng. A. 382 (2004) 64–81. doi:10.1016/j.msea.2004.04.024.

[40] E.C.W. Perryman, Recrystallization Characteristics of Superpurity Base Al-Mg Alloys Containing 0 to 5 Pet Mg, Trans. AIME. (1955) 369–378. doi:10.1007/BF03377512.

[41] M. Muzyk, Z. Pakiela, K.J. Kurzydlowski, Ab initio calculations of the generalized stacking fault energy in aluminium alloys, Scr. Mater. 64 (2011) 916–918. doi:10.1016/j.scriptamat.2011.01.034.

[42] M.T.. Thornton P.R., The dependence of cross-slip on stacking fault energy in face centered cubic metals and alloys, Philos. Mag. A J. Theor. Exp. Appl. Phys. 7 (1962) 1349–1369. doi:doi.org/10.1080/14786436208213168.

[43] J. Kreyca, E. Kozeschnik, State parameter-based constitutive modelling of stress strain curves in Al-Mg solid solutions, Int. J. Plast. (in Press) (2018). doi:10.1016/j.ijplas.2018.01.001.

Paper II

A state parameter-based model for static recrystallization interacting with precipitation

Heinrich Buken and Ernst Kozeschnik

A model for static recrystallization with simultaneous precipitation and solute drag

Heinrich Buken[a] and Ernst Kozeschnik[a, b]

[a] Institute of Materials Science and Technology, TU Wien, Getreidemarkt 9, 1060 Vienna, Austria
[b] MatCalc Engineering GmbH, Getreidemarkt 9, 1060 Vienna, Austria

In the present work, we introduce a state parameter based microstructure evolution model, which incorporates the effect of solute atoms and precipitates on recrystallization kinetics. The model accounts for local precipitate coarsening at grain boundaries, which promotes an average grain boundary movement even if the Zener pinning force exceeds the driving force for recrystallization. The impact of solute drag on the grain boundary mobility as well as simultaneous precipitation is discussed in detail. The model is verified on experimental data on recrystallization in V- micro-alloyed steel, where excellent agreement is achieved.

Keywords: Recrystallization; Precipitation; Zener pressure; Solute drag; micro-alloyed steel, Vanadium

1. Introduction

During thermo-mechanical processing of crystalline materials, the growth velocity of recrystallizing grains can strongly be affected by the presence of precipitates and solute atoms. Precipitates interact with the moving grain boundaries via the well-known Zener pinning effect [1], which acts as a retarding force on the velocity of boundary movement. The magnitude of the Zener pressure is mainly determined by the precipitate phase fraction and size, which are commonly evolving in the course of thermo-mechanical treatment. In case of micro-alloyed steel, this effect is experimentally well analysed for the case of carbo-nitrides forming with minor additions of Al, V, Ti and Nb [2].

In addition to Zener pinning, the grain boundary mobility can also be drastically influenced by the solute drag effect [3]. In this case, elements that are segregated into the grain boundary must be "dragged along" with the moving boundary, thus exerting a retarding effect on the movement. The absolute value of the solute drag effect is mainly determined by the nominal concentration of the solute drag elements and their binding

energy to the grain boundary. Detailed experiments in steel [4] show that V, Mo, Ti and Nb are probably the most practically relevant elements with regard to solute drag in austenite of Fe-based alloys. A proper consideration of both effects, Zener drag and solute drag, is therefore essential for a successful simulation of recrystallization kinetics.

In literature, two types of simulation approaches exist for a description of these effects in micro-alloyed steel: phenomenological and physically-based models. On one hand, Medina and co-workers [2,5] utilize a phenomenological approach based on the Avrami model [6]. In this approach, the impact of precipitation on recrystallization is described by means of two coupled Avrami equations. The fast reaction term reproduces recrystallization kinetics in the regime before the Zener pressure exceeds the driving pressure for recrystallization. As soon as precipitation starts to control the grain boundary mobility, the slower Avrami kinetics becomes dominant. By interconnecting both solutions (slow and fast kinetics), Medina et al. are able to describe the evolution of the recrystallized fraction for a large amount of precipitation-controlled recrystallization experiments. The additional effect of solute atoms on grain boundary mobility is taken into account indirectly by an empiric formula, which accounts for the nominal chemical composition of the steel with a composition-dependent activation energy for recrystallization.

In contrast, Zurob et al. [7,8] suggest a physically-based approach, where the growth of recrystallized grains is expressed in terms of mobility and driving pressure. The impact of precipitation on growth kinetics is incorporated in the driving pressure term via the effective driving force resulting from the difference between recrystallization driving and Zener pinning pressure. This approach is well in line with former models suggested by Hillert [9] and Nes [10]. The solute drag impact in the Zurob et al. model is accounted for on basis of the work of Cahn [3] and it is, thus, included inherently in the grain boundary mobility.

In the present work, a comprehensive state parameter-based model coupling a multi-component multi-phase framework for precipitation kinetics simulation with a physically-based grain boundary movement and recrystallization approach including the impact of precipitation is introduced. The precipitation kinetics simulations are utilizing the comprehensive thermokinetic simulation environment MatCalc [11], where precipitation kinetics are computed as a function of temperature, deformation conditions and alloy compositions in a more or less fitting parameter-free manner. The successful applicability of MatCalc to precipitation problems in microalloyed steel has been

demonstrated many times, see, for instance, refs. [12–14]. The nucleation and growth models utilized in the precipitation kinetics simulations are described in detail in refs. [15–21]. The recrystallization model is introduced subsequently.

2. The Model

2.1 Recrystallization

The evolution of the polycrystalline microstructure after deformation is expressed in terms of the nucleation and growth kinetics of recrystallized grains. The formation of recrystallization nuclei is assumed to occur on the junctions of high angle grain boundaries (HAGB) and low angle grain boundaries (LAGB), as experimentally confirmed in low alloyed steel in ref. [22]. Consequently, the nucleation rate, $\dot{N}_{rx}$, is written as

$$\dot{N}_{rx} = \begin{cases} C_{rx}\left(\dfrac{\pi}{6}\delta^2 D\right)^{-1}\exp(\dfrac{-Q_{rx}}{RT})(1-X_{rx}) & ,\delta \geq \delta_{crit} \\ 0 & ,\delta < \delta_{crit} \end{cases} \qquad (1)$$

where δ is the subgrain diameter, D is the mean unrecrystallized grain diameter, C_{rx} is a calibration coefficient, Q_{rx} is an activation energy similar in value to that for substitutional self-diffusion along grain boundaries, X_{rx} is the recrystallized fraction and R is the universal gas constant. The parent austenite grain is assumed to be of spherical geometry. The criterion for nucleation is determined by the ratio between the surface energy of a subgrain, γ_{LB}, and the driving force for recrystallization, P_D, which is provided by the excess of deformation-induced dislocations. The corresponding relation [23] reads as

$$\delta_{crit} = \frac{3\gamma_{LB}}{P_D} = \frac{3\gamma_{LB}}{0.5\mu b^2 \rho}. \qquad (2)$$

The energy contribution of dislocations is calculated via the shear modulus, μ, the burgers vector, b, and the excess dislocation density ρ. Once the nucleus exceeds a critical size, its further growth rate, $\dot{D}_{rx}$, is expressed in terms of an effective HABG mobility, $M_{eff,HB}$, and the driving force as

$$\dot{D}_{rx} = M_{eff,HB}P_D(1-X_{rx}). \qquad (3)$$

In the course of recrystallization, the overall growth velocity of recrystallizing grains is assumed to decrease as a consequence of decreasingly available unrecrystallized volume. The evolution of the recrystallized fraction, which represents the ratio between the

velocity of recrystallized volume gain, $\dot{V}_{rx}$, and total volume, V_{tot}, is expressed as superposition of a term related to the nucleation of newly recrystallized grains and growth of existing ones as

$$\dot{X}_{rx} = \frac{\pi}{6}\left(\dot{N}_{rx}D_{rx}^3 + 3\dot{D}_{rx}D_{rx}^2\right) = \frac{\dot{V}_{rx}}{V_{tot}}. \qquad (4)$$

The evolution of the dislocation density is described by means of an extended Kocks-Mecking model considering the processes of dislocation generation as well as dynamic and static recovery. In this context, we closely follow the approach introduced by Sherstnev et al. [24] describing the rate of the total dislocation density evolution as

$$\dot{\rho} = \frac{M\sqrt{\rho}}{Ab}\dot{\varphi} - 2B\frac{d_{ann}}{b}\rho\, M\dot{\varphi} - 2CD_{Dis}\frac{\mu b^3}{k_B T}(\rho - \rho_{RS}), \qquad (5)$$

with the Taylor factor, M, the critical dislocation annihilation distance, d_{ann}, the substitutional self-diffusion coefficient at dislocations, D_{Dis}, the strain rate $\dot{\varphi}$, and material parameters A, B, C. However, in contrast to the original Sherstnev et al. model, where the authors assume that the driving force for static recovery is given by the difference of actual and equilibrium dislocation density, we introduce a limiting degree of static recovery, here, given by the amount of geometrically necessary dislocations, ρ_{RS}, for maintaining the subgrain microstructure. In the Read-Shockley model [25], which is adopted here, the mean subgrain misorientation angle, θ_{mean}, and the mean subgrain size, δ, in a periodic network in the grain boundary plane, define the required dislocation density, ρ_{RS}, as

$$\rho_{RS} = \frac{\tan(\theta_{mean})}{b\delta}. \qquad (6)$$

The deformation-induced subgrain size is assumed to be correlated with the dislocation density by means of the principle of similitude [26,27]. This mainly empirical relation delivers a cell/subgrain size, which is directly linked to the dislocation density evolution during deformation with

$$\delta = \frac{K}{\sqrt{\rho}}, \qquad (7)$$

where K is a material parameter. After deformation, and before the onset of recrystallization, subgrain coarsening takes place. The mean growth rate of subgrains is expressed in terms of an effective LAGB mobility, $M_{eff,\,LB}$, and a driving force provided by curvature

$$\dot{\delta} = M_{\text{eff,LB}} \frac{3\gamma_{\text{LB}}}{\delta}, \qquad (8)$$

with $M_{\text{eff,LB}}$ as an effective LAGB mobility.

2.2 Precipitates and solute atoms

Micro-alloying elements in steel can have two effects on recrystallization kinetics: Zener pinning by carbo-nitride particles and solute drag by solid solution atoms [7]. For the effect of precipitates, the Zener pressure, P_Z, can be expressed [10] as

$$P_Z = \frac{3f\gamma_{\text{HB}}}{2r}, \qquad (9)$$

with f being the precipitated phase fraction and r being the mean precipitate radius. Since the MatCalc precipitation kinetics framework offers detailed information on the size distribution of precipitates also, in the simulations, a size class-based formulation of the Zener pressure is used as introduced by Rath and Kozeschnik [28] in a recent treatment of coupled precipitation and grain growth. To account for different precipitate types, i, and size classes, k, we use the following expression which reads

$$P_Z(k,i) = \frac{3}{2}\gamma_{\text{HB}} \sum_i \sum_k \frac{f_{k,i}}{r_{k,i}}. \qquad (10)$$

To describe the impact of precipitation on recrystallization, we assume that the precipitates, which potentially pin the boundaries, are interconnected along high velocity diffusion paths, i.e. the grain boundaries. Due to the fast diffusion kinetics along the boundaries, the precipitates are subject to significantly accelerated coarsening. When the number density of precipitates pinning the boundary decreases due to coarsening, the Zener pressure decreases and the grain boundary becomes locally released. The free grain boundary then continues to move further into the deformed microstructure until it encounters a new front of pinning precipitates, where the local coarsening procedure repeats. On average, the grain boundary can thus continuously move through the material even if the Zener pressure determined by the initial precipitate distribution exceeds the driving pressure for recrystallization. This issue is discussed in detail in ref. [29].

In support of this concept, Yazawa et al. [30] and Jones and Ralph [31] experimentally observed this special precipitate coarsening behaviour in the presence of recrystallization. The precipitates in front of the moving boundary and behind had significantly different average size and number density. To mimic this behaviour in our model, we include the Zener pressure into the mobility term instead of reducing the

available driving force by the Zener pressure to obtain an effective driving force. The resulting mobility taking into account the particle pinning effect reads as

$$M_{prec} = \begin{cases} \left(\dfrac{P_D - P_Z}{P_D} \right) M_{free} + \left(1 - \dfrac{P_D - P_Z}{P_D} \right) M_{pinned} & , P_D > P_Z \\ M_{pinned} & , P_D \leq P_Z \end{cases} \qquad (11)$$

where M_{prec} is the effective mobility of the grain boundary in the presence of precipitates, M_{free} is the free mobility without any dragging and retarding influences of particles and/or solute atoms, and M_{pinned} is the limiting (non-zero) mobility, which is adopted by the grain boundary when the Zener pressure exceeds the driving pressure for recrystallization.

In the present model, the impact of solute drag is modelled on basis of the work of Cahn [3]. Accordingly, the dragging effect of solute atoms, which are segregated into the grain boundary, is incorporated into the mobility term with

$$M_{SD} = \frac{1}{\alpha C_{GB}}, \qquad (12)$$

where M_{SD} is the mobility of the grain boundary in the presence of solute drag, C_{GB} is the grain boundary concentration of the solute drag element and α is an inverse mobility. The latter determines the temperature dependency of the solute drag effect via the grain boundary/atom interaction energy, E_B, given as

$$\alpha = \frac{\omega (RT)^2}{E_B D_{CB} V_M} \left(\sinh\left(\frac{E_B}{RT} \right) - \left(\frac{E_B}{RT} \right) \right), \qquad (13)$$

where ω is the grain boundary width, V_M is the molar volume of the matrix phase and D_{CB} is the cross boundary diffusion coefficient of the solute drag element. For convenience, in the present analysis, the grain boundary concentration is assumed to be identical to that of the matrix without any regard of additional element segregation into the boundary.

The integral effective mobility is finally evaluated as

$$M_{eff,HB} = \left(\frac{1}{M_{prec}} + \frac{1}{M_{SD}} \right)^{-1}, \qquad (14)$$

which is in accordance with Cahn´s original suggestion of combining the solute drag mobility with the free mobility.

2.3 Materials

To verify the present model, we analyze the experimental observations on simultaneous recrystallization and precipitation reported by Medina et al. [32]. The selected materials have been investigated at different degrees of supersaturation, determined by the V and N content. The chemical composition, thus, also determines the solution temperature, T_{Sol}, listed in Table 1, in addition to the starting grain size. The experiments are carried out in a temperature range between 825°C and 1100°C, at a strain rate of 3.63s^{-1} and at a strain of 0.35.

Table 1:   Chemical composition of simulated materials [32].

ID.	V [wt.-%]	C [wt.-%]	N [wt.-%]	T_{Sol} [°C]	D_0 [μm]
V1	0.043	0.11	0.0105	1023	172
V2	0.06	0.12	0.0123	1058	167
V3	0.09	0.12	0.0144	1106	165

2.4 Model parameters

Apart from the parameters C_{rx} and Q_{rx}, eq. (1), which determine the nucleation rate of recrystallizing grains, a major input quantity into the recrystallization simulations is the effective mobility of the recrystallization front, i.e., the grain boundary mobility. This quantity (eq. 14) is basically determined by three partial mobilities: (i) M_{free}, (ii) M_{pinned} and (iii) M_{SD}, which are discussed in more detail next.

(i) The free mobility is parameterized in accordance to the suggestion of Turnbull [33] as

$$M_{free} = \eta_{free} \cdot M_{TB} = \eta_{free} \cdot \frac{\omega D_{GB} V_m}{b^2 RT}, \qquad\qquad (15)$$

where η_{free} is a linear pre-factor, M_{TB} is the Turnbull mobility, ω is the grain boundary width and D_{GB} is the substitutional self-diffusion coefficient along grain boundaries. The latter is adopted from a recent independent assessment of Stechauner and Kozeschnik [34], providing the essential information on the temperature-dependence of the free mobility, which thus becomes a fixed quantity in our treatment instead of being an unknown fitting parameter. The absolute value of this quantity is adjusted such that it is in accordance to the mobility suggestion for low alloyed austenite reported in ref. [35]. A pre-factor of η_{free} =1.5% is chosen in the present work. A grain boundary width of ω =1nm is adopted from ref. [36].

(ii) The pinned mobility concept, as utilized in the present work, is based on the assumption of local precipitate coarsening along grain boundaries. This concept has been introduced recently in ref. [29] and it was briefly described earlier in section 2.2. In an analysis of grain boundary precipitate coarsening, Kirchner [37] showed that coarsening at grain boundaries should obey a temperature-dependence determined by the grain boundary diffusion coefficient. We thus conclude that the temperature-dependence of the Turnbull mobility is also determining the local coarsening kinetics. Therefore, we adopt this concept for the pinned mobility and express it as a fraction of the Turnbull mobility with

$$M_{pinned} = \eta_{pinned} \cdot M_{free} = \eta_{pinned} \cdot \eta_{free} \cdot M_{TB} \ , \qquad (16)$$

with a dimensionless pre-factor, η_{pinned}. In the present work, its value is set to 3%.

(iii) The empirical studies by Andrade et al. [4] show that the solute drag effect of V during recrystallization is considerably smaller than that of Ti or Nb, however, it is supposed to be still conceivable at lower temperatures. Unfortunately, Andrade et al. do not report absolute values for the binding energy of V to the grain boundary within the framework of the Cahn model [3]. We assume that the trapping energy of V to the austenite grain boundaries is of the order of 2.5 kJ/mol, because this value delivers good agreement with experimental evidence.

The driving pressure for recrystallization is mainly determined by the amount of excess defects (dislocations) that are introduced into the material during deformation. The dislocation density evolution is, in turn, determined by the material parameters A, B and C (eq. 5) and, in the present work, adjusted to the flow curve data of Hernandez et al. [38] utilizing the Taylor forest hardening law. For the deformation conditions reported there and used here, the computed dislocation densities reach maximum values below $8 \cdot 10^{14}$ m^{-2}. The parameters used in the present study are summarized in table 2. These are used without further adjustment in all simulations presented subsequently.

Table 2:   Input parameters for recrystallization simulation

Parameter	Value	Unit	Ref.
D_{Dis}	$4.5 \cdot 10^{-5} \exp(185000/RT)$	m²/s	[34]
D_{GB}	$5.5 \cdot 10^{-5} \exp(145000/RT)$	m²/s	[34]
D_{CB}	$2D_B$	m²/s	[36]
Q_{rx}	145	kJ/mol	[34]
C_{rx}	$1.5 \cdot 10^6$	-	This work
γ_{HB}	$1.3111 - 0.0005T$	J/m2	[7]
γ_{LB}	$0.5\gamma_{HB}$	J/m2	This work
A, B, C	$50; 5; 5 \cdot 10^{-5}$	-	This work
θ_{mean}	3	degree	This work
$E_{B,V}$	2.5	kJ/mol	This work
ω	$1 \cdot 10^{-9}$	m	[36]
$\eta_{free,HB}$	$1.5 \cdot 10^{-2}$	-	[34,35]
$\eta_{pinned,HB}$	$3 \cdot 10^{-2}$	-	This work

3. Results and discussion

In this section, we compare our simulations with the experimental data obtained by Medina and co-workers [32] on a series of V-microalloyed steels (see table 1). In the simulations, we apply the same thermo-mechanical treatment as reported in the corresponding study. To obtain information on the initial grain size for recrystallization after solution heat treatment at 1230°C for 600s, Medina et al. [32] utilize metallographic methods. The double hit deformation experiments are performed as torsion tests at different temperatures ranging from 825°C to 1100°C. The deformation conditions are kept constant during every measurement with a strain rate of $3.63s^{-1}$ and a strain of 0.35. Figure 1 shows our simulation results in comparison to the experiments from ref.[32]. With the single set of input parameters, we obtain excellent agreement for all three steels investigated here. For illustration of the effect of solute drag, we have computed the recrystallization kinetics at the two lowest temperatures for each alloy with and without solute drag (dashed grey lines).
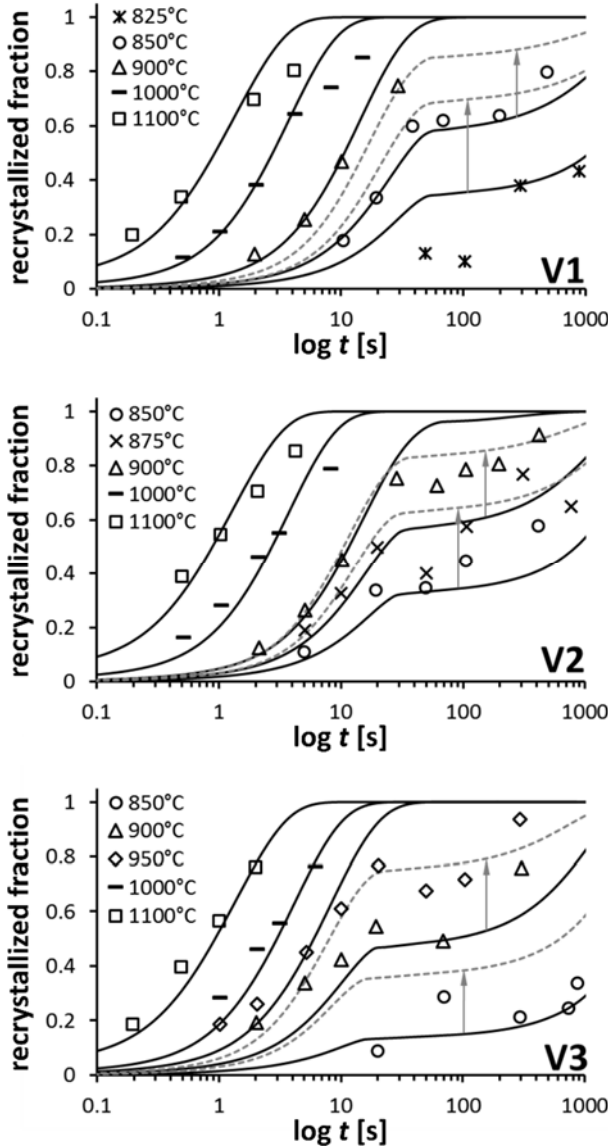
Figure 1: Calculated and experimental recrystallization kinetics for steels V1, V2 and V3 from ref. [32]. Dashed lines: Computed curves neglecting the solute drag effect.

In each of the considered alloys, the recrystallized fractions exhibit distinct plateaus of recrystallization stasis, which are caused by the pinning effect of V(C,N) precipitates on the moving grain boundaries. With increasing V-carbonitride supersaturation from alloy V1 to V3, the increasing pinning potential affects recrystallization in two ways: (i) the plateaus start at earlier times and (ii) the plateaus occur at higher testing temperatures. Both trends are well captured by the simulations and can clearly be attributed to the corresponding differences in precipitation kinetics. With increasing V and N contents, the driving force for precipitation increases and, thus, the driving pressure for

recrystallization is compensated by the retarding Zener pressure at earlier times and at higher temperatures.

As soon as the Zener pressure equals the driving pressure for recrystallization, the effective grain boundary mobility is drastically reduced and a slower recrystallization kinetics is observed. Figure 2 illustrates the occurrence of these thresholds for each considered alloy by plotting the time-temperature-precipitation (TTP) kinetics for the 5% precipitated phase fraction lines and for the lines where P_D equals P_Z. For the present set of investigated alloys, a time range within approximately a factor of four is spanned and a corresponding temperature interval of approximately 70°C. The precipitation simulations clearly support the interpretation that the recrystallization plateaus are caused by Zener pinning.

In analyses of results from double-deformation experiments, the nature of softening fractions and their relation to recrystallized fraction is discussed controversially in literature. On the one hand, Zurob et al. [39] suggest that dislocation pinning by precipitates represents the origin of the measured plateaus. These authors argue that static recovery is severely hindered if the number density of precipitates exerts a certain limit. By virtue of a pinned dislocation network, no further energy loss and, thus, softening would be measured if a softening fraction method is used for evaluation. Consequently, if recrystallization and precipitation occur simultaneously, these authors argue that softening fraction measurements neither deliver information on the recrystallized fraction, nor is classic Zener pinning the reason for the observed plateaus.

On the other hand, Medina et al. [40] relate the observed plateaus directly to the recrystallized fraction and the interaction of recrystallization with particle pinning. These authors claim that their softening fraction data measured with the back-extrapolation method correlate well with the recrystallized fraction. To support their arguments, they analyze a substantial amount of experimental data and confirm their analysis with metallographic characterization of recrystallization at different stages during their experiments [41–43]. In the present work, we adopt the interpretation of Medina et al., however being aware that some controversy exists in this field.
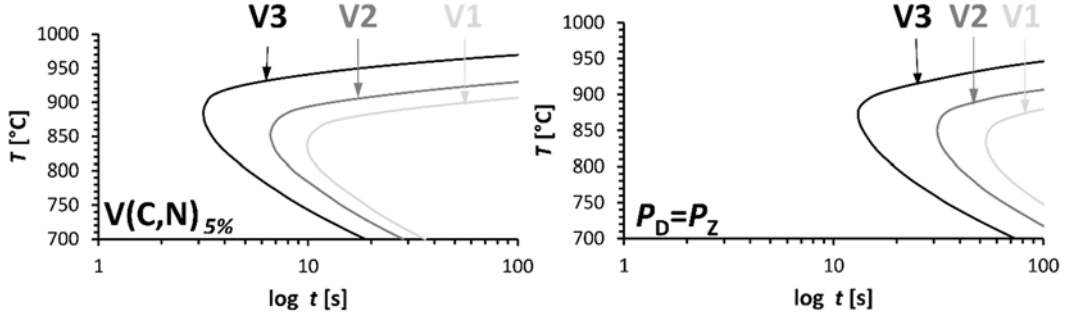
Figure 2: Simulated TTP-curves for 5% precipitated fraction and the position where the driving pressure for recrystallization equals the Zener pinning pressure.

In Fig. 1, the recrystallized fraction curves are calculated with and without consideration of the solute drag effect caused by V atoms. Apparently, the impact of solute drag is rather substantial at lower temperatures, whereas it appears to be negligible at higher temperatures. The calculated partial mobilities plotted in Fig. 3 support this observation. The black dashed line shows the mobility suggested by the Turnbull approach, which is based on the grain boundary diffusion coefficient assessed in ref. [34]. The grey dashed line denoted by M_{free} represents the effective mobility of the unpinned and solute drag-free boundary. M_{SD} is the mobility calculated from the Cahn model, eqs. (11) and (12), and using a binding energy between V atoms and grain boundary of 2.5 kJ/mol. The effective mobility for the unpinned grain boundary, $M_{eff,HB}$, is deviating from M_{free} only at the lowest temperatures, whereas they converge at the higher temperatures. The grain boundary mobility accounting for the pinning effect of precipitates is effective only after the driving force for recrystallization balances the Zener pressure, i.e., P_D equals P_Z. Once the grain boundary is pinned by precipitates, solute drag is ineffective in the present steels under consideration.
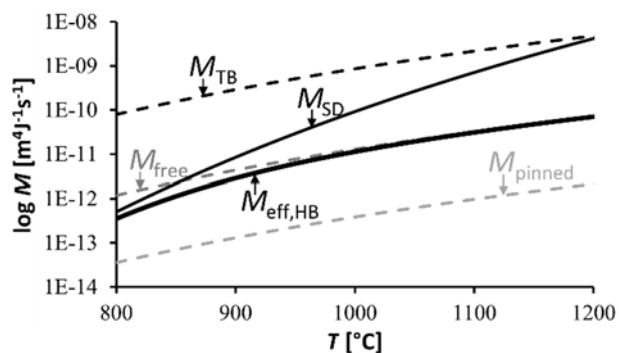
Figure 3: Partial mobilities utilized in the simulations for alloy V3

4. Summary

In the present work, we propose a comprehensive model for thermokinetic modeling of simultaneous recrystallization, precipitation and solute drag. The impact of precipitation on the observed recrystallization stasis is assumed to be determined by Zener particle pinning and the kinetics of local precipitate coarsening at grain boundaries. In contrast to conventional modeling approaches, this effect is included into the mobility term instead of evaluating a threshold value for complete recrystallization stasis with zero grain boundary mobility. This consideration is essential for a consistent simulation of experimentally evidenced recrystallization plateaus. In addition to Zener pinning, the solute drag effect is incorporated in the sense of the Cahn solute drag approach. It is demonstrated that this effect has significant impact on the recrystallization kinetics at the lowest testing temperatures. We observe good agreement between simulations and experiments with a binding energy of 2.5 kJ/mol.

References

1. C. S. Smith, Trans. AIME **175**, 15 (1948).

2. M. Gomez, A. Quispe, and S. F. Medina, Steel Res. Int. **85**, 1440 (2014).

3. J. W. Cahn, Acta Metall. **10**, 789 (1962).

4. H. L. Andrade, M. G. Akben, and J. J. Jonas, Metall. Trans. A **14**, 1967 (1983).

5. S. F. Medina and a. Quispe, ISIJ Int. **41**, 774 (2001).

6. M. Avrami, J. Chem. Phys. **8**, 212 (1940).

7. H. S. Zurob, Y. Brechet, and G. Purdy, Acta Mater. **49**, 4183 (2001).

8. K. Rehman and H. S. Zurob, Mater. Sci. Forum **753**, 417 (2013).

9. M. Hillert, Acta Metall. **13**, 227 (1965).

10. E. Nes, Acta Metall. **24**, 391 (1976).

11. E. Kozeschnik, Http://matcalc.tuwien.ac.at/ (n.d.).

12. R. Radis and E. Kozeschnik, Model. Simul. Mater. Sci. Eng. **20**, 055010 (2012).

13. R. Radis and E. Kozeschnik, Steel Res. Int. **81**, 681 (2010).

14. R. Radis and E. Kozeschnik, Model. Simul. Mater. Sci. Eng. **18**, 055003 (2010).

15. J. Svoboda, F. D. Fischer, P. Fratzl, and E. Kozeschnik, Mater. Sci. Eng. A **385**, 166 (2004).

16. E. Kozeschnik, J. Svoboda, P. Fratzl, F. D. Fischer, P. Fratzl, and E. Kozeschnik, Mater. Sci. Eng. A **385**, 166 (2004).

17. B. Sonderegger and E. Kozeschnik, Metall. Mater. Trans. A **40**, 499 (2009).

18. B. Sonderegger and E. Kozeschnik, Scr. Mater. **60**, 635 (2009).

19. B. Sonderegger and E. Kozeschnik, Metall. Mater. Trans. A **41**, 3262 (2010).

20. E. Kozeschnik, *Modeling Solid-State Precipitation* (Momentum Press, 2012).

21. E. Kozeschnik, J. Svoboda, and F. D. Fischer, Calphad **28**, 379 (2004).

22. S. S. Hansen, J. B. Vander Sande, and M. Cohen, Metall. Trans. A **11A**, 387 (1980).

23. Y. Huang and F. J. Humphreys, Acta Mater. **48**, 2017 (2000).

24. P. Sherstnev, P. Lang, and E. Kozeschnik, Eccomas 2012 8 (2012).

25. W. T. Read and W. Shockley, Phys. Rev. **78**, 275 (1950).

26. Y. . Estrin, L. S. . Tóth, A. . Molinari, and Y. . Bréchet, Acta Mater. **46**, 5509 (1998).

27. E. Nes, Prog. Mater. Sci. **41**, 129 (1997).

28. M. Rath and E. Kozeschnik, Mater. Sci. Forum **753**, 357 (2013).

29. H. Buken, P. Sherstnev, and E. Kozeschnik, *Unpuplished Research* (2016).

30. Y. Yazawa, T. Furuhara, and T. Maki, Acta Mater. **52**, 3727 (2004).

31. A. . Jones and B. Ralph, Acta Metall. **23**, 355 (1975).

32. S. F. Medina, J. E. Mancilla, and C. a. Hernández, ISIJ Int. **34**, 689 (1994).

33. D. Turnbull, Trans. AIME **191**, 661 (1951).

34. G. Stechauner and E. Kozeschnik, Calphad **47**, 92 (2014).

35. T. Zhou, R. J. O'Malley, and H. S. Zurob, Metall. Mater. Trans. A Phys. Metall. Mater. Sci. **41**, 2112 (2010).

36. M. K. Rehman and H. S. Zurob, Metall. Mater. Trans. A Phys. Metall. Mater. Sci. **44**, 1862 (2013).

37. H. O. K. Kirchner, Metall. Trans. **2**, 2861 (1971).

38. C. A. Hernandez, S. F. Medina, and J. Ruiz, Acta Metall. **44**, 155 (1996).

39. H. S. Zurob, C. R. Hutchinson, Y. Brechet, and G. R. Purdy, Mater. Sci. Eng. A **382**, 64 (2004).

40. M. Gómez, L. Rancel, and S. F. Medina, Mater. Sci. Eng. A **506**, 165 (2009).

41. A. Quispe, S. F. Medina, M. Gómez, and J. I. Chaves, Mater. Sci. Eng. A **447**, 11 (2007).

42. A. Quispe, S. F. Medina, and P. Valles, ISIJ Int. **37**, 783 (1997).

43. M. Gómez, S. F. Medina, a. Quispe, and P. Valles, ISIJ Int. **42**, 423 (2002).

Paper III

A state parameter-based model for static recrystallization interacting with precipitation

Heinrich Buken, Pavel Sherstnev and Ernst Kozeschnik

Modelling and Simulation in Materials Science and Engineering

Volume 24, Year 2016, 35006.

A state parameter-based model for static recrystallization interacting with precipitation

Heinrich Buken[a], Pavel Sherstnev[b] and Ernst Kozeschnik[a, c]

[a] Institute of Materials Science and Technology, Vienna University of Technology, Getreidemarkt 9, 1060 Vienna, Austria

[b] LKR-Leichtmetallkompetenzzentrum Ranshofen GmbH, AIT-Austrian Institute of Technology, Austria; now at LLC "Linhardt-Altai", Bijsk, Russian Federation

[c] MatCalc Engineering GmbH, Getreidemarkt 9, 1060 Vienna, Austria

In the present work, we develop a state parameter-based model for the treatment of simultaneous precipitation and recrystallization based on a single-parameter representation of the total dislocation density and a multi-particle multi-component framework for precipitation kinetics. In contrast to conventional approaches, the interaction of particles with recrystallization is described with a non-zero grain boundary mobility even for the case where the Zener pressure exceeds the driving pressure for recrystallization. The model successfully reproduces the experimentally observed particle-induced recrystallization stasis and subsequent continuation in micro-alloyed steel with a single consistent set of input parameters. In addition, as a state parameter-based approach, our model naturally supports introspection into the physical mechanisms governing the competing recrystallization and recovery processes.

Keywords: Recrystallization; Precipitation; Zener pressure; micro-alloyed steel; MatCalc

Introduction

The original work of Smith and Zener [1], introducing a formalism for the energetic interaction between second phase particles and grain boundaries, triggered significant scientific effort into further exploration of this topic. In modeling grain growth based on the concept of mobility and driving pressure, Hillert [2] incorporates the effect of second phase particles as integral part of the driving pressure term, which ultimately leads to a limiting grain size determined by the balance of retarding and driving forces. Subsequent investigations focusing on recrystallization modeling, such as, among many others, the

ones by Nes [3], Humphreys [4] and Zurob et al. [5,6], confirm the applicability of this concept.

Despite an apparent success in describing the onset of recrystallization stasis caused by precipitates, the processes governing the continuation of the recrystallization process and its interaction with the ongoing precipitate evolution are not well understood and inconsistently described in literature. Although the experimentally observed completion of recrystallization is commonly attributed to precipitate coarsening and the accompanying reduction of the Zener pressure, its kinetics is not related to conventional Ostwald ripening, but to some faster coarsening mechanism. In a recent contribution [7], the assumption of local coarsening along the pinned grain boundaries has been suggested, however, no corresponding local coarsening model has been formulated, there.

In the present work, we present a novel approach describing static recrystallization and its interaction with precipitation. The latter is simulated on basis of the thermokinetic software MatCalc, which delivers phase fraction and size distribution of precipitates in the framework of the multi-particle SFFK model [8-9], extended multi-component classical nucleation theory as described in detail in ref. [10] and interfacial energies calculated in the generalized broken bond (GBB) approach [11-13]. From the simulated particle distributions, the retarding pressure due to grain boundary pinning is evaluated and utilized further in the recrystallization model, which is introduced next.

A model for simultaneous recrystallization and precipitation

The evolution of polycrystalline grains during recrystallization is expressed in terms of the mean grain sizes of recrystallized and non-recrystallized (deformed) grains. The formation of newly recrystallized grains is assumed to occur on the junctions of high angle grain boundaries (HAGB) and low angle grain boundaries (LAGB) [14]. The latter are assumed to be introduced throughout the deformation process. Accordingly, the nucleation rate, $\dot{N}_{rx}$, is given as

$$\dot{N}_{rx} = \begin{cases} C_{rx}\left(\dfrac{\pi}{6}\delta^2 D\right)^{-1} \exp(\dfrac{-Q_{rx}}{RT})(1-X_{rx}) & ,\delta \geq \delta_{crit} \\ 0 & ,\delta < \delta_{crit} \end{cases}, \qquad (1)$$

where δ is the subgrain diameter, D is the mean non-recrystallized grain diameter, C_{rx} is a calibration coefficient, Q_{rx} is an activation energy similar in value to that for substitutional self-diffusion along grain boundaries, X_{rx} is the recrystallized fraction, R is the universal gas constant and T is temperature. A stable nucleus is assumed to be a

(deformation-induced) subgrain that is (i) in contact with a HAGB and (ii) exceeds a critical size, δ_{crit}, given by the ratio of the interfacial energy of the LAGB, γ_{LB}, and the driving pressure, P_D, with

$$\delta_{crit} = \frac{3\gamma_{LB}}{P_D} = \frac{3\gamma_{LB}}{0.5\mu b^2 \rho} \tag{2}$$

where the driving pressure originates from the removal of stored energy of dislocations introduced by deformation. It is characterized by the mean dislocation density, ρ, the shear modulus, μ, and the Burgers vector, b. The curvature expression in terms of subgrain diameter and surface energy is adopted from ref. [15]. After nucleation, the growth rate of recrystallizing grains, $\dot{D}_{rx}$, is expressed by the product of an effective HAGB mobility ($M_{eff,\ HB}$) and the driving pressure, scaled by the remaining non-recrystallized volume fraction, $(1-X_{rx})$, as

$$\dot{D}_{rx} = M_{eff,\ HB}\, P_D\, (1 - X_{rx}) \tag{3}$$

The evolution of the recrystallized fraction, which represents the ratio between recrystallized volume, $\dot{V}_{rx}$, and total volume, V_{tot}, is expressed as superposition of a term related to the nucleation of new recrystallized grains and growth of existing ones as

$$\dot{X}_{rx} = \frac{\pi}{6}\left(\dot{N}_{rx} D_{rx}^3 + 3\dot{D}_{rx} D_{rx}^2\right) = \frac{\dot{V}_{rx}}{V_{tot}} \tag{4}$$

The essential quantity for evaluation of the nucleation rate of recrystallized grains, $\dot{N}_{rx}$, is apparently the mean dislocation density, ρ, which is directly corresponding to the energy that is stored in the polycrystalline microstructure as a consequence of deformation. In our work, the evolution of the dislocation density is described by means of an extended Kocks-Mecking model considering deformation-induced dislocation generation as well as dynamic and static recovery. We closely follow the approach introduced in ref. [16], where the evolution of the total dislocation density has been proposed as

$$\dot{\rho} = \frac{M\sqrt{\rho}}{Ab}\dot{\varphi} - 2B\frac{d_{ann}}{b}\rho M\dot{\varphi} - 2CD_{Dis}\frac{\mu b^3}{k_B T}\rho \tag{5}$$

with the Taylor factor, M, the critical dislocation annihilation distance, d_{ann}, the substitutional self-diffusion coefficient along dislocations, D_{Dis}, the Boltzmann constant, k_B, the strain rate, φ, and material parameters A, B, C.

The strain-induced subgrain size is assumed to be correlated with the mean dislocation density by the principle of similitude [16-17]. This mainly empirical relation delivers a cell/subgrain size, which is directly linked to the dislocation density evolution during deformation with

$$\delta = \frac{K}{\sqrt{\rho}}.$$
(6)

Here, K is a material parameter. After deformation and before the onset of static recrystallization, subgrain growth and coarsening take place simultaneously, leading to a reduction of the total dislocation density. To describe this process, the mean growth rate of subgrains is expressed in terms of an effective LAGB mobility, $M_{eff, LB}$, and a driving force provided by the mean subgrain curvature with

$$\dot{\delta} = M_{eff,LB}\frac{3\gamma_{LB}}{\delta}.$$
(7)

The expression for the LAGB mobility is taken from Sandström [19], where the LAGB-mobility is proposed as

$$M_{eff, LB} = \eta_{eff, LB}\frac{D_B b^2}{k_B T} \quad ,$$
(8)

with the substitutional self- diffusion coefficient in the bulk, D_B, and a linear parameter $\eta_{eff, LB}$.

For the interaction of recrystallization with precipitation, we assume that the precipitates nucleate and grow in a random spatial distribution within the grains. In the sense of the Smith and Zener model [1], the recrystallization front comes to a stop once the retarding pressure exerted by the precipitates equals or exceeds the driving pressure. After the grain boundary has become immobile, the pinning precipitates are, now, interconnected by a high-velocity diffusion path, i.e., the grain boundary, and they are therefore exposed to fast local coarsening. As a consequence, the density of strain induced precipitates, pinning the boundary, decreases locally at a substantially increased rate and the pinning pressure quickly decreases. Thus, the grain boundary becomes locally released and moves on until it is pinned again by the next generation of strain induced precipitates in front of the moving boundary. Local coarsening sets in again and the process is continuously repeated, leaving behind a recrystallized volume with precipitates that have undergone a local coarsening process as sketched in Fig. 1. This process has been observed and confirmed experimentally by Yazawa et al. [20] for VC particles and by Jones and Ralph [21] for NbC- particles in austenite.
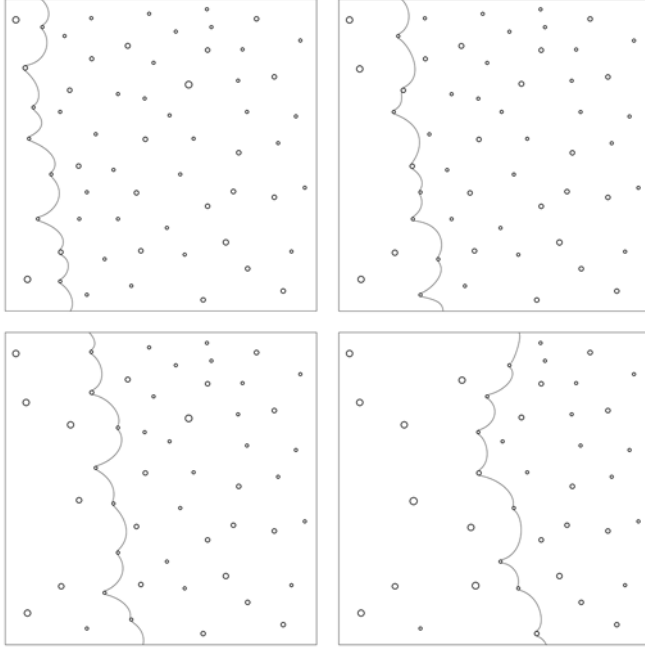
Figure 1: Sketch of a recrystallizing grain boundary passing through a forest of obstacles (precipitates).

In the presence of local coarsening and on an average basis, the recrystallization front thus never comes to a complete stop, but alternating individual segments of the boundary continuously progress into the unrecrystallized volume. Consequently, this process is comparable in nature to the movement of an interface through a viscous medium, which can be expressed by a characteristic mobility governed by the kinetics of local coarsening. In contrast to most other modeling approaches [2–7], in the present work, the Zener pressure, P_Z, is therefore not incorporated in the driving force term for recrystallization but accounted for indirectly in an effective grain boundary mobility, expressed in terms of a weighted superposition of an obstacle-free mobility, M_{free}, representing the mobility of the grain boundary in the absence of precipitates, and a pinned mobility, M_{pinned}, describing the effective mobility of the grain boundary in the presence of particles subject to the mechanism of local coarsening, as

$$M_{\text{eff,HB}} = \begin{cases} \left(\dfrac{P_D - P_Z}{P_D}\right)M_{\text{free}} + \left(1 - \dfrac{P_D - P_Z}{P_D}\right)M_{\text{pinned}} & , P_D > P_Z \\ M_{\text{pinned}} & , P_D \leq P_Z \end{cases} \qquad (9)$$

In this approach, the boundary mobility maintains a finite, non-zero value even in the case where the retarding pressure exceeds the driving pressure. Thereby we simplify and treat growing precipitates and precipitates which have already undergone the classical growth

process with the same pinned mobility value. The Zener pressure itself is given for a spatial distribution of spherical precipitates in dependence of the precipitate radius, r_p, and the precipitate phase fraction, f_p, by Nes et al. [3] as

$$P_Z = \frac{3 f_p \gamma_{HB}}{2 r_p} .$$ (10)

Input parameters to the microstructure model

A crucial aspect for the quantitative reproduction of experimental data on the recrystallization stasis in the present context is the appropriate choice of values for the grain boundary mobilities, M_{free} and M_{pinned}. In the present work, we adopt a model proposed by Turnbull [22], relating the free mobility of a HAGB to the grain boundary diffusivity, D_{GB}, of the majority substitutional element as

$$M_{free} = \eta_{free,HB} \cdot M_{TB} = \eta_{free} \cdot \frac{\omega D_{GB} V_m}{b^2 RT} ,$$ (11)

with the grain boundary thickness, ω, the grain boundary mobility suggested by Turnbull, M_{TB}, and the molar volume V_m. In the simulations, the grain boundary diffusivity of fcc Fe is adopted from the recent independent assessment of Stechauner and Kozeschnik [23]. As a major consequence, this choice delivers the principal temperature-dependence of the grain boundary mobility interrelated with the temperature-dependence of the grain boundary diffusion coefficient. Thus, the necessity of taking the activation energy for grain boundary movement as an unknown fitting parameter is eliminated. The absolute value for the free mobility is calibrated on basis of the experiments of Zhou et al. [24] in the parameter $\eta_{free,\,HB}$, which delivers excellent agreement with a value of 1,5%.

The temperature-dependency of the pinned mobility should be somehow related to that of the free mobility [25], since precipitate coarsening along grain boundaries, as well as the grain boundary mobility itself, are controlled by substitutional diffusion inside the grain boundary. Thus, we model the pinned mobility as a linear fraction of the free mobility with

$$M_{pinned} = \eta_{pinned,\,HB} \cdot M_{free} ,$$ (12)

again with the principal temperature-dependence determined by the grain boundary diffusivity.

The driving pressure for recrystallization is mainly determined by the stored energy of the deformation-induced dislocations. Therefore, the calibration parameters (A, B, C) of the extended Kocks- Mecking model (Eq. 5) are adjusted such as to reproduce flow curves reported by Hernandez et al. [26]. The observed dislocation densities do not

exceed $8 \cdot 10^{14}$ m^{-2} and deliver appropriate flow stresses in the sense of the Taylor forest hardening law with the input parameters similar to those mentioned in ref. [6]. A collection of input parameters obtained in the present work is given in table 1. These values are consistently used over the whole range simulation conditions.

Table 1.   Simulation input parameters

Parameter	Value	Ref.
$\eta_{\text{free, HB}}$	$1.5 \cdot 10^{-2}$	[20- 21]
$\eta_{\text{pinned, HB}}$	$3 \cdot 10^{-2}$	This work
$\eta_{\text{eff, LB}}$	$7.5 \cdot 10^{-3}$	This work
γ_{HB} [J/m²]	1.3111-0.0005T	[6]
γ_{LB} [J/m²]	$0.5\gamma_{\text{HB}}$	This work
Q_{rx} [kJ/mol]	145	[23]
C_{rx}	10^6	This work
A (Eq. 5)	50	This work
B	5	This work
C	$5 \cdot 10^{-5}$	This work

Simulation results and discussion

The performance of our model is verified exemplarily on experimental data reported by Quispe et al. [27], analyzing the recrystallization behavior of V micro-alloyed steel in dependence of different starting austenite grain sizes and temperatures. Figure 2 presents the essential results of our simulation approach in the form of recrystallized fractions compared to the experimental softening fractions reported in Ref. [27]. Below 1000°C, the precipitation of V(C, N) particles increasingly interacts with the recrystallization process by exerting a retarding pressure on the moving grain boundary. Once the retarding pressure exceeds the driving pressure for recrystallization, the effective mobility of the recrystallization front decreases to a value given by the pinned mobility, M_{pinned}, which is taken as 3% of the free mobility. The physical meaning of this value is related to the critical time that is required for the local coarsening until P_Z decreases below P_D. Thus, a different alloy could require a different linear prefactor for the calculation of M_{pinned}.
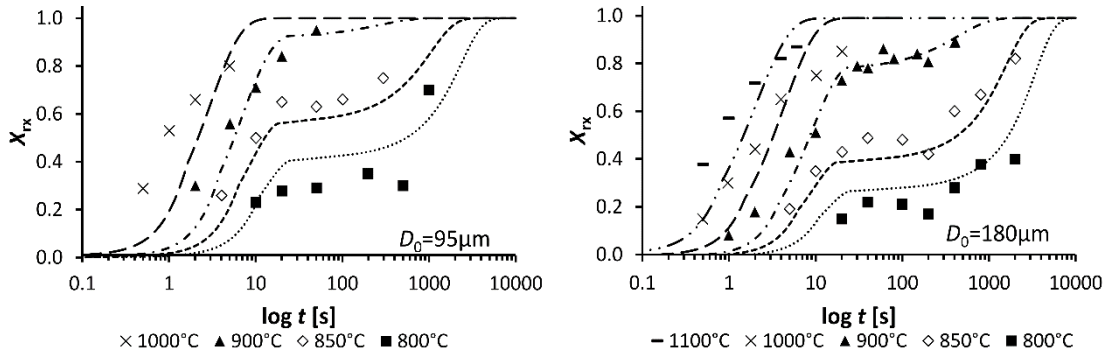
Figure 2:   Simulated recrystallized fraction as a function of temperature compared to experimental results from Quispe et al. [27] with different grain sizes

In the present work, so far, the softening fractions observed by means of torsion tests performed by Quispe et al. [26] have been interpreted as being identical to our calculated recrystallized fractions. This is in line with the interpretation of these authors, however, it has been discussed controversial approaches in literature and we want to address this issue, therefore, in the following. There exist mainly two interpretations of the recrystallization stasis plateaus as measured via the softening fraction method: On the one hand, Zurob et al. [6] suggest to explain the occurrence of the measured softening plateaus as a result of dislocation pinning by precipitates. According to their theory, static recovery is not possible if precipitates pin the dislocation network. Consequently, the deformation-induced excess energy remains stored in the material. Based on this assumption, Zurob et al. [28] formulate general recrystallization maps, where almost no recrystallization occurs till the "end" of the softening plateaus. Thus, these authors identify no direct relation between softening and recrystallized fractions in their consideration of simultaneous precipitation and recrystallization, which is supported by the key experiments of Llanos et al. [29,30] and Kang et al. [31]. On the other hand, Medina and coworkers [32] directly relate the measured softening plateaus as calculated by their back extrapolation method to recrystallized fractions even if precipitation interacts with recrystallization. This method is experimentally confirmed for a significant amount of softening data, where metallographic measurements have been made directly in the plateau regions of V and Nb alloyed steel. These authors observe excellent agreement between softening and recrystallized fractions in their analysis [27,33,34]. Without further going into this discourse, the present authors adopt the interpretation of Quispe et al. [26] and analyze their simulation results accordingly.

A major advantage of the present model is that the progress of recrystallization is described on basis of fundamental state parameters, such as dislocation density, grain size, subgrain size and distribution of precipitates. Consequently, our approach provides considerable potential for introspection, i.e., the possibility of shedding insight into the physical mechanisms of recrystallization and its interaction with, e.g., deformation, recovery and precipitation. For illustration, Figure 3 displays the simulated grain size evolution in comparison to metallographic observations, which have been reported by Quispe et al [27] for two temperatures exhibiting a pronounced recrystallization plateau (850°C, 50s and 900°C, 70s).

Three types of calculated grain sizes may be compared to experiments: (i) the former austenite grain size, (ii) the recrystallized grain size and (iii) a mean grain size, D_{mean}, which is calculated as volumetric weighted superposition of (i) and (ii) by means of the recrystallized fraction. The metallographic analysis at 850°C shows a microstructure with approximately 50% recrystallized grains and an overall heterogeneous size distribution. The observed microstructure is well reproduced by our simulation, with a significant gap between the mean sizes of recrystallized and non-recrystallized grains. In contrast, at 900 °C, a more homogeneous microstructure is observed, which is attributed to the high recrystallized fraction of approximately 85%. This situation is also well reproduced by our simulation. To complement this comparison, we also display predicted grains sizes from an empirical relation for the recrystallized grain size of microalloyed steel as suggested by Sellars [35] with

$$D_{\text{rx,Sellars}} = 0.5 \frac{D^{0.67}}{\varepsilon^{0.67}} \, .$$
(13)

This relation delivers a recrystallized grain size of 33 µm, when using the corresponding parameters, D=180µm and ε=0.35. These results are shown in Fig. 3 as symbols, in close agreement with our simulation at 99% recrystallized fraction.
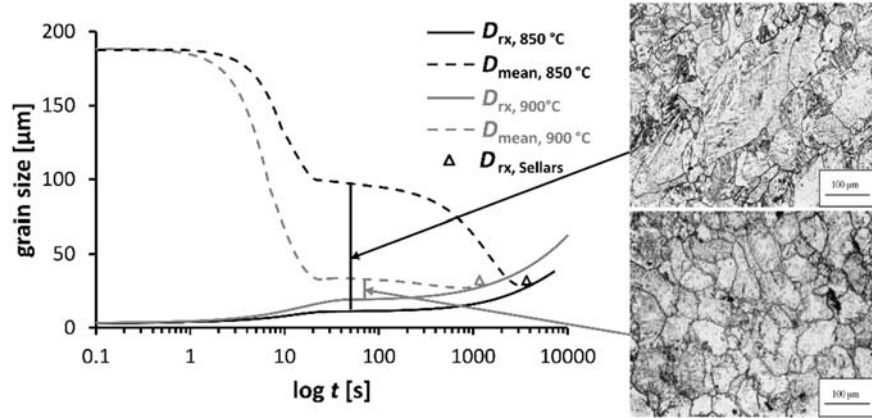
Figure 3.   Simulated grain size evolution for simultaneous recrystallization and precipitation at different temperatures. Metallographic results reproduced from ref. [27], with permission of Elsevier.

In addition, our simulation approach provides insight into details of the nucleation process by evolving the mean subgrain size as critical condition for the number of newly formed supercritical nuclei, Eq. (1). In their work, Quispe et al. [27] observe that recrystallization kinetics are accelerated with decreasing starting austenite grain size. This is attributed to a higher nucleation site density due to an increasing total grain boundary surface area. Yoshie et al. [36] claim that the specific grain boundary area scales with the inverse of grain size, in accordance with Eq. 1. Figure 4 illustrates the evolution of the simulated state parameters, where the nucleation period and amount of stable nuclei are depicted for both considered starting grain sizes (95µm and 180 µm) at 850°C. The interesting observation from the considered experiments is that the impact of the starting grain size on recrystallization remains the same even in the presence of the retarding effect of precipitates. This is particularly prominent in the 850°C results, where the plateau height changes by approximately 20% due to a different starting grain size (Fig. 2). The same is indicated by our simulation, which explicitly relates the different plateau heights to the grain size dependence of recrystallization nucleation rate.
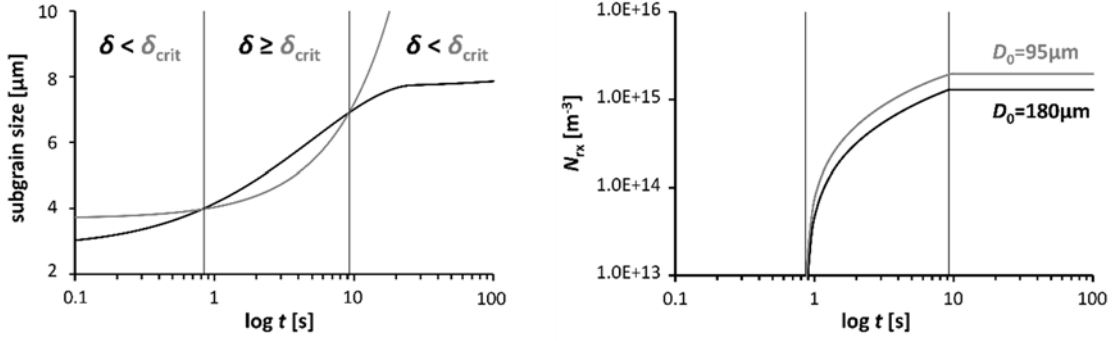
Figure 4: Evolution of some simulation state variables for different starting grain sizes at 850°C.

Finally, figure 5 summarizes the calculated kinetics of precipitation and recrystallization in the form of a Recrystallization-Time-Temperature-Precipitation (RTTP) plot. The diagram displays the progress of recrystallization for several iso-recrystallization lines together with the simulated 5% and 90% precipitation phase fraction lines. The plot clearly shows that the onset of recrystallization stasis is directly related to the precipitated phase fraction and the increasing Zener drag accompanying the precipitation progress. For illustration, the diagram also shows the line where the recrystallization driving pressure equals the Zener drag, i.e., the line where P_D equals P_Z, which is qualitatively in good agreement with experimental observation from refs. [29,37], who claim that this line is located between 5% and 27% of precipitated phase fraction. Furthermore, the simulated start of conventional Ostwald ripening in the deformed microstructure, $V(C,N)_{LSW}$ is depicted, which clearly shows that the kinetics of bulk diffusion-controlled precipitate coarsening has too low kinetics to explain the measured onset of recrystallization after the stasis plateau.
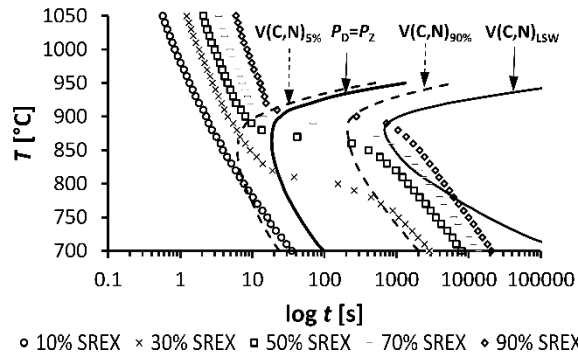

Figure 5: Simulated RTTP- diagram for V-microalloyed steel with 180μm starting austenite grain size

Conclusion

In this work, we introduce a new approach for modeling the interaction of precipitation with static recrystallization kinetics in a consistent way. The experimentally observed plateaus of recrystallization stasis are clearly caused by Zener pinning, however, in contrast to other models, we assume that the recrystallization front never comes to a stop and maintains a non-zero value even if the retarding pressure exceeds the driving pressure for recrystallization. We interpret this behavior in terms of the retarded movement (flow) of an interface through a viscous medium, the velocity of which is determined by local coarsening of precipitates along the grain boundary. Our choice of grain boundary mobilities (free and pinned) delivers the temperature-dependence of the kinetic processes naturally from independent experiments and avoids that these quantities must be considered as fitting parameters.

References

[1]   Smith C S 1948 Introduction to Grains, Phases, and Interfaces—an Interpretation of Microstructure *Trans. AIME* **175** 15–51

[2]   Hillert M 1965 On the theory of normal and abnormal grain growth *Acta Metall.* **13** 227–38

[3]   Nes E 1976 The effect of a fine particle dispersion on heterogeneous recrystallization *Acta Metall.* **24** 391–8

[4]   Humphreys F J 1997 A unified theory of recovery, recrystallization and grain growth, based on the stability and growth of cellular microstructures—II. The effect of second-phase particles *Acta Mater.* **45** 5031–9

[5]   Zurob H S, Brechet Y and Purdy G 2001 A model for the competition of precipitation and recrystallization *Acta Mater.* **49** 4183–90

[6]   Zurob H S, Hutchinson C R, Brechet Y and Purdy G 2002 Modelling recrystallization of microalloyed austenite: effect of coupling recovery, precipitation and recrystallization *Acta Mater.* **50** 3075–92

[7]   Rehman K and Zurob H S 2013 Novel Approach to Model Static Recrystallization of Austenite during Hot-Rolling of Nb-Microalloyed Steel: Effect of Precipitates *Mater. Sci. Forum* **753** 417–22

[8]   Svoboda J, Fischer F D, Fratzl P and Kozeschnik E 2004 Modelling of kinetics in multi-component multi- phase systems with spherical precipitates I: Theory *Mater. Sci. Eng. A* **385** 166–75

[9]   Kozeschnik E, Svoboda J, Fratzl P and Fischer F D 2004 Modelling of kinetics in multi-component multi-phase systems with spherical precipitates II: Numerical solution and application *Mater. Sci. Eng. A* **385** 157–65

[10]   Kozeschnik E 2012 *Modeling Solid-State Precipitation* (Momentum Press)

[11]   Sonderegger B and Kozeschnik E 2009 Generalized Nearest-Neighbor Broken-Bond Analysis of Randomly Oriented Coherent Interfaces in Multicomponent Fcc and Bcc Structures *Metall. Mater. Trans. A* **40** 499–510

[12]   Sonderegger B and Kozeschnik E 2009 Size dependence of the interfacial energy in the generalized nearest-neighbor broken-bond approach *Scr. Mater.* **60** 635–8

[13]   Sonderegger B and Kozeschnik E 2010 Interfacial Energy of Diffuse Phase Boundaries in the Generalized Broken-Bond Approach *Metall. Mater. Trans. A* **41** 3262–9

[14]   Hansen S S, Vander Sande J B and Cohen M 1980 Niobium carbide precipitation and austenite recrystallization in hot rolled microalloyed steels *Metall. Trans. A* **11A** 387–402

[15]   Huang Y and Humphreys F J 2000 Subgrain growth and low angle boundary mobility in aluminium crystals of orientation {110}|<001> *Acta Mater.* **48** 2017–30

[16]   Sherstnev P, Lang P and Kozeschnik E 2012 Treatment of Simultaneous Deformation and Solid- State Precipitation in Thermo-Kinetic Calculations *Eccomas 2012* 8

[17]   Estrin Y ., Tóth L S ., Molinari A . and Bréchet Y . 1998 A dislocation-based model for all hardening stages in large strain deformation *Acta Mater.* **46** 5509–22

[18]   Nes E 1997 Modelling of work hardening and stress saturation in FCC metals *Prog. Mater. Sci.* **41** 129–93

[19]   Sandstrom R 1977 Subgrain Growth Occuring by Boundary Migration *Acta Metall.* **25** 905–11

[20]   Yazawa Y, Furuhara T and Maki T 2004 Effect of matrix recrystallization on morphology, crystallography and coarsening behavior of vanadium carbide in austenite *Acta Mater.* **52** 3727–36

[21]   Jones A . and Ralph B 1975 The influence of recrystallization on carbide particle distributions in a fully stabilized austenitic steel *Acta Metall.* **23** 355–63

[22]   Turnbull D 1951 Theory of grain boundary migration rates *Trans. AIME* **191** 661–5

[23]   Stechauner G and Kozeschnik E 2014 Assessment of substitutional self-diffusion along short-circuit paths in Al, Fe and Ni *Calphad* **47** 92–9

[24]   Zhou T, O'Malley R J and Zurob H S 2010 Study of grain-growth kinetics in delta-ferrite and austenite with application to thin-slab cast direct-rolling microalloyed steels *Metall. Mater. Trans. A Phys. Metall. Mater. Sci.* **41** 2112–20

[25]   Kirchner H O K 1971 Coarsening of grain-boundary precipitates *Metall. Trans.* **2** 2861–4

[26]   Hernandez C A, Medina S F and Ruiz J 1996 Modelling Alloy Flow Curves in Low and Microalloyed Steels *Acta Metall.* **44** 155–63

[27]   Quispe A, Medina S F, Gómez M and Chaves J I 2007 Influence of austenite grain size on recrystallisation–precipitation interaction in a V-microalloyed steel *Mater. Sci. Eng. A* **447** 11–8

[28]   Zurob H S, Hutchinson C R, Brechet Y and Purdy G R 2004 Rationalization of the softening and recrystallization behaviour of microalloyed austenite using mechanism maps *Mater. Sci. Eng. A* **382** 64–81

[29]   Llanos L, Pereda B and López B 2015 Interaction Between Recovery, Recrystallization, and NbC Strain-Induced Precipitation in High-Mn Steels *Metall. Mater. Trans. A* **46** 5248–65

[30]   Llanos L, Pereda B, Lopez B and Rodriguez-Ibabe J M 2016 Hot deformation and static softening behavior of vanadium microalloyed high manganese austenitic steels *Mater. Sci. Eng. A* **651** 358–69

[31]   Kang K B, Kwon O, Lee W B and Park C G 1997 Effect of precipitation on the recrystallization behavior of a Nb containing steel *Scr. Mater.* **36** 1303–8

[32]   Gomez M, Quispe A and Medina S F 2014 Influence of the microalloying elements on the temporary inhibition of static recrystallization by strain induced precipitates *Steel Res. Int.* **85** 1440–5

[33]   Quispe A, Medina S F and Valles P 1997 Recrystallization-induced a Medium Carbon Vanadium Microalloyed Steel *ISIJ Int.* **37** 783–8

[34]   Gómez M, Medina S F, Quispe a. and Valles P 2002 Static Recrystallization and Induced Precipitation in a Low Nb Microalloyed Steel. *ISIJ Int.* **42** 423–31

[35]   Beynon J and Sellars C M 1992 Modelling Microstructure and its effects during multipass hot rolling *ISIJ Int.* **32** 359–67

[36]   Yoshie A, Fujita T, Fujioka M, Okamoto K, Morikawa H and Mabuchi H 1996 Effect of dislocation density in an unrecrystallized part of austenite on growth rate

of recrystallizing grain *ISIJ Int.* **36** 444–50

[37]   Iparraguirre C, Fernández A I, López B, Scott C, Rose A, Kranendonk W, Soenen B and Paul G 2005 Characterization of Strain Induced Precipitation of Nb in Microalloyed Austenite using Classical and Novel Techniques *Mater. Sci. Forum* **500-501** 677–84

Paper IV

State parameter-based modelling of microstructure evolution in micro-alloyed steel during hot forming

Heinrich Buken and Ernst Kozeschnik

State parameter-based modelling of microstructure evolution in micro-alloyed steel during hot forming

Heinrich Buken[1] and Ernst Kozeschnik[1, 2]

[1] Institute of Materials Science and Technology, Vienna University of Technology, Getreidemarkt 9, 1060 Vienna, Austria

[2] Materials Center Leoben Forschung GmbH, Roseggerstraße 12, 8700 Leoben, Austria

In steel production, thermo-mechanical treatment at elevated temperatures is an inevitable step for controlling the microstructure and, thus, the mechanical-technological properties of the final product. One of the main goals in modelling microstructure evolution is the prediction of progress and interaction of hardening and softening mechanism at temperatures, where reheating, hot rolling, finish rolling and coiling are typically carried out. The main mechanisms that need to be accounted for are precipitation, grain growth, solute drag, recovery, recrystallization and phase transformation, which are to be described as functions of temperature, external loading and chemical composition of the material. In the present work, we present a new approach for dealing with these problems and apply it to the thermal and mechanical loading of microalloyed steel. Within this model, we quantitatively predict, for instance, the phenomenon of recrystallization stop in the presence of precipitation. The computational treatment is verified against experimental data from literature, where good agreement is achieved.

1. Introduction

For the case of single phase alloys that is, e.g., C- Mn- steel in the austenitic range, many constitutive laws are available that are capable of providing more or less sufficient knowledge about the static recrystallization behaviour [1]. In multiphase alloys, such as V-microalloyed steel, recrystallization kinetics can become more complicated and constitutive laws are inappropriate to describe recrystallization kinetics since a further dimension enters and influences the system: Particles cause a pinning pressure on grain boundaries. The magnitude of this Zener Drag effect is mainly determined by the precipitated phase fraction and the precipitate size but has its physical roots in the saving of energetically unfavourable total grain interface area.

Deformation provides a higher dislocation density in the material and affects the precipitation process by providing a higher nucleation site density and a higher diffusion rate in the matrix. As a consequence of this interplay of mechanisms, a description of microstructure kinetics with a single Avrami- curve [2] is not possible. Amongst many others, Medina et al. [3] show recrystallization plateaus in the presence of the common microelements Ti, Nb and V.

Modelling approaches are available in literature describing the simultaneous precipitation and recrystallization kinetics either phenomenological or physically based. Medina et al. [3] use a framework of interrelated Avrami based equations. Developing for each composition a grain size and strain dependent formula to calculate a critical maximum temperature where barely a plateau can be measured, they classify recrystallization kinetics into two regimes: a fast one with a low activation energy and a slow one where precipitates pin the grain boundaries. Nonetheless, this approach is not capable of illustrating the experimentally observed curve shapes but shows an assessment of transformation times in dependence of various material conditions and thermo-mechanical processing routes.

Zurob et al. [4] suggest a physical approach for modelling those plateaus. By simulating both, strain-induced precipitation and recrystallization kinetics, they interconnect the microstructure and precipitate evolution by the integral value of driving and retarding pressures. Once the Zener force exceeds the driving force, grain growth and recrystallization progresses come to a stop. Due to coarsening, (Ostwald ripening), the number density of precipitates decreases, they exert less influence on grain boundary movement and the Zener pressure decreases. At this point, the sum of driving pressure and retarding pressure are positive again and grains continue to grow. In this approach, Zurob et al. deliver simulation results, which show the experimentally observed curve progression.

Although some models describing coupled precipitation kinetics and microstructure evolution are available, in most approaches, either the precipitation and recrystallization kinetics are modelled implicitly, such that one set of parameters is only valid for one composition, or that the modelling of precipitation kinetics is fitted with phenomenological parameters (usually interface energies), such that the coupled model delivers microstructure results (e.g. recrystallized fraction) being in good agreement with experimental results.

In the present work and in contrast to the conventional approaches, we utilize a precipitate kinetics framework that is based on independent thermo-physical quantities (thermodynamic

and kinetic databases). From these, temperature, composition and size dependent system parameters, such as interfacial energies [5–7], are computed. The state parameters are then evolved as a function of chemical composition, heat treatment and deformation regime as well as microstructure (grain size, dislocation density, etc.). For simulation of microstructure evolution, we utilize a recently developed single class recrystallization model, in which the driving forces and mobilities are computed by means of the approaches introduced subsequently. In this framework, we describe the precipitation and recrystallization interaction of low carbon steel, where the recrystallization kinetics are influenced by precipitate phases.

2. Modelling approach

2.1 Model development

The thermo-kinetic simulations of precipitation with coupled microstructure evolution are carried out with the software package MatCalc (version 6.00.007). The physical concept and functionality of the precipitate evolution, as delivered by MatCalc, is explained for the case of micro alloying elements in steel elsewhere [8,9]. To the precipitation kinetics routines of MatCalc, we couple a microstructure evolution model, which is introduced next.

The nucleation rate of recrystallized grains is modelled as

$$\dot{N}_{rx} = \begin{cases} C_{rx}\left(\dfrac{\pi}{6}\delta^2 D\right)^{-1} \exp(\dfrac{-Q_{rx}}{RT})(1 - X_{rx}) & ,\delta \geq \delta_{crit} \\ 0 & ,\delta < \delta_{crit} \end{cases}, \qquad (1)$$

where δ is the subgrain diameter, D is the mean un-recrystallized grain diameter, C_{rx} is a calibration coefficient, Q_{rx} is an activation energy equal to the value for substitutional self-diffusion along grain boundaries, X_{rx} is the recrystallized fraction, R is the universal gas constant and T is temperature. The inverse term including the grain size and the subgrain size captures the condition that only subgrains (LAGB), which are in contact with a high-angle grain boundary can become nuclei for recrystallization as experimentally observed in ref. [10].

A second condition for nucleation is that the subgrain exceeds a critical size, δ_{crit}. This is given by the ratio of the interfacial energy of the LAGB, γ_{LB} and the driving pressure, P_D, with

$$\delta_{crit} = \frac{3\gamma_{LB}}{P_D} = \frac{3\gamma_{LB}}{0.5\mu b^2 \rho}. \qquad \qquad \wedge \qquad \qquad (2)$$

The driving pressure is introduced by deformation and calculated by means of a total dislocation density, ρ, the shear modulus, μ, and the Burgers vector, b. Before nucleation takes place, the subgrain has to grow in order to overcome this critical size. On the one hand, the subgrain size is reduced by the deformation-induced dislocation that are stored in the subgrain boundaries. Nes [11] and Estrin [12] introduced the principle of similitude, where the dislocation density is correlated to a subgrainsize, δ_0, by means of a material parameter K, which is taken as starting subgrain size directly after deformation. On the other hand, the subgrain grows due to the driving pressure of capillary, where $M_{eff,LB}$ is the effective LAGB mobility.

$$\delta = \delta_0 + \dot{\delta} \cdot t = \left(\frac{K}{\sqrt{\rho}} \right) + \left(M_{eff,LB} \frac{3\gamma_{LB}}{\delta} \right) \cdot t \qquad (3)$$

The growth velocity of stable nuclei, $\dot{D}_{rx}$, is expressed by the product of an effective HAGB mobility, $M_{eff, HB}$, and the driving pressure as

$$\dot{D}_{rx} = M_{eff, HB} P_D (1 - X_{rx}). \qquad (4)$$

With increasing degree of recrystallization, less deformed volume is available in which the recrystallized grains can grow into. To account for that, the growth velocity is balanced with the unrecrystallyzed volume fraction, $1\text{-}X_{rx}$.

Deformation induces an increased dislocation density in the material and originates a driving pressure for recrystallization. The deformation-induced dislocation density is calculated by means of a Kocks- Mecking-type approach [13], which has been extended for static recovery by Sherstnev et al. [14].

$$\dot{\rho} = \frac{M\sqrt{\rho}}{Ab}\dot{\varphi} - 2B\frac{d_{ann}}{b}\rho M\dot{\varphi} - 2CD_{Dis}\frac{\mu b^3}{k_B T}\rho \qquad (5)$$

with the Taylor factor, M, the critical dislocation annihilation distance, d_{ann}, the substitutional self-diffusion coefficient at dislocations, D_{Dis}, the Boltzmann constant, k_B, the strain rate φ, and material parameters A, B, C.

The influence of precipitates on recrystallization kinetics is incorporated via the Zener pressure, P_Z, which is given for a spatial distribution of spherical precipitates by Nes et al. [15] as

$$P_Z = \frac{3f\gamma_{HB}}{2r}, \qquad (6)$$

where γ_{HB} is the HAGB energy, f is the phase fraction of precipitates and r is the precipitate radius. In contrast to most other approaches [16–18], we do not incorporate the Zener pressure into the driving force term, which may lead to a complete growth stop of the recrystallization front if the retarding force exceeds the driving force. In our treatment, we assume that the precipitates, which are arranged at the pinned grain boundary, are interconnected along a high velocity diffusion path, which allows for fast local coarsening of precipitates. Hence, the Zener pressure locally decreases and allows for a further boundary movement till a new front of precipitates is encountered, where the process of local coarsening is repeated. We aggregate this mechanism in the form of an effective mobility, which is written as

$$M_{\text{eff}} = \begin{cases} \left(\dfrac{P_D - P_Z}{P_D}\right)M_{\text{free}} + \left(1 - \dfrac{P_D - P_Z}{P_D}\right)M_{\text{pinned}} & , P_D > P_Z \\ M_{\text{pinned}} & , P_D \le P_Z \end{cases} \qquad (7)$$

where the effective boundary mobility is calculated as superposition between a free mobility, M_{free}, in the absence of pinning, and a minimum mobility M_{pinned}, caused by precipitate pinning. This new approach provides a possibility for boundary movement even if the mean Zener pressure of the system exceeds the driving pressure for recrystallization.

2.2 Model Parameters

To verify the new model on experimental data, an evaluation of important parameters is performed first, which is summarized in table 1. Since the grain boundary mobility is a most important input parameter in our recrystallization model, we express this quantity in relation to well-assessed diffusion coefficients. Turnbull [19] suggests an upper bound for the boundary mobility, M_{TB}, with

$$M_{\text{free}} = \eta_{\text{free,HB}} \cdot M_{TB} = \eta_{\text{free,HB}} \cdot \frac{\omega D_{GB} V_m}{b^2 RT}, \qquad (8)$$

with the substitutional diffusion coefficient at grain boundaries, D_{GB}, the grain boundary width, ω and the molar volume of the material, V_m. Since atomic attachment kinetics are not accounted for within this approach, we introduce a dimensionless linear factor, $\eta_{\text{free,HB}}$, which conserves the temperature dependency of the free mobility as the ratio of the grain boundary diffusion coefficient and temperature. We adopt D_{GB} in austenite from a recent diffusion assessment of Stechauner and Kozeschnik [20]. The linear factor

is adjusted to the mobility measurements of Zhou et al. [21] of plain C-Mn steel in austenite, where good agreement is achieved with a value of 1.5%.

The temperature dependency of the pinned mobility should be equal to the free mobility. Kirchner [22] suggests for precipitate coarsening at grain boundaries the same temperature dependency as Turnbull for the grain boundary mobility. Thus, we model the pinned mobility as fraction of the free mobility, which delivers with Eq. 4 a reduced growth rate in the presence of precipitates as

$$M_{pinned} = \eta_{pinned,HB} \cdot M_{free}. \qquad\qquad (9)$$

Application of this concept (section 3) shows that the mobility decreases by two orders of magnitude to 3% due to the retarding pressure exerted by the precipitates. The driving pressure for recrystallization is mainly determined by the deformation-induced dislocations and interacts with both nucleation and growth of the new microstructure. Therefore, the parameters (*A*, *B*, *C*) of the extended Kocks- Mecking model (Eq. 5) are adjusted such as to reproduce flow curve results of Hernandez et al. [23]. The observed dislocation densities do not exceed $7 \cdot 10^{14}$ m^{-2} and deliver appropriate flow stresses in the sense of the Taylor forest hardening law with input parameters similar to those mentioned in ref. [4]. The activation energy for nucleation of recrystallization (Eq. 1) mainly determines the temperature dependency of the nucleation rate. Occurring at the grain boundary, nucleation is assumed to obey the temperature dependency of grain boundary diffusion. Thus, this value is also taken from ref. [20]. The linear factor, C_{rx}, is an adjusting parameter, which balances the nucleation suppressing effect of the activation energy, but it is left constant over the range of considered materials (section 3). A collection of the elaborated parameters is given in table 1.

Table 1.   Simulation input parameters

| Parameter	Unit	Value	Ref.
$\eta_{free,HB}$	-	0.015	[19–21]
$\eta_{pinned,HB}$	-	0.03	This work
A	-	50	This work
B	-	5	This work
C	-	$5 \cdot 10^{-5}$	This work
Q_{rx}	kJ mol^{-1}	145	[20]
Crx	s^{-1}	1e6	This work
γ_{HB}	J m^{-2}	$1.311 - 0.005 \cdot T$	[4]
γ_{LB}	J m^{-2}	$0.5 \cdot \gamma_{HB}$	This work

3. Validation

Finally, the present microstructure model with combined precipitation kinetics is verified on experimental results from Medina et al. [24], who measured the progress of static recrystallization in diverse V-microalloyed steels. Table 2 summarizes the different compositions, starting grain sizes, D_0 and solid solution temperatures, T_{sol}, of the investigated materials.

Table 2. Considered materials at $\varepsilon = 0.35$ and $\dot{\varepsilon} = 3.62 s^{-1}$

Steel	C [wt.-%]	V [wt.-%]	N [wt.-%]	T_{sol} [°C]	D_0 [μm]
S1	0.125	0.065	0.0123	1056	167
S2	0.113	0.095	0.0144	1106	162

The two considered materials are experimentally analysed at a constant strain, , strain rate, $\dot{\varepsilon}$, and at different temperatures. The different precipitate solution temperatures, which are calculated with the thermokinetic software MatCalc, indicate different driving forces for precipitation. Steel S1 has a lower driving force for precipitation than steel S2 due to lower V and N contents. Therefore, the retardation of recrystallization due to precipitation is more pronounced in the more supersaturated alloy S2. At lower temperatures (below 1000°C), recrystallization starts to interact with precipitation and both steels show in that temperature range a recrystallization plateau. The more supersatured system S2 shows, in comparison to steel S1, recrystallization plateaus at lower levels of recrystallized fractions, because the Zener pressure exceeds the driving pressure for recrystallization earlier. When the retarding pressure exceeds the driving pressure, further kinetics are limited by the pinned mobility and the progress of recrystallization is decelerated. At higher temperatures ($T \geq 1000$°C), there is no interaction between precipitation and precipitation observed and both alloys show nearly the same microstructure evolution kinetics. Figure 1 depicts the results of our simulation approach in comparison to the experimental measurements of Medina et al [24].
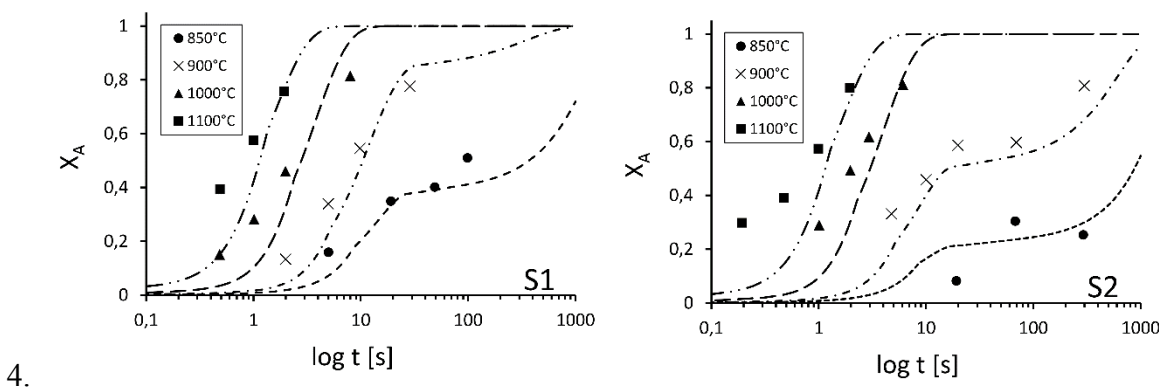
Figure 1.   Recrystallization experiments vs. simulation for steel S1 and S2 at different temperatures

5. Summary

A new microstructure model is presented, where the static recrystallization process is described by the mechanisms of nucleation and growth. The growth rate of recrystallized grains is given by the product of grain boundary mobility and driving pressure. In contrast to several other models, the precipitate influence is incorporated into the mobility term and not the driving pressure term, which allows for a further growth of the recrystallized fraction even if the Zener force exceeds the driving force. The model is verified against experimental data from ref. [24], where good agreement is achieved.

References

[1]   Beynon J and Sellars C M 1992 Modelling Microstructure and its effects during multipass hot rolling *ISIJ Int.* **32** 359–67

[2]   Avrami M 1940 Kinetics of Phase Change. II Transformation-Time Relations for Random Distribution of Nuclei *J. Chem. Phys.* **8** 212–24

[3]   Medina S F and Mancilla J E 1996 Static recrystallization modelling of hot deformed microalloyed steels at temperatures below the critical temperature *ISIJ Int.* **36** 1077–83

[4]   Zurob H S, Brechet Y and Purdy G 2001 A model for the competition of precipitation and recrystallization *Acta Mater.* **49** 4183–90

[5]   Sonderegger B and Kozeschnik E 2009 Generalized Nearest-Neighbor Broken-

Bond Analysis of Randomly Oriented Coherent Interfaces in Multicomponent Fcc and Bcc Structures *Metall. Mater. Trans. A* **40** 499–510

[6]   Sonderegger B and Kozeschnik E 2009 Size dependence of the interfacial energy in the generalized nearest-neighbor broken-bond approach *Scr. Mater.* **60** 635–8

[7]   Sonderegger B and Kozeschnik E 2010 Interfacial Energy of Diffuse Phase Boundaries in the Generalized Broken-Bond Approach *Metall. Mater. Trans. A* **41** 3262–9

[8]   Radis R and Kozeschnik E 2010 Concurrent Precipitation of AlN and VN in Microalloyed Steel *Steel Res. Int.* **81** 681–5

[9]   Radis R and Kozeschnik E 2012 Numerical simulation of NbC precipitation in microalloyed steel *Model. Simul. Mater. Sci. Eng.* **20** 055010

[10]   Hansen S S, Vander Sande J B and Cohen M 1980 Niobium carbide precipitation and austenite recrystallization in hot rolled microalloyed steels *Metall. Trans. A* **11A** 387–402

[11]   Nes E 1997 Modelling of work hardening and stress saturation in FCC metals *Prog. Mater. Sci.* **41** 129–93

[12]   Estrin Y, Tóth L S, Molinari A and Bréchet Y 1998 A dislocation-based model for all hardening stages in large strain deformation *Acta Mater.* **46** 5509–22

[13]   Kocks U F and Mecking H 2003 Physics and phenomenology of strain hardening: The FCC case *Prog. Mater. Sci.* **48** 171–273

[14]   Sherstnev P, Lang P and Kozeschnik E 2012 Treatment of Simultaneous Deformation and Solid- State Precipitation in Thermo-Kinetic Calculations *Eccomas 2012* 8

[15]   Nes E, Ryum N and Hunderi O 1985 On the Zener drag *Acta Metall.* **33** 11–22

[16]   Nes E 1976 The effect of a fine particle dispersion on heterogeneous recrystallization *Acta Metall.* **24** 391–8

[17]   Humphreys F J 1997 A unified theory of recovery, recrystallization and grain growth, based on the stability and growth of cellular microstructures—II. The effect of second-phase particles *Acta Mater.* **45** 5031–9

[18]   Zurob H S, Hutchinson C R, Brechet Y and Purdy G 2002 Modelling recrystallization of microalloyed austenite: effect of coupling recovery, precipitation and recrystallization *Acta Mater.* **50** 3075–92

[19]   Turnbull D 1951 Theory of grain boundary migration rates *Trans. AIME* **191** 661–5

[20]   Stechauner G and Kozeschnik E 2014 Assessment of substitutional self-diffusion along short-circuit paths in Al, Fe and Ni *Calphad* **47** 92–9

[21]   Zhou T, O'Malley R J and Zurob H S 2010 Study of grain-growth kinetics in delta-ferrite and austenite with application to thin-slab cast direct-rolling microalloyed steels *Metall. Mater. Trans. A Phys. Metall. Mater. Sci.* **41** 2112–20

[22]   Kirchner H O K 1971 Coarsening of grain-boundary precipitates *Metall. Trans.* **2** 2861–4

[23]   Hernandez C A, Medina S F and Ruiz J 1996 Modelling Alloy Flow Curves in Low and Microalloyed Steels *Acta Metall.* **44** 155–63

[24]   Medina S F, Mancilla J E and Hernandez C A 1993 Influence of Vanadium on the static recrystallization of austenite in microalloyed steels *J. Mater. Sci.* **28** 5317–24

Paper V

A Model for the Influence of Micro-Alloying Elements on Static
Recrystallization of Austenite

Heinrich Buken, Sabine Zamberger and Ernst Kozeschnik

A Model for the Influence of Micro-Alloying Elements on Static Recrystallization of Austenite

Heinrich Buken[1], Sabine Zamberger[2], Ernst Kozeschnik[1,3]

[1]Institute of Materials Science and Technology, Vienna University of Technology, Getreidemarkt 9, 1060 Vienna, Austria

[2]voestalpine Stahl Donawitz GmbH & Co KG, Kerpelystrasse 199, 8700 Leoben, Austria

[3]MatCalc Engineering GmbH, Getreidemarkt 9, 1060 Vienna, Austria

Abstract

After and during hot rolling of steel, recrystallization can occur and impact severely on the resulting product properties. Recrystallization kinetics are, in particular, influenced by the addition of micro-alloying elements. On the one hand, micro-alloying elements in solid solution, such as Nb, Ti and V, exert a solute drag effect, which reduces the mobility of the grain boundaries. On the other hand, micro-alloying elements form precipitates, which exert a particle pinning force on the grain boundaries. In the present work, we formulate a physically-based recrystallization model with grain boundary mobilities that account simultaneously for the solute drag and Zener drag impact of Nb, Ti and V. We verify the model on numerous experiments on static recrystallization from literature, where good agreement is observed with a single set of simulation input parameters.

Introduction

The mechanism of recrystallization determines the final product quality during hot deformation of steel. Recrystallization kinetics are mainly influenced by the steel composition, the deformation velocity, the degree of deformation, the starting austenite grain size and the deformation temperature, which is phenomenologically demonstrated by Medina and Quispe [1].

The addition of micro-alloying elements to the steel composition has a particular influence on the recrystallization behavior of steel. On the one hand, micro-alloying elements, such as Nb, Ti and V, can form carbo-nitride precipitates, which exert a

retarding pressure on the grain boundaries [2]. This pinning force may even change the appearance of the recrystallized fraction vs. time curves and "pinning plateaus" become observable [3]. On the other hand, micro-alloying elements exert a solute drag effect on grain boundary movement. Andrade et al. [4] experimentally confirmed this for Nb, Ti and V additions in steel. In literature, a substantial amount of empirical and physical based approaches for predicting recrystallization behavior is available. Medina and Quispe [1] present an empirical and Avrami- based [5] model, where the recrystallization plateaus are modelled with two interrelated transformation curves. The solute drag impact is accounted for with different activation energies. Rehman et al. [6,7] suggest a physically-based approach for Nb micro-alloyed steel, where the recrystallization plateaus are considered to be caused by pinned dislocations. The solute drag impact is modelled with the Cahn approach [8], which reduces the grain boundary mobility in dependence of the solute type and solute concentration.

In this work, we introduce an advancement of a recently published state parameter-based microstructure evolution model [9], which accounts for both effects, the solute drag and the Zener drag. We compare the model results to various experiments on micro-alloyed steel in literature. Thereby, we formulate a new nucleation model for recrystallization, which is introduced next.

The model

The nucleation rate of newly formed recrystallized grains can be described by the product of the number of potential nucleation sites, N_{pot}, the flux of subgrains becoming supercritical from a distribution function, $\dfrac{\partial R}{\partial t}$, and a factor accounting for the already consumed nucleation sites, B_{Nuc}, with

$$\frac{\partial N_{rx}}{\partial t} = N_{pot} \frac{\partial R}{\partial t} B_{Nuc} \qquad\qquad (1)$$

Potential nucleation sites are subgrains, which are located at the grain boundary and exceed a critical size in the sense of the Bailey-Hirsch mechanism [10]. We express the number density of potential recrystallization nuclei as surface weighted ratio between the specific available high angle grain boundary (HAG) surface area, a_{av}, and the cross section of a supercritical low angle grain boundary (LAG), $A_{crit,LAG}$. Thereby, we approximate the HAG geometry with a truncated octahedron, as

$$N_{pot} = a_{av} \frac{1}{A_{crit,LAG}} f(\varepsilon) = \frac{1}{8\sqrt{2}\left(\dfrac{3R}{2}\right)^3} \frac{1}{\pi r_{crit}^2} f(\varepsilon) \qquad (2)$$

where R is the mean grain radius, r_{crit} is the critical LAG radius and $f(\varepsilon)$ is a surface factor for the deformed grain geometry. The latter is taken from Zhu et al. [11] for the case of plane strain compression.

The LAG distribution can be characterized with a Rayleigh function [6]. The fraction of the subgrains, which are larger than the critical size is given by the function

$$R(t) = \exp\left(-\frac{\pi}{4} X_{crit}^2(t)\right), \qquad (3)$$

where X_{Crit} is the critical subgrain size normalized by the mean subgrain size. The flux of subgrains that become super-critical and serve as stable nuclei during and after hot deformation is then obtained by differentiation with respect to time as

$$\frac{\partial R(t)}{\partial t} = -\frac{1}{2}\pi R(t) X_{crit} \dot{X}_{crit}. \qquad (4)$$

The normalized critical subgrain diameter and its rate, $\dot{X}_{crit}$, can be the calculated in dependence of a mean LAG size, r_{mean}, and critical LAG size.

$$X_C = \frac{r_{crit}}{r_{mean}}, \qquad (5)$$

$$\dot{X}_C = \frac{\dot{r}_{crit}}{r_{mean}} - \frac{r_{crit}\,\dot{r}_{mean}}{r_{mean}^2}. \qquad (6)$$

The evolution of the mean and critical subgrain diameter values has been described in a previous contribution [9]. During the nucleation period, already stable nuclei consume grain boundary area, which becomes unavailable for further nucleation. Again, we use a surface weighted approach in dependence of the recrystallized grain density, N_{rx}, in order to approximate the effect of occupied nucleus sites on the nucleation rate with

$$B_{Nuc} = 1 - \frac{N_{rx}\pi\left(r_{crit}\right)^2}{a_{av}}. \qquad (7)$$

The subsequent growth of stable nuclei is influenced by precipitates and solute atoms, which both affect the grain boundary mobility [8,9].

In contrast to most other approaches [12,13], in the present work, the Zener pressure term is not included into the driving pressure term. We assume that the precipitates, which are arranged at the pinned grain boundary, are interconnected along high velocity diffusion

paths (grain boundaries), which trigger fast local precipitate coarsening. We approximate the effect of this local coarsening mechanism on recrystallization kinetics by means of an effective mobility for each considered precipitate type T, which is written as

$$
M_{\text{prec, T}} =
\begin{cases}
\left(\dfrac{P_{\text{D}} - P_{\text{Z}}}{P_{\text{D}}} \right) M_{\text{free}} + \left(1 - \dfrac{P_{\text{D}} - P_{\text{Z}}}{P_{\text{D}}} \right) M_{\text{pinned}} & , P_{\text{D}} > P_{\text{Z}} \\
M_{\text{pinned}, T} & , P_{\text{D}} \leq P_{\text{Z}}
\end{cases}
, \qquad (8)
$$

where the precipitate effected boundary mobility, $M_{\text{prec, T}}$, is calculated as superposition between a free mobility, M_{free}, in the absence of pinning, and a minimum mobility M_{pinned}, caused by precipitate pinning. This treatment allows for a slower grain boundary movement even if the Zener pressure, P_{Z}, exceeds the driving pressure for recrystallization, P_{D}.

The impact of solute drag is modelled with the Cahn approach [8], where the dragging effect of solute atoms is incorporated into the mobility term for the solute drag exerting element E with

$$
M_{\text{SD},E} = \frac{1}{\alpha_E C_{\text{GB,E}}}, \qquad (9)
$$

where $M_{\text{SD,E}}$ is the mobility of the grain boundary in the presence of solute drag, $C_{\text{GB,E}}$ is the grain boundary concentration and α is an inverse mobility. The latter is mainly determined by a grain boundary/atom interaction energy, E_{B}, and is given as

$$
\alpha = \frac{\omega (RT)^2}{E_{\text{B,E}} D_{\text{CB,E}} V_{\text{M}}} \left(\sinh\left(\frac{E_{\text{B,E}}}{RT} \right) - \left(\frac{E_{\text{B,E}}}{RT} \right) \right), \qquad (10)
$$

where ω is the grain boundary width, V_{M} is the molar volume of the matrix phase, $D_{\text{CB},E}$ is the cross boundary diffusion coefficient, R is the universal gas constant and T is the temperature. The effective HAGB mobility can then be calculated in dependence of precipitates and solutes with

$$
M_{\text{eff,HB}} = \left(\frac{1}{M_{\text{prec,T}}} + \frac{1}{M_{\text{SD, E}}} \right)^{-1}. \qquad (11)
$$

Input parameters and validation

Since the grain boundary mobility is a central input parameter in our recrystallization model, we further detail the evaluation procedure for mobilities, below. For the mobility

of a free, un-pinned grain boundary, we use an expression suggested by Turnbull [14], in which the grain boundary mobility, M_{TB}, is described by

$$M_{\text{free}} = \eta_{\text{free}} \cdot M_{\text{TB}} = \eta_{\text{free}} \cdot \frac{\omega D_{\text{GB}} V_{\text{m}}}{b^2 RT},$$ (12)

with an average substitutional diffusion coefficient at grain boundaries, D_{GB}, and a dimensionless linear factor, η_{free}. We adopt D_{GB} in austenite from a recent assessment of Stechauner and Kozeschnik [15]. The linear factor is adjusted to the mobility measurements of Zhou et al. [16] of plain C-Mn steel in austenite, where good agreement is achieved with a value of 1.5%.

The temperature dependence of the pinned mobility should be equal to that of the free mobility. Kirchner [17] suggests, for precipitate coarsening at grain boundaries, the same temperature dependency as Turnbull for the grain boundary mobility. Thus, we model the pinned mobility as fraction of the free mobility, which delivers with Eq. 4 a reduced growth rate in the presence of different precipitate types, T, as

$$M_{\text{pinned, } T} = \eta_{\text{pinned, } T} \cdot M_{\text{free}}.$$ (13)

The solute drag impact is mainly determined by the binding energy of the solute drag exerting element to the grain boundary. Andrade et al. [4] determined corresponding values for Nb, Ti and V and gives an order for the solute drag strength, where Nb is the strongest and V is the weakest solute drag exerting element. Maintaining the given hierarchy, we define the element dependent trapping energies accordingly. The key values for the simulations carried out in this work are summarized in table 1.

Table 1: Input parameters for recrystallization simulation

Parameter	Value	Unit	Ref.
γ_{HB}	1.3111-0.0005T	J/m2	[12]
$E_{\text{B,Nb}}$	17	kJ/mol	This work
$E_{\text{B,Ti}}$	10	kJ/mol	This work
$E_{\text{B,V}}$	2.5	kJ/mol	This work
η_{free}	$1.5 \cdot 10^{-2}$	-	[15,16]
$\eta_{\text{pinned,Nb}}$	$0.6 \cdot 10^{-2}$		This work
$\eta_{\text{pinned,Ti}}$	$1 \cdot 10^{-2}$	-	This work
$\eta_{\text{pinned, V}}$	$3 \cdot 10^{-2}$	-	This work

To validate the present model, we analyze the experimental observations on simultaneous recrystallization and precipitation in Nb, Ti and V alloyed steels reported by Medina et al. [18–20]. The selection of experiments offers a wide range of recrystallization affecting parameters. Among them are different strains, ε, starting grain sizes, D_0, temperatures and compositions. Solely the strain rate is held constant during every experiment at $3.63s^{-1}$. Table 2 summarizes the materials and experiments considered further.

Table 2: Chemical composition of simulated materials

alloy	Ti, Nb, V [wt.-%]	C [wt.-%]	N [wt.-%]	T [°C]	ε	D_0 [μm]	Ref.
Ti- steel	0.075 (Ti)	0.15	0.0102	850-1100	0.35	90	[18]
Nb- steel	0.042 (Nb)	0.11	0.0112	900-1100	0.2	122	[20]
V- steel	0.06 (V)	0.12	0.0123	850-1100	0.2-0.35	167	[19]

Figure 1 summarizes our simulation results in comparison to experimental data by Medina et al. [18–20]. Both, the simulation results and the experimental data of the V steel show that increasing strain accelerates recrystallization kinetics. The height of recrystallization "plateaus" are strongly dependent on the accumulated strain. The strain range changes the plateau heights by approximately 20% recrystallized fraction. In comparison to the V and Ti alloy, the Nb alloy shows a retarded recrystallization behavior, which is caused by the strong solute drag impact. The grain size dependence is also reproduced well by our simulation. This is clearly observable on the Ti alloy, which starts at the highest temperature at a recrystallized fraction of approximately 15%, attributable to the lowest starting grain size of 90μm. One interesting observation is, that the pinned mobility delivers, for each precipitate type, a plausible temperature dependency, supporting the pinned mobility concept applied in the present work.
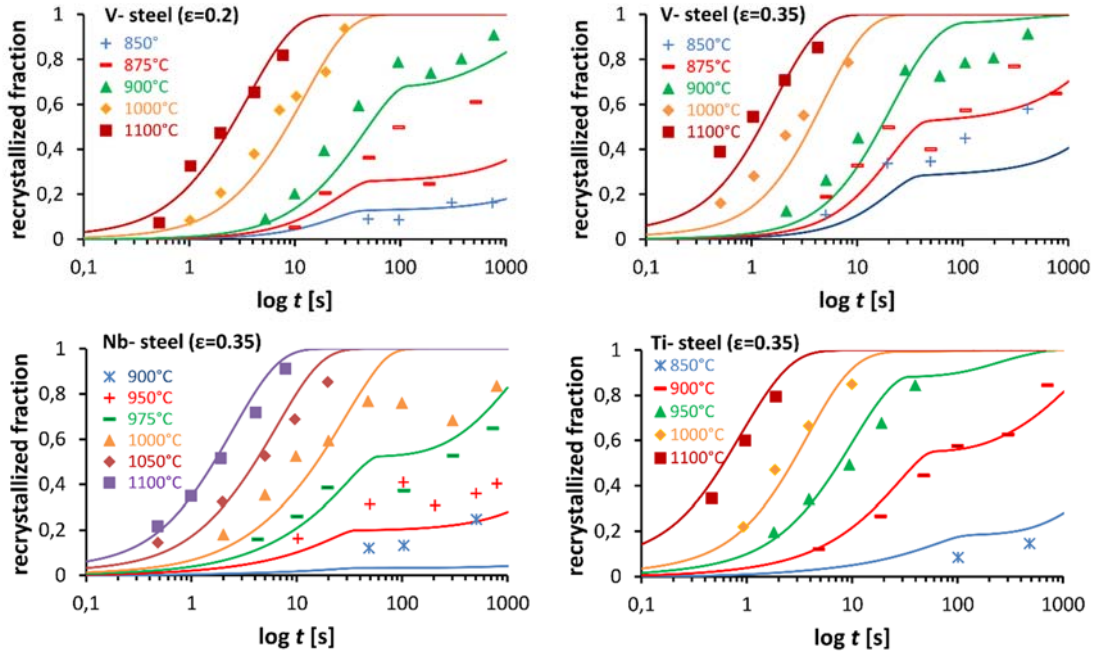
Figure 1: Simulation results vs. experimental data of Medina et al. [18–20]

Summary

A state parameter-based microstructure model is presented, which successfully integrates the impact of precipitates and solutes on recrystallization kinetics. The precipitate influence is incorporated into the grain boundary mobility, which allows for a further growth of the recrystallized fraction even if the Zener force exceeds the driving force for recrystallization. The solute drag impact is modelled with the Cahn approach and captures the different impact of Nb, Ti and V on grain boundary motion. The model is validated against several experiments from literature [18–20].

References

[1]   S.F. Medina, a. Quispe, ISIJ Int. 41 (2001) 774–781.

[2]   C.S. Smith, Trans. AIME 175 (1948) 15–51.

[3]   M. Gomez, A. Quispe, S.F. Medina, Steel Res. Int. 85 (2014) 1440–1445.

[4]   H.L. Andrade, M.G. Akben, J.J. Jonas, Metall. Trans. A 14 (1983) 1967–1977.

[5]   M. Avrami, J. Chem. Phys. 8 (1940) 212–224.

[6]   M.K. Rehman, H.S. Zurob, Metall. Mater. Trans. A Phys. Metall. Mater. Sci. 44 (2013) 1862–1871.

[7]   K. Rehman, H.S. Zurob, Mater. Sci. Forum 753 (2013) 417–422.

[8]   J.W. Cahn, Acta Metall. 10 (1962) 789–798.

[9]   H. Buken, P. Sherstnev, E. Kozeschnik, Model. Simul. Mater. Sci. Eng. 24 (2016) 11pp.

[10]   J.E. Bailey, P.B. Hirsch, Proc. R. Soc. London A 267 (1962) 11–37.

[11]   Q. Zhu, C.M. Sellars, H.K.D.H. Bhadeshia, Mater. Sci. Technol. 23 (2007) 757–766.

[12]   H.S. Zurob, Y. Brechet, G. Purdy, Acta Mater. 49 (2001) 4183–4190.

[13]   E. Nes, Acta Metall. 24 (1976) 391–398.

[14]   D. Turnbull, Trans. AIME 191 (1951) 661–665.

[15]   G. Stechauner, E. Kozeschnik, Calphad 47 (2014) 92–99.

[16]   T. Zhou, R.J. O'Malley, H.S. Zurob, Metall. Mater. Trans. A Phys. Metall. Mater. Sci. 41 (2010) 2112–2120.

[17]   H.O.K. Kirchner, Metall. Trans. 2 (1971) 2861–2864.

[18]   S.F. Medina, a. Quispe, ISIJ Int. 36 (1996) 1295–1300.

[19]   S.F. Medina, J.E. Mancilla, C. a. Hernández, ISIJ Int. 34 (1994) 689–696.

[20]   S.F. Medina, Scr. Metall. Mater. 32 (1995) 43–48.